UNIVERSITY OF READING

Department of Meteorology

Evaluating Numerical Model Cloud Parameterizations using Radar and Lidar Simulation

Jonathan Mark Wilkinson

A thesis submitted for the degree of Doctor of Philosophy

March 2007

I confirm that this is my own work and the use of all material from other sources has been properly and fully acknowledged.

Jonathan Mark Wilkinson

Abstract

Clouds are an important constituent of the Earth's atmospheric radiation budget and are one of the major uncertainties in predicting future climate. In order to predict how clouds will behave in future climate, we first have to evaluate how they are represented in numerical models in the present day.

This thesis explores the evaluation of model cloud parameterization schemes using two simulation methods, where radar and lidar observations are predicted from model variables. Simulation of ground-based radar data is used to investigate why many operational models have a deep evaporation zone when compared to radar observations and has allowed the rejection of many possible causes of the deep evaporation zone. However, when comparing radiosonde and model humidity profiles it can be seen that, in many cases, there is a sharp drop in humidity within the evaporating layer. A simple numerical model is created that uses the Met Office model parameterization scheme to test the sensitivity of evaporation zones to atmospheric variables. Using radiosonde temperature and humidity profiles, the evaporation model shows that, given the correct humidity gradient, the Met Office model could accurately represent the evaporation zone depth.

Secondly, simulation is used to make a global evaluation of the ECMWF model's cloud scheme. A forward model is used to predict lidar backscatter from the ICESat satellite using ECMWF model variables. This accounts for the extinction of the lidar signal and removes any cloud that would not be detected by the lidar. Over nine million kilometers of ICESat data are compared to the corresponding ECMWF model output. Results show that the ECMWF ice cloud is too frequent, tropical boundary layer clouds are poorly represented and the model has greatest skill at high altitudes and over the land.

Acknowledgements

I am very grateful for the contribution to this thesis made by my supervisors **Robin Hogan** and **Anthony Illingworth**. Thanks to Robin for his patient yet critical viewpoint of my work and for the large number of times he prevented me from taking a totally wrong turning. Thanks must go also to Anthony for casting his eye over my results and applying the wide knowledge of radar and clouds he has acquired; it's amazing how much you actually know!

I must also give thanks to other members of the radar group. To **Ewan O'Connor** for his help with all the programming, data reading and data storage and to **Rob Thompson** for help with some of my Matlab problems. Thanks must also go to **Richard Forbes** for his knowledge of the Met Office model.

A Ph.D. could not even start without data and so I am grateful for the contribution of the Rutherford Appleton Laboratory and the staff at the Chilbolton Observatory for the ground-based radar data. Thanks must also go to the Cloudnet team for data. The ICESat data was obtained from the National Snow and Ice Data Center (NSIDC), at Boulder in Colorado, USA; many thanks to all those over there who allowed me to transfer such a huge quantity of data with few problems. The corresponding ECMWF data was provided by **Angela Benedetti**; many thanks to her and the team at the ECMWF.

Special thanks to all the Ph.D. students at Reading who have made my time here special. You provided me with all those lunchtime runs around campus, support when I felt like my work was going nowhere, numerous evenings out and plenty other non-work activities. Thanks also to the numerous organists who have provided me with thesis relief through music.

Finally I should like to thank my family and friends outside of work for financial and moral support. In particular, I should like to thank my parents **Thelma Wilkinson** and the late **Peter Wilkinson** for their support and encouragement in my meteorological career.

"If you care enough for a result, you will most certainly attain it."

- William James (1842–1910)

"Logic will get you from A to B. Imagination will take you everywhere."

- Albert Einstein (1879–1955)

"*Everybody talks about the weather, but nobody does anything about it.*"

- Charles Dudley Warner (1829–1900)

Contents

1 Introduction and Motivation **1**

1.1 The Importance of Clouds within Climate and Weather Forecasting Models . . . 1

1.2 Two Methods of Evaluating Models . . . 2

1.3 This Thesis . . . 5

2 Using Radar and Lidar for Model Evaluation **7**

2.1 Introduction . . . 7

2.2 Principles of Radar Remote Sensing . . . 8

2.2.1 The Radar Equation . . . 8

2.2.2 Using Radar to Study Clouds . . . 11

2.3 Principles of Lidar Remote Sensing . . . 15

2.3.1 The Lidar Equation . . . 16

2.3.2 Using Lidar to Study Clouds . . . 17

2.4 Model Representation of Clouds . . . 19

2.4.1 Liquid Water Content . . . 20

2.4.2 Ice Water Content . . . 23

2.4.3 Cloud Fraction . . . 24

2.4.4 Cloud Overlaps . . . 26

2.5 Comparisons Between Radar/Lidar and Models . . . 29

2.5.1 Radar and Lidar Evaluation of Liquid Water Content . . . 29

2.5.2 Radar and Lidar Evaluation of Ice Water Content . . . 31

2.5.3 Radar and Lidar Evaluation of Model Cloud Fraction and Cloud Occurrence 33

2.5.4 Radar and Lidar Simulation . . . 37

2.5.5 Overlap Evaluation . . . 38

2.5.6 Skill Scores . . . 39

2.6 Future Remote Sensing of Clouds and Model Comparisons 42

3 Doppler Radar Evaluation of Evaporating Ice in Operational Models 44

3.1 Introduction 44

3.1.1 Structure of a Warm Front 47

3.2 Model Parameterization Scheme 49

3.3 Description of the Radar and Model Data 54

3.3.1 94-GHz Radar Data 54

3.3.2 Met Office Model Data 57

3.3.3 Selection of Data 57

3.3.4 Definition of an Evaporation Zone 58

3.4 Methodology 58

3.5 Profiles of Radar Reflectivity and Fall Velocity 59

3.5.1 Preferential Sampling of Updraughts and Downdraughts within the Radar Data 60

3.5.2 Using Velocity Measurements in the Middle of the Cloud to Test the Accuracy of the Model Parameterization 62

3.6 Examining the Effects of Turbulence 65

3.7 The Effect of Ice Particle Density 66

3.7.1 The Effects of Changing the Density Relationship 67

3.8 Humidity and Evaporation Rate Studies 68

3.8.1 Model Representation of Sonde Humidity Profiles 69

3.8.2 Comparison Between Radar and Model Evaporation Rates 74

3.8.3 Summary of Humidity and Evaporation Rate Studies 77

3.9 Other Operational Models 77

3.9.1 Comparison with the ECMWF Model 78

3.9.2 Comparison with the Météo-France Model 79

3.9.3 Comparison with the RACMO Model 80

3.9.4 Summary of Results from the Other Models 82

3.10 Conclusions and Summary 82

4 A 1D Explicit Microphysics Model of Ice Evaporation 85

4.1 Introduction 85

4.2 Description of the Model 86

4.2.1 Model Constraints and Simplifications 89

4.3 Evaporation Depth Sensitivity to Temperature, Pressure, Humidity and Initial Ice Water Content . . . 90
4.4 Evaporation Depth Experiments Using Radiosonde Data . . . 93
4.5 Issues with Modelled Capacitance . . . 96
4.6 Conclusions and Summary . . . 98
4.7 Future Work . . . 99

5 A Lidar Forward Model for Comparisons Between ICESat and the ECMWF Model 100
5.1 Introduction . . . 100
5.2 Processing of Model Data . . . 103
5.2.1 Converting Model Variables to Extinction Coefficient . . . 103
5.2.2 Calculation of the Multiple-Scattering Factor . . . 104
5.2.3 Lidar Ratio . . . 105
5.2.4 Interpolation of model data on to an ICESat height grid . . . 105
5.2.5 Selecting Model Grid Points . . . 108
5.2.6 Cloud Overlap . . . 108
5.2.7 Cloud Fraction Resampling . . . 110
5.3 Processing of Lidar Data . . . 110
5.3.1 Rejection of Unwanted (Non-Cloud) Signal . . . 111
5.3.2 Averaging of ICESat Backscatter Data . . . 113
5.4 Results . . . 113
5.4.1 The Effect of the Lidar Forward Model . . . 114
5.4.2 Location of Cloud with Latitude . . . 115
5.4.3 Land and Sea Comparisons . . . 119
5.4.4 Backscatter Comparison . . . 121
5.4.5 Skill Scores . . . 123
5.4.6 Sensitivity to Effective Radius . . . 126
5.5 Conclusions . . . 129
5.6 Future Work . . . 131

6 Summary, Conclusions and Future Work 133
6.1 Summary of Findings and Conclusions . . . 133
6.1.1 Evaporating Ice within Operational Models . . . 134
6.1.2 Assessment of the Performance of the ECMWF model using ICESat . . . 136
6.1.3 Spacebourne Radar and Lidar Cloud Climatology . . . 138
6.2 Future Work . . . 139
6.2.1 Ice Evaporation . . . 140

6.2.2 ICESat and the ECMWF model 140
6.2.3 Simulation 141

Glossary **143**

Symbols **152**

References **158**

CHAPTER ONE

Introduction and Motivation

1.1 The Importance of Clouds within Climate and Weather Forecasting Models

Clouds are important within the climate system as they interact with both solar (short wave) and terrestrial (long wave) radiation. With recent estimates of the future increase in carbon dioxide, climate models have predicted a rise of global mean temperature from 2 to 5 K, over the next 100 years (IPCC, 2007). The difference between a 2 K rise and a 5 K rise may result in dramatic differences in the frequency of severe weather events, the likelihood of a thermohaline shutdown (e.g. Manabe and Stouffer, 1999), sea level rise (e.g. Bengtsson *et al.*, 2005) and the action required by policymakers and politicians to tackle climate change (IPCC, 2007). It is well known that much of the uncertainty in the global mean temperature rise is due to the frequency and behaviour of clouds in a future climate (Arking, 1991; IPCC, 2007; Quante, 2004).

In order to understand how clouds are likely to behave in a future climate, we must first understand how they behave in the present climate. As the microphysical processes that form, evolve and dissipate clouds occur on scales much smaller than the size of a model grid box, parameterization is needed for models to represent clouds. An accurate knowledge of the processes that form, dissipate and modify cloud are necessary to develop accurate cloud parameterization schemes for general circulation models (GCMs).

In addition to their importance in the climate system, clouds are also important in short-term forecasts produced by numerical weather prediction (NWP) models, for a number of reasons. The first is that they produce precipitation, and good forecasts of cloud position and nature are the first step in good forecasts of precipitation location and intensity. Another reason is that low-lying cloud tends to reduce visibility of mountains, taller buildings and trees, which can affect the flight patterns of civilian and military aircraft, as well as military operations.

Also, clouds affect the radiation budget and hence correct representation of clouds is important to ensure accurate surface temperature forecasts; in warm conditions this will affect the

evaporation rate and soil moisture content, while in cold conditions the amount of cloud is important for forecasting of frosts. Finally, the amount of aircraft wing icing is dependent on the water contents, cloud phase and temperatures of clouds the aircraft fly through, so correct representation of clouds is important in this case to ensure flight conditions for aircraft are not dangerous.

The complexity of cloud parameterizations is always increasing; however, this is no guarantee of improved accuracy. When a new cloud parameterization scheme is in place, it is important to evaluate the scheme's performance by comparing properties of the modelled clouds to the same, or similar, observed properties. Evaluation of model parameterization schemes can lead to improvements in a model's parameterization of clouds. Within a GCM, this should lead to an increased confidence in the behaviour of clouds within a future climate, reducing some of the uncertainty in any future predictions of global climate. Better representation of clouds within NWP models has been the focus of recent research (e.g. Wilson and Ballard, 1999; Tompkins, 2002; Jakob, 2003; Illingworth *et al.*, 2007). Improvements within some NWP models due to change in cloud scheme have been noted. For example, Wilson and Ballard (1999) implemented changes in the Met Office cloud scheme and state that these changes result in drier boundary layers and better visibility estimates, better representation of deep precipitating systems and improved forecasts of freezing rain and drizzle, which led to more accurate forecasts of visibility, heavy rain events and freezing conditions that produce icy roads. In addition, Illingworth *et al.* (2007) showed that improvements in the Météo-France model led to better estimates of model Ice Water Content (IWC) which should improve the way the model represents radiative transfer as well as surface temperature forecasts.

1.2 Two Methods of Evaluating Models

As clouds can exist as high as 20 km in places, in-situ measurements from aircraft are sparse in nature, often quite expensive and hence do not lend themselves easily to making long-term observations of clouds that are useful for model evaluation, but are more suited to making microphysical measurements that can evaluate parameterization schemes. Remote sensing methods, either from ground-based stations beneath the cloud or satellites above the cloud, tend to be used for evaluation of model cloud climatology.

Cloud parameterization schemes in NWP models and GCMs are formulated in terms of prop-

erties, such as the cloud water content within a model grid box and the fraction of cloud filling a grid box. However, radar[1] and lidar[2] instruments do not directly measure water contents. Instead they measure the backscattered intensity of the electromagnetic radiation returned from the cloud. Due to the narrow beamwidth of the instrument when compared to the size of the model grid box, a vertically pointing radar or lidar is not capable of obtaining the instantaneous cloud fraction of the entire grid box, just an echo showing the location of cloud in the atmosphere above the instrument. Hence the variables measured by radar and lidar are distinctly different to those used within the model cloud scheme. This presents a challenge when one wishes to evaluate a model cloud parameterization scheme. By contrast, to compare radiosonde measurements of temperature, humidity and pressure with model profiles is relatively straightforward; all three variables exist as prognostic variables within the model and, providing the radiosonde has correct calibration, data assimilation methods can be used to equate the model temperature profiles to those obtained from sondes. However, as radar and lidar measurements are different from model prognostic variables, one quantity must be converted to the other before any evaluation of the performance of the model cloud parameterization scheme can take place. There are two methods of doing this, shown in figure 1.1. The first is to convert the radar or lidar observations into model variables, or alternatively, the model variables can be used to simulate the observations.

An example of converting observed quantities to model variables is the conversion of radar reflectivity to an ice water content that can be compared with the model. This has been attempted using radar measurements with theoretical particle size distributions (Sassen, 1987; Sassen and Liao, 1996) to derive the ice water content. Alternatively, radar measurements can be combined with aircraft-measured particle size distributions and model temperature (Liu and Illingworth, 2000; Hogan *et al.*, 2006) to obtain estimates of ice water content.

The second method is to use the model variables to predict or simulate the signal that would be observed by the radar or lidar. Although there have been some cloud-resolving and single-column model simulations of radar and lidar data, (Luo *et al.*, 2003, 2005), these have not specifically been intended to evaluate the performance of an operational model; hence the simulation of radar and lidar signals of cloud using model variables for model evaluation purposes is a fairly novel idea. There are only two known previous examples of simulation of radar and lidar data:

[1] Radar is an acronym for RAdio Detection And Ranging.

[2] Similarly, lidar, (after Middleton and Spilhaus, 1953) stands for LIght Detection And Ranging.

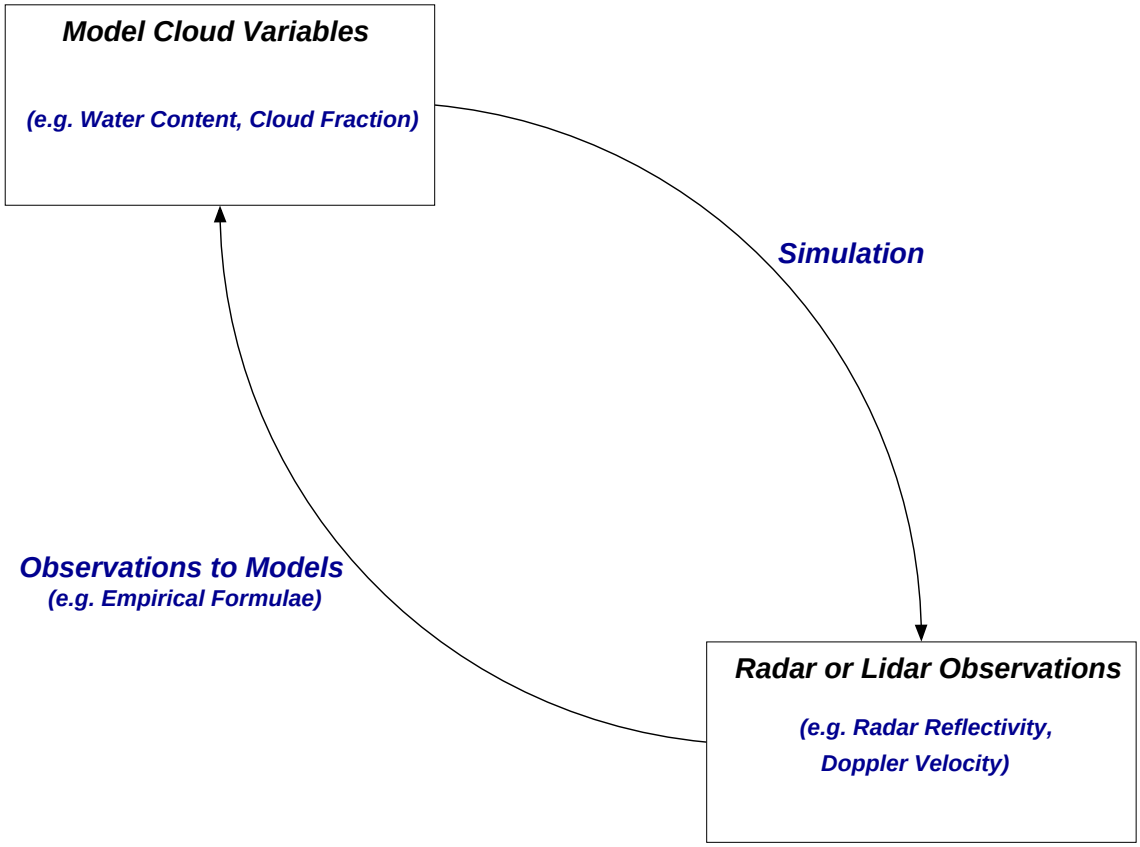

Figure 1.1: *Schematic diagram showing the two different methods that evaluate model cloud parameterizations using radar and lidar.*

Yeh *et al.* (1995), who used a cloud resolving model in order to predict the observations of the Tropical Rainfall Measuring Mission (TRMM) radar, in particular to note the attenuation of the radar signal; and Chiriaco *et al.* (2006), who examined the ability of the joint Pennsylvania State University and National Centre for Atmospheric Research Mesoscale Model (MM5) to simulate radar and lidar cloud profiles, which were compared with measurements in France.

The simulation technique is useful to allow data assimilation to take place. Once the radar or lidar measurements are simulated by the model, differences between the measured and simulated data can be examined. This is the first step in data assimilation. Simulated data from model analysis of the atmosphere can then be compared to radar or lidar data and the model adjusted so that the model simulations agree with the observations.

With the launch of the CloudSat and CALIPSO (Cloud-Aerosol Lidar and Infrared Pathfinder Satellite Observation) satellites, which use a spaceborne radar and lidar to measure clouds, there

has been an interest in the use of radar and lidar simulation, because of the possibility of signal attenuation. By using the simulation method, the signal attenuation can be predicted by the model water contents. However, it is tricky to predict model ice or liquid water contents given a signal that has been attenuated and hence a fairer comparison between model and radar or lidar can result from use of a simulation method.

Examples of CloudSat simulators are currently being developed at the Met Office (Bony-Lena, 2006) and elsewhere (Stephens, 2006; Haynes and Stephens, 2006, document in preparation), while examples of CALIPSO simulators are being trialled in France (Bony-Lena, 2006). In addition, they can also be used to test new model parameterization schemes and it is already planned to assimilate CloudSat data into models using the simulation (or as it is also known, forward modelling) technique (Stephens, 2006). In both cases, simulation techniques prove useful and hence development of the methodology, including this thesis, is important.

1.3 This Thesis

The purpose of this thesis is to evaluate a number of aspects of model cloud parameterization schemes using radar and lidar. This thesis will use two examples of the simulation method outlined above to convert model variables into observations measured by active remote sensors, using both ground-based radar and spaceborne lidar observations.

In chapter 2, we shall look at the origins of radar and lidar as a tool for cloud studies and the important principles of radar detection of cloud hydrometeors. Issues of sensitivity and radar wavelength to be used will be discussed, due to their importance in detection of cloud. The second half of the chapter will examine how models parameterize clouds and their microphysical processes. This is important in order to take the model variables, apply the simulation method to convert them into observed quantities. A number of previous evaluations of model cloud schemes using radar and lidar will be reviewed and there will be some examination into where model evaluation and development using radar and lidar may lead in the future.

Chapter 3 focuses on the problem of evaporating ice representation within the operational models. Previous studies (Forbes and Hogan, 2006) have identified that the evaporation of ice beneath warm fronts takes place in a shallow layer around 500 metres deep, whereas in the Met Office model this layer is represented as being 2–3 times the depth of radar observations. In this

chapter it is shown that the deep ice evaporation problem is not unique to the Met Office model; in fact a number of operational models from across Europe produce similarly deep evaporation depth scales when tested. Several hypotheses are suggested for the occurrence of this phenomena and tested accordingly using simulation techniques to predict radar reflectivity and Doppler velocity. Doppler parameters were not available for the work of Forbes and Hogan (2006). By comparing observed and simulated data, several of the hypotheses can be rejected and evidence is presented that the deep model evaporation is caused by incorrect humidity profiles within the Met Office model.

In order to completely test the hypotheses raised in chapter 3, a simple numerical model concerning the mechanics of ice evaporation is developed in chapter 4. This utilises the evaporation parameterizations from the Met Office model upon a high resolution (5m) grid. It is first used to test the sensitivity of the evaporation rate to fundamental atmospheric quantities of temperature, humidity and pressure, as well as cloud ice water content. Further experiments are carried out using radiosonde and radar data to simulate the evaporation beneath a number of ice cloud evaporation case studies using the model parameterization scheme. The model data available from these cases can also be used to simulate the model evaporation of ice. The validity of the Met Office model parameterization scheme can be tested and the cause of the Met Office model's deep evaporation layers will be identified.

Chapter 5 uses simulation techniques to make a fair comparison between the ICESat lidar and the ECMWF model. Due to the near-global coverage of the ICESat satellite, the performance of the ECMWF model can be assessed at locations where there are no ground-based radar or lidar instruments. A sample of 15 days of data, equivalent to a distance of 9 million kilometres on the Earth's surface is used to derive statistics of the performance of model cloudiness with latitude and height. Differences in model performance above land and sea surfaces can be obtained; previously model performance statistics over the sea have been difficult to obtain due to a lack of observations of cloud profiles in these regions. In addition, two skill scores are used to test the validity of model forecasts across the globe.

Concluding remarks to this thesis and the possibility of future work in developing simulation techniques for model validation and development are drawn in chapter 6.

CHAPTER TWO

Using Radar and Lidar for Model Evaluation

2.1 Introduction

In chapter 1, clouds were identified as one of the greatest sources of uncertainty in GCM predictions of future climate. Active remote sensing (and in particular, radar and lidar) has the ability to obtain profiles of cloud data in the direction of the beam emitted from the instrument, making it an ideal choice for evaluating model cloud parameterization schemes.

As NWP and GCM model performance is of interest to meteorologists, their evaluation has already been the subject of a number of studies. For cloud schemes it is difficult to make direct measurements of cloud properties on a global scale and on a frequent basis, so remote sensing is often used. This can be in the form of satellites measuring the outgoing long wave radiation from cloud top, radiometers on the surface measuring the downwelling radiation from clear sky and cloudy conditions, and a few radar and lidar stations making active remote sensing observations of the cloud. Although ground based radar and lidar stations are very useful to evaluate model performance at a single point, they tend to be located over the land and are limited to a few sites across the globe, most often in the Northern Hemisphere (examples include the ARM (Atmospheric Radiation Measurement) sites in America and the Cloudnet sites in Europe).

Passive instruments have been used for many years to monitor global cloud coverage from space in projects like ISCCP (Schiffer and Rossow, 1983). However, in the last decade or so, the use of active instruments in space has been discussed (e.g. Atlas *et al.*, 1995; Brown *et al.*, 1995; Hogan and Illingworth, 1999). At the time of writing, there have already been lidar studies from space using LITE and ICESat (McCormick *et al.*, 1993; Zwally *et al.*, 2002). An active radar has been used in space for the tropical rainfall measuring mission (TRMM, launched 27 November 1997, Simpson *et al.*, 1988). CloudSat, the first active radar from space directly intended for cloud observations (Stephens *et al.*, 2002) was launched on 28 April 2006 along with its sister

satellite CALIPSO (Cloud-Aerosol Lidar and Infrared Pathfinder Satellite Observation) and both instruments are making satisfactory measurements of clouds. These are part of the A-train of satellites (Stephens *et al.*, 2002; Vaughan *et al.*, 2004). Future space based cloud observations are planned for the future, such as EarthCARE (due for launch in 2012).

In this chapter, the principles behind radar and lidar remote sensing are examined with particular attention to their use in evaluating operational models. Previous studies in model performance are discussed. Section 2.2 concentrates on the principles behind operational radar, including the scattering by atmospheric particles, the sensitivity of wavelengths used and which wavelengths are suitable for studying clouds. The history of radar for meteorological purposes will be discussed briefly, with suitable equations given. Section 2.3 examines how lidar works, from the earliest studies, to some of the more recent works and the development of modern lidars for atmospheric measurements and how they can be used to detect cloud. Section 2.4 looks at how clouds are represented in numerical models, including the main variables of water contents and cloud fraction, including a discussion on whether they are better as prognostic or diagnostic variables. There will be a number of cases from existing models to explain the principles behind representing clouds in terms of these three variables. There will be an insight into the different cloud overlap schemes used in GCMs, providing supporting evidence for the validity of assumptions made in the cloud schemes. Section 2.5 reviews the previous work published using radar and lidar observations to evaluate the performance of weather and climate models. This includes a review of previous work in retrieving water contents, cloud fraction and overlap statistics from radar and lidar measurements. In addition, the evaluation of individual forecasts is examined using skill scores; this methodology will be explained and previous examples cited. Finally, section 2.6 provides an insight into how numerical models might develop in the future, with use of radar and model studies to improve model representation of clouds within the Earth's climate system.

2.2 Principles of Radar Remote Sensing

2.2.1 The Radar Equation

The radar principle involves transmitting a high powered pulse (P_T) towards a target and measuring a much smaller power (P_R) that is backscattered to the instrument. The meteorological form of the radar equation, neglecting attenuation due to atmospheric gases, is given as follows (after

Probert-Jones, 1962):

$$P_R(r) = C_{rad}\frac{P_T}{r^2}\sum_{\Delta V}(\sigma_i), \tag{2.1}$$

where C_{rad} is a constant that depends on the hardware of the radar equipment (such as antenna gain and dish size), r is the mean distance of the targets with backscatter cross section σ from the radar. The subscript i refers to an individual target within the unit volume ΔV.

The backscatter cross-section, σ, of a spherical particle (such a cloud droplet or small raindrop) can be expressed using the Rayleigh approximation as follows (Battan, 1973):

$$\sigma = \frac{\pi^5}{\lambda^4}|K|^2 D^6, \tag{2.2}$$

where λ is the wavelength of the electromagnetic radiation, D is the particle diameter and K is the dielectric factor, defined as

$$K = \frac{m^2 - 1}{m^2 + 1}, \tag{2.3}$$

where m is the complex refractive index of the scatterer and m^2 is the dielectric constant. Equation 2.2 can then be substituted into equation 2.1 to give the following form:

$$P_R = \frac{\hat{C}_{rad}|K|^2}{r^2}\sum_{\Delta V} D^6. \tag{2.4}$$

In determining equation 2.4 we have incorporated the constant C_{rad} and the other constants to form a new hardware constant $\hat{C}_{rad}$. It is also assumed that all particles within the radar beam have the same value of $|K|^2$. If this is not the case, the $|K|^2$ should lie within the summation. The values of $|K|^2$ change for water droplets as the radar wavelength decreases from centimetres to millimetres and are also a function of temperature. From equation 2.4 we can define the radar reflectivity, Z. In simple terms, this is a parameter of the cloud to which the radar is sensitive. We have incorporated the wavelength dependence in equation 2.2 into $\hat{C}_{rad}$ in equation 2.4. In defining radar reflectivity, we should like to remove this dependence on wavelength so that two radars with the same hardware but operating at different wavelengths will give the same value of reflectivity. Hence, radar reflectivity is determined as follows:

$$Z = \sum_i N_i D_i^6. \tag{2.5}$$

Here, D_i is the diameter of the particles per unit volume and N_i is the number of particles of size D_i per unit volume. Taking a distribution of liquid water drops in a cloud, equation 2.5 can be

expressed as

$$Z = \int_0^\infty N(D)D^6 dD, \tag{2.6}$$

with $N(D) \times dD$ being the number of particles with diameter from D to $D + dD$.

The Rayleigh approximation introduced in equation 2.2, is reliable for when the wavelength of the radiation is significantly larger than the diameter of the particle. As the ratio of wavelength to particle size decreases to the point where the particle size is of the same order of magnitude as the radar wavelength, Mie theory (as described in Carswell and Pal, 1980; Born and Wolf, 1999) should be used. This can be done quite simply by adding the Mie-to-Rayleigh ratio (γ) into equation 2.6:

$$Z = \int_0^\infty \gamma(D)N(D)D^6 dD. \tag{2.7}$$

The consequences of adding the Mie-to-Rayleigh ratio into our calculations are to allow Rayleigh scattering for the smallest particles, but for the backscattered power to significantly reduce as the particles get larger and enter the Mie size region, hence the magnitude of the reflectivity decreases compared to if the scattering was entirely within the Rayleigh regime.

Figure 2.1 shows the electrical size of a spherical particle (defined as $\pi D/\lambda$) versus the normalised backscatter cross section ($\sigma/(\pi(D/2)^2)$). The lines for the Rayleigh regime are superimposed and it can be seen that as the normalised backscatter cross section approaches unity (wavelength of the radiation is roughly the same size as the particle diameter), then the particle curves diverge from the Rayleigh regime into the Mie regime. For larger particles, the size of the oscillations in the curve gradually gets smaller, until the principles of geometric optics can be applied.

From figure 2.1, it can be seen that curves behave differently for ice and liquid water particles. In fact, the reflectivity values for liquid and ice need to be treated separately. For ice this can be done by modifying equation 2.7 as follows:

$$Z = \int_0^\infty \frac{|K_{ice}|^2}{|K_{water}|^2} \gamma(D)N(D)D^6 dD, \tag{2.8}$$

where $|K_{ice}|$ is the dielectric factor for ice and $|K_{water}|$ is the dielectric factor for liquid water. The value of $|K_{ice}|^2$ is 0.197 for solid ice, but lower as the density decreases, with the ratio of $|K_{ice}|$ to ice density constant. Ice density reduces with increasing particle diameter (e.g. Brown and Francis (1995) give ice density to be $0.07D^{-1.1}$, where ice density is in g cm^{-3} and D is in

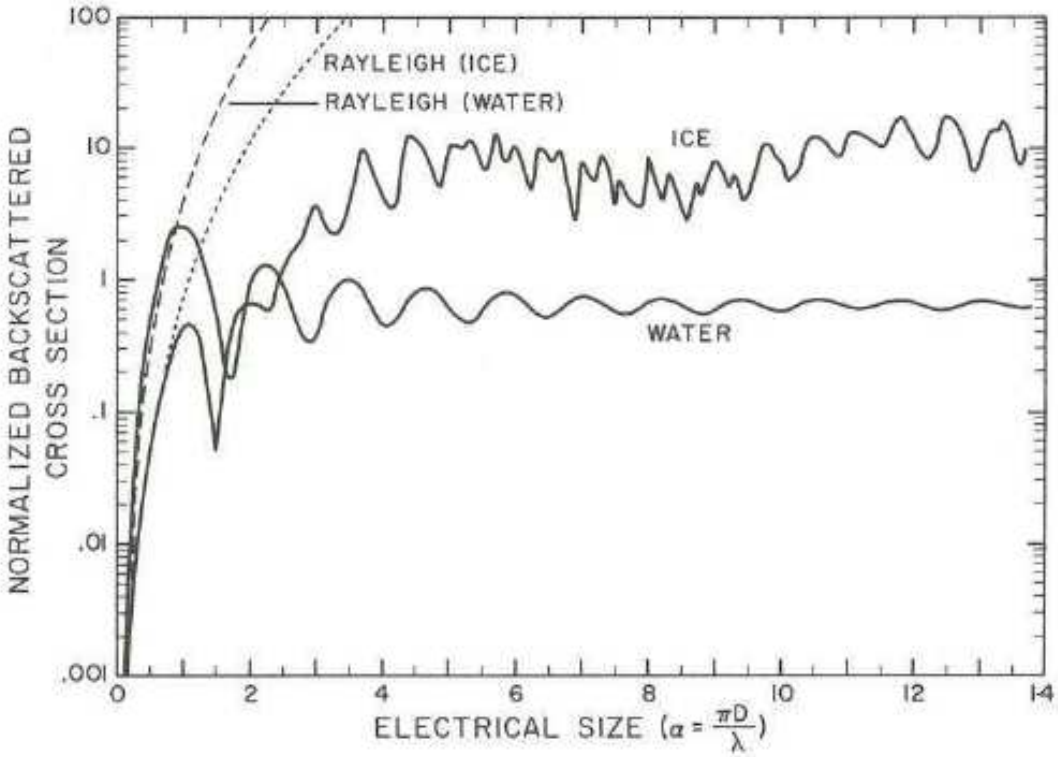

Figure 2.1: *Backscatter cross sections for ice and water at 0 °C, with the Rayleigh approximation lines superimposed. The normalised backscatter cross section is defined as the backscatter cross section, σ, divided by the cross sectional area of the particle. From Burgess and Ray (1986).*

mm) and hence the dielectric factor decreases for larger particle sizes. The result is that values of $|K_{ice}|^2$ are much lower than for water and hence the values of Z are lower in ice clouds than in water clouds.

2.2.2 Using Radar to Study Clouds

The choice of radar wavelength for cloud studies has implications on the amount of cloud detected. From equation 2.2, we can see that the backscatter cross section, (and hence the returned power in equation 2.1) is inversely proportional to the fourth power of the radar wavelength. Hence the shorter the wavelength, the greater the sensitivity of the radar, all else being equal. A radar with greater sensitivity will be able to detect smaller particles, especially those which exist in the thinnest ice clouds. However, the shorter the radar wavelength, the more likely the radar is to be affected by attenuation as it passes through clouds, as we shall see shortly.

Although radar in meteorology is traditionally thought of as a means for detecting precipitation, studies of clouds using radar have been carried out for the past 50 years. Early studies were limited by radar technology to use centimetre wavelengths (and hence low frequency) measurements of clouds (e.g. Marshall, 1953; Wexler, 1955; Wexler and Atlas, 1959).

It is well established that higher frequency radars are limited by atmospheric absorption to just a few spectral windows. This can be shown using a millimetre-wave propagation model (e.g. Liebe, 1985). The spectral windows result in frequencies for vertical operation of cloud radar at roughly 35 GHz, 94 GHz, 140 GHz and 220 GHz. Following advances in radar technology, millimetre wavelength radars were in operation by the 1980s: Hobbs *et al.* (1985) verified the use of 35-GHz radar (8.6 mm wavelength) for cloud experiments and the first 94-GHz (3.2 mm wavelength) radar intended for cloud studies was constructed by Lhermitte (1987).

Despite the sensitivity improvements that occur as a result of a shorter wavelength, there are also attenuation problems. Table 2.1 shows the one-way attenuation of the electromagnetic waves produced by radars at various frequencies and through various mediums encountered in the atmosphere, over a range of atmospheric temperatures. As the wavelength of the radar decreases, the attenuation also increases through each medium. Although attenuation by atmospheric gases (mostly due to oxygen and water vapour) is relatively small at low temperatures for 35-GHz, at high temperatures and frequencies, the attenuation is significantly higher and should be corrected for. The attenuation due to liquid water (γ_w) is largest for the highest frequencies. For 35-GHz and 94-GHz, attenuation is larger for the lower temperatures. The results of ice attenuation from table 2.1 show that in general, ice attenuation can be neglected for Rayleigh scattering.

Figure 2.2 shows the attenuation coefficients due to rain rate, assuming a temperature of 20°C. It can be seen that for a rain rate of 1 mm hr^{-1}, the attenuation coefficient of a 94-GHz would be of the order of 1 dB km^{-1}. For 35-GHz, this value would be closer to 0.2 dB km^{-1}. This relationship between rainfall rate and attenuation coefficient is roughly linear for all frequencies. Attenuation by rain is significant for 35-GHz and 94-GHz radar data, but there is an additional attenuation due to rain on the radome of the radar. Using a 94-GHz radar, Hogan *et al.* (2003a) reported a difference of 9 dB between measurements where the radar was vertically pointing and exposed to the rain and where the radar was sheltered at an angle of 45°C in rain. They blame the difference in measurements entirely on wet radomes. Given the attenuation from figure 2.2 and the results of Hogan *et al.* (2003a), it is unwise to use data from millimetre wavelength radars for

	$\gamma_{g(\text{saturated})}$ dB km^{-1} Hogan (1998)		γ_w (dB km^{-1})/(g m^{-3}) Meneghini and Kozu (1990)			γ_i $\times 10^{-4}$(dB km^{-1})/(g m^{-3}) Meneghini and Kozu (1990)		
	35-GHz	94-GHz	35-GHz	94-GHz	140-GHz	35-GHz	94-GHz	140-GHz
$-20°$C	0.0541	0.1128	1.77	5.41	6.60	0.28	0.37	0.42
$-10°$C	0.0620	0.1785	1.36	5.15	6.82	0.38	0.49	0.54
0°C	0.0843	0.3230	1.05	4.82	7.06	1.40	1.80	2.10
10°C	0.1355	0.6358	0.82	4.37	7.12			
20°C	0.2455	1.3101	0.64	3.85	6.91			
30°C	0.4773	2.7544	0.52	3.32	6.45			

Table 2.1: *One-way attenuation of radar signals for atmospheric gases (γ_g), liquid water cloud (γ_w) and ice water cloud (γ_i). Pressure is assumed to be constant at 1013 mb and Rayleigh scattering is assumed.*

cloud studies during rain events.

There have been further experiments on higher frequency radar observations. In a trial for a highly sensitive radar with small vertical resolution, Mead *et al.* (1989) used a 215 GHz (1.4 mm wavelength) radar for remote sensing of cloud and fog. However, at these high frequencies, Mead *et al.* (1989) noted that the results depended highly on the amount of water vapour in the atmosphere. In addition, from table 2.1 we see that attenuation increases as frequency increases. Although detection of stratocumulus and fog was still possible with the Mead *et al.* (1989) study, the radar beam would rapidly extinguish in thicker liquid water clouds and reflectivity values will be variable dependent on the humidity between the radar and any clouds being sensed. However, the high sensitivity and small beamwidth could, in theory allow good measurements of thinner ice clouds with smaller particles if the radar was mounted on an aircraft or a satellite. However, since the frequency is above 100-GHz, there could be some attenuation problems in thick ice cloud (Brussaard and Watson, 1995).

Throughout the last twenty years, there have been many studies suggesting the possibility of spaceborne radar (Lhermitte, 1989; Atlas *et al.*, 1995; Brown *et al.*, 1995). As radars from space encounter the higher and cooler ice clouds before they reach the liquid water cloud, they are less liable to attenuation and thus shorter wavelength radar systems can be used (Hogan and Illingworth, 1999). However, radar measurements from space have to be mounted on satellites in low

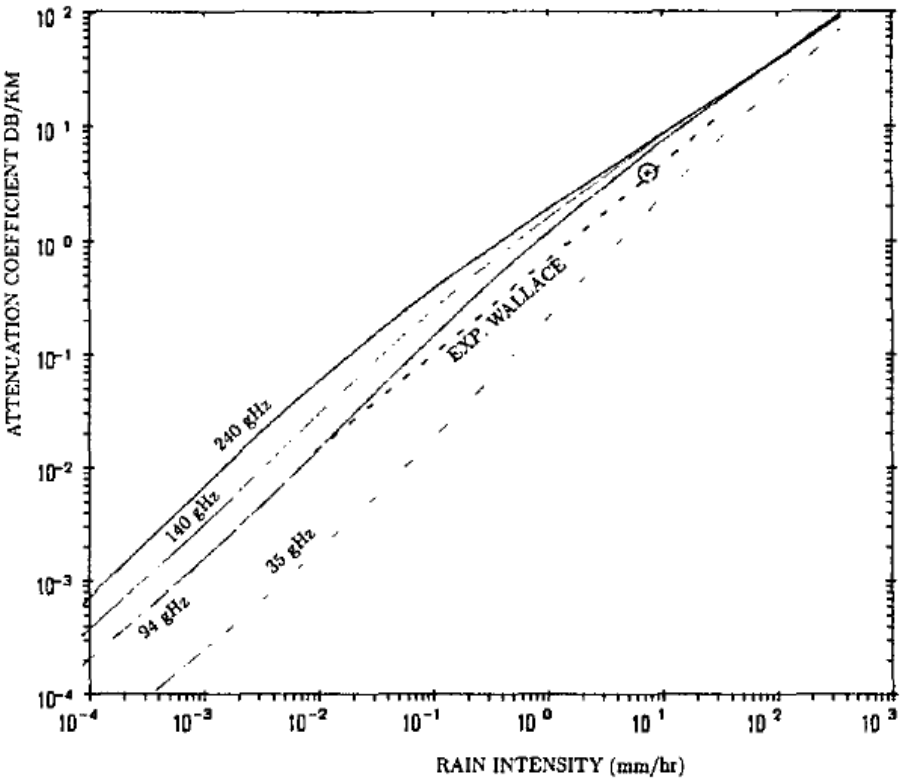

Figure 2.2: *Attenuation coefficient at various radar frequencies with rain rate and at a temperature of 20° C from the results of Lhermitte (1990). The dashed line marked "EXP. WALLACE" denotes an experiment by Wallace (1988) for 94-GHz and the circled cross shows one 94-GHz measurement by Lhermitte (1990).*

earth orbits at altitudes of less than 1000 km. Higher orbits would lead to larger pulse volumes, lower sensitivity and hence a radar on a geostationary satellite would give little information on the clouds below. As the radars are in low Earth orbits, they travel around the globe, profiling snapshots of clouds rather than making climatological profiles in one place.

To summarise, in planning a new ground-based radar system for the long-term monitoring of clouds would depend on the number of radars to be used and the location of the study. For a single wavelength study, a 35-GHz or 94-GHz radar would be the most useful as they have high sensitivity and would be able to detect the maximum amount of cloud. However, the results when precipitation takes place would have to be looked at with great care and in most cases, discarded from the study. If the radar was to be located in an area of the tropics where frequent heavy rain occurs, a lower frequency radar would probably be more suitable, but this would limit the detection of thinner ice clouds. In these locations, a 35-GHz radar would be preferable as it has less attenuation to liquid, gas and will Rayleigh scatter more particles than a 94-GHz radar. A

94-GHz radar will have greater attenuation and will be able to detect more of the small non-cloud signals such as birds and insects. In addition, in the tropics, the water content of clouds can be higher and hence attenuation due to liquid water could be greater for a 94-GHz radar.

For spaceborne radar studies, the situation is different. The first consideration is the physical size of the dish; trying to launch a satellite with a radar dish larger than 2 m diameter is difficult. Attenuation of the higher radar frequencies takes place in rain, liquid cloud and water vapour, so from space the radar will be able to penetrate a significant depth of atmosphere. Considering these factors together, a wavelength of at least 94-GHz should be chosen for its physical dish size and greater sensitivity. Meneghini and Kozu (1990) noted that for a 94-GHz radar the attenna diameter is 1.8 m, as opposed to 5 m for 35-GHz and 10 m for 15-GHz. The pulse power will be lower for 94-GHz radar and at 300 km from the radar, the footprint would be 500 m for the 35 and 94-GHz radars and 600 m for the 15-GHz radar. Hence, the 94-GHz radar is more suitable for spacebourne use. However, as the radar receiver has a wider field-of-view from space, multiple scattering will take place, which may be a problem at 94-GHz (Battaglia *et al.*, 2007).

2.3 Principles of Lidar Remote Sensing

Lidar works on the same principles as radar, but instead of using radiation at microwave wavelengths, it uses laser radiation and operates at ultraviolet to infrared wavelengths. The basic principle is the same as for radar, with a transmitter emitting pulsed power towards a target, which is sent back to the instrument's receiver. However, due to the much shorter wavelength used, lidar observations of cloud particles tend to use Mie and geometric optics approximations rather than Mie and Rayleigh scattering approximations used by millimetre cloud radars.

As reported in Weitkamp (2005), the origins of lidar were from attempts to measure air density profiles using telescopes and searchlight beams (Hulbert, 1937; Johnson *et al.*, 1939), but rapid development of the instrument followed the invention of the laser in the 1960s (Maiman, 1960; McClung and Hellwarth, 1962). Since then, there has often been close collaboration between laser and lidar, with development linked to technological innovation (Weitkamp, 2005).

2.3.1 The Lidar Equation

As lidar tends to work on similar principles to radar, it is possible to derive the lidar equation based on similar work for the radar equation, shown in equation 2.1, taking account of the extinction of the signal due to particles in the atmosphere.

The lidar equation in its most common form and in the single-scattering limit is as follows Weitkamp (2005):

$$P_R(r,\lambda) = P_T \frac{C_{lid}}{r^2} \beta(r,\lambda) \exp\left[-2\int_0^{r'} \alpha(r',\lambda) dr'\right], \tag{2.9}$$

where P_R is the small amount of power backscattered to the instrument from the targets, P_T is the transmitted power, r is the range of the targets and λ is the lidar wavelength. The hardware of the lidar is represented by the constant C_{lid}. The term within the exponential is the transmission term, which relates to the extinction of the lidar signal as it passes through a medium (such as cloud), with a depth r' and extinction coefficient α. The term β is the backscatter coefficient of the particles interacting with the radiation. Following the same way that radar reflectivity can be defined from backscattered power, the lidar attenuated backscatter β' can be defined, with units of sr^{-1} m^{-1}. It can be seen that this is different to radar reflectivity (Z), with different units. It is perfectly valid to express radar reflectivity as a backscatter, but by tradition, radar scientists have used reflectivity as most targets are in the Rayleigh regime and the value of reflectivity is independent of wavelength for Rayleigh scatterers. Dividing σ in equation 2.2 by unit volume does not give attenuation in the same way attenuated backscatter does. Lidar works mostly in the geometric optics region and historically worked independently of radar and defined backscatter as a wavelength-dependent quantity with little reference to radar science.

In addition, with many particles, we often wish to consider multiple scattering and can do so by including the multiple-scattering factor, η (after Platt, 1973), within the exponent. Although multiple scattering can be calculated numerically (Kattawar and Plass, 1971; Eloranta, 1998), it can potentially be very computationally expensive and hence the approximation of Platt (1973) is more frequently used. Values of η vary from 0.5 in the wide telescope receiver field-of-view limit to 1. With a value of 0.5, the maximum amount of multiple scattering is assumed to take place, meaning that all the scattered photons remain within the field of view of the lidar receiver. With an η value of 1, the photons entering the receiver have only been scattered once. Accounting for

multiple scattering, equation 2.9 can be written in terms of β' as

$$\beta'(r,\lambda) = \beta(r,\lambda)\exp\left[-2\eta\int_0^{r'}\alpha(r',\lambda)dr'\right]. \tag{2.10}$$

In addition to the approximation of the multiple-scattering factor, we can define the extinction-to-backscatter ratio (sometimes called the lidar ratio) as $s = \alpha/\beta$ and express equation 2.10 in terms of α:

$$\beta'(r,\lambda) = \frac{\alpha(r,\lambda)}{s}\exp\left[-2\eta\int_0^{r'}\alpha(r',\lambda)dr'\right]. \tag{2.11}$$

From this expression, it can be seen that large value of the extinction coefficient results in a large signal returned to the telescope receiver, but also an attenuation of the signal as it passes through the medium, and a reduced sensitivity to detecting the medium further down the beam.

For most wavelengths, scattering depends on the ratio of the wavelength of the lidar radiation to the size of the particles. The values of α and β in equation 2.11 depend on the wavelength of the laser light. Weitkamp (2005) give the extinction coefficient, α as a function of range (r) and wavelength (λ) as follows:

$$\alpha(r,\lambda) = \sum_j N_j(r)\sigma_{j,ext}(\lambda), \tag{2.12}$$

where N_j are the number of particles of extinction cross section $\sigma_{j,ext}$ per unit volume.

2.3.2 Using Lidar to Study Clouds

For cloud detection, the most common lidar type used is elastic-backscatter lidar. Where the particle radius is much smaller than the lidar wavelength (such as for lidar scattering of the smallest aerosol particles or molecular gases), Rayleigh scattering occurs and the sensitivity to extinction and scattering is inversely proportional to the fourth power of the wavelength. However, for most of the larger particles found in clouds, there is little wavelength dependence on backscatter as the scattering is in the geometric optics region (where the wavelength of the lidar is much smaller than the particle diameter), although the refractive index may be wavelength dependent.

However, in equation 2.11, the value of the lidar ratio, s is variable and depends on the medium the lidar signal is passing through. For liquid water, values of s vary with drop size and wavelength. There is also a dependence on the dielectric constant, but this changes very little with the temperature within liquid water clouds and as cloud droplets are spherical, s can be assumed to vary with drop size and wavelength alone, as in O'Connor *et al.* (2005).

Using a variety of droplet size distributions, Pinnick *et al.* (1983) find s for liquid water between 14.2 and 19.9 sr, dependent on wavelength. However, a later study by O'Connor *et al.* (2005) using a gamma shaped drop distribution found that s is almost constant between drop sizes of 10 and 50 μm, despite changing the shape of the gamma distribution. O'Connor *et al.* (2004) calculate s for a 905 nm lidar and liquid water drops to be 18.8 ± 0.8 sr. They also note that this result varies little for shorter wavelengths of 532 nm, where s is 18.6 ± 1 sr and 355 nm, where s is 18.9 ± 0.4 sr. For ice, the value of s is highly variable, as changes in temperature may result in changes in ice particle habits and sometimes aggregates can form. At any given temperature, there may be a range of ice particle habits that occur.

Hence, Platt *et al.* (1987) gave s to be approximately 50 sr in tropical cirrus clouds between -40 and -80 °C, and proposed a link between the lidar ratio and temperature. In later studies, data from the Atmospheric Radiation Measurement (ARM) Pilot Radiation Observation Experiment (PROBE) were used (Platt *et al.*, 1998), with results showing s ranging from 28.6 to 44.9 sr, with higher values of s at colder temperatures. Data from the Lidar In-Space Technology Experiment (LITE) were used (Platt *et al.*, 1999) to provide similar calculations of s, which ranged between 12 and 21 sr dependent on temperature. Although these values may seem much smaller than those used for the PROBE experiment, it should be noted that LITE has a much larger receiver field-of-view and thus a smaller value of the multiple scattering factor.

Once this multiple scattering factor variation is taken into account, it is sometimes found (Platt *et al.*, 1999) that the values of s are of similar sizes. Chen *et al.* (2002) examined s values in ice clouds at different heights and temperatures and found that s varies from 20.4 sr at 15–16 km altitudes (-70 to -75 °C) to 36.7 sr at 12–13 km (-48 to -58 °C), with an average lidar ratio of 29$\pm$12 sr.

Although the variability of s can sometimes be explained by different instruments having different fields of view and different values of the multiple scattering factor, η, a more likely explanation is due to the temperature dependence of s. Whereas individual cloud droplets are roughly spherical and thus can be shown to have the same lidar ratio over a large range of sizes, this is not true for ice. Ice crystals can have a variety of habits (plates, dendrites, columns and so forth) and can experience aggregation. Hence the optical properties of ice can differ very rapidly within the cloud and producing very different lidar ratios. The temperature dependence we see in the studies of Platt *et al.* (1998, 1999) and Chen *et al.* (2002) are likely to be due to different lidar

ratios for the predominant crystal habit at these different temperatures.

The choice of wavelength used by lidar depends also on the laser and its properties (Weitkamp, 2005). Early studies (Maiman, 1960; McClung and Hellwarth, 1962) used ruby lidars (694nm). More recently, Neodymium gases combined with yttrium aluminium garnet crystalline lattices (Nd:YAG) has been one type of lidars manufactured for modern studies (Weitkamp, 2005), with a wavelength of 1064 nm (near infra-red). Using nonlinear crystals, this frequency can be doubled to 532nm and tripled to 355nm, which are more sensitive to the smaller particles and can detect molecular backscatter. Reduction of molecular backscatter can then be used for detecting optical depth through a medium. Using other gases, lidars can be developed to work at almost any wavelength from 250 nm to 11μm.

2.4 Model Representation of Clouds

Representation of cloud within general circulation models (GCMs) and in climate models has always been important for radiative transfer calculations and surface temperature calculations. In operational models, clouds are also important for visibility, aircraft icing and forecasting of precipitation, to name but a few reasons. In this section, current methods of parameterizing cloud will be examined.

Although early GCMs were developed within the 1950s and 1960s (Randall, 2000), at this stage clouds were not specifically represented in weather forecast models. In some studies, climatological zonal values were used, which tended to ignore longitude and time variations of the cloud amounts (e.g. Manabe *et al.*, 1965; Smagorinsky *et al.*, 1965; Holloway and Manabe, 1971). During the 1970s the need for more physically based cloud schemes was recognised. By the mid 1970s the National Center for Atmospheric Research (NCAR), in the USA had a scheme where the cloud amount at each grid box was diagnosed empirically from relative humidity (Washington, 1974). Although these schemes remained within models for some years (e.g. Slingo, 1980, 1987), since the 1990s most models have a prognostic cloud water content (sometimes separated into different phases of liquid, ice and mixed phase). In addition, some parameterizations treat cloud fraction as a prognostic variable. This section examines cloud schemes for liquid water content (section 2.4.1), ice water content (section 2.4.2) and cloud fraction (section 2.4.3). Also of importance to radiation calculations is the amount of cloud the radiation passes through. How-

ever, the only information carried within the model is the value of cloud fraction. If a vertical column of model grid boxes is not completely clear and not completely cloudy, some assumptions must be made as to how different layers of cloud are overlapped within the model. This is discussed in section 2.4.4.

2.4.1 Liquid Water Content

The first step in developing a prognostic cloud scheme involves deriving an equation for the rate of change of liquid cloud water mixing ratio (q_l). The simplest schemes make no distinction between liquid water mixing ratio and cloud ice mixing ratio (q_i) at this stage, so that q_l actually incorporates both phases. The rate of change of q_l depends on various source and sink terms as follows (following, Smith, 1990):

$$\frac{dq_l}{dt} = \left(\frac{dq_l}{dt}\right)_{ADV} + \left(\frac{dq_l}{dt}\right)_{DIFF} + \left(\frac{dq_l}{dt}\right)_{TM} + \left(\frac{dq_l}{dt}\right)_{ST} + \left(\frac{dq_l}{dt}\right)_{P} + \left(\frac{dq_l}{dt}\right)_{CV}. \quad (2.13)$$

In equation 2.13, the subscripts of each term are as follows: ADV refers to advection; $DIFF$ refers to horizontal diffusion; TM refers to vertical turbulent mixing from the boundary layer; ST refers to stratiform cloud formation (due to condensation) or dissipation (due to evaporation); P refers to the loss by formation of precipitation and CV refers to the source of cloud water by detrainment from cumulus convection. The advection term will be positive if there is a net flow of cloud into the grid box from neighbouring cloudy grid boxes. The diffusion term will act to move cloud water from where there is a large amount to where there is little. This can either be positive or negative, depending on whether the grid box has more or less cloud water than its neighbours. The turbulent mixing term can either mix in dry air into the clouds from a less humid boundary layer, or in the case of a warm front, where the cloud base gradually descends with time, moist air can be mixed in from a humid boundary layer. The stratiform cloud term can have either sign, depending on whether the air is rising, cooling and condensing, or whether it is sinking and the cloud is evaporating. The precipitation term is always negative; cloud water is never gained by rain production. The detrainment from cumulus convection is always positive; there is never a sink of cloud water by this process.

The principle of having a cloud water content represented by a prognostic variable was first developed by Sundqvist (1978), who used only the terms for advection, diffusion, stratiform cloud formation/dissipation and precipitation formation. The basis for the cloud schemes used for the

last 15 years in the Met Office unified model is Smith (1990), which uses equation 2.13, ignoring only the convection term, as in his model version, the convection scheme was not coupled to the cloud water content scheme. The Smith (1990) scheme carried a single water content, making the distinction of liquid or ice phase only for the precipitation and not for cloud, which was assumed to have just one water content. The distinction of precipitation phase was based on a linear function of temperature as shown in equation 2.14, with α_{CP} being the fraction of the total water content of the grid box which is liquid. The variables T_{ice} and T_0 are the temperatures at which all the precipitation is assumed to be solid and all liquid, respectfully. In the Smith (1990) scheme the value of T_{ice} is 264.16 K and the value of T_0 is 273.16 K.

$$\begin{aligned} \alpha_{CP} &= 0 & T \leq T_{ice} \\ \alpha_{CP} &= \tfrac{T-T_0}{T_0-T_{ice}} + 1 & T_{ice} < T < T_0 \\ \alpha_{CP} &= 1 & T \geq T_0 \end{aligned} \tag{2.14}$$

In a similar manner to the Smith (1990) scheme, the ECMWF model (Tiedtke, 1993), still uses just one variable for cloud liquid water, with the phase (based on earlier work by Matveev, 1984) being a function of temperature as shown in equation 2.15, with the value of T_{ice} for this model being 250.16 K and T_0 being the same as in Smith (1990).

$$\begin{aligned} \alpha_{CP} &= 0 & T \leq T_{ice} \\ \alpha_{CP} &= \left(\tfrac{T-T_{ice}}{T_0-T_{ice}}\right)^2 & T_{ice} < T < T_0 \\ \alpha_{CP} &= 1 & T \geq T_0 \end{aligned} \tag{2.15}$$

Figure 2.3 shows the change in phase (α_{CP}) with temperature for the two different schemes. It can be seen that for the Matveev (1984) scheme that there is a tendency for the model to maintain a water phase at lower temperatures than the Smith scheme. Cloud phase schemes such as Matveev (1984) and Smith (1990) have been evaluated in a number of aircraft and ground-based studies. Bower *et al.* (1996) found that there was generally a sharp change in phase between zero and -10 °C over both maritime and continental clouds; they also found that the then-current Met Office parameterization of phase was biased by about 3 °C so that more ice clouds were occurring at higher temperatures. This work is verified by Field *et al.* (2004), who also noted the sharp drop in phase by -10 °C in the majority of flights made over Chilbolton. Finally, Hogan *et al.* (2003b) found using flights from data over Chilbolton, that both the Met Office and ECMWF models

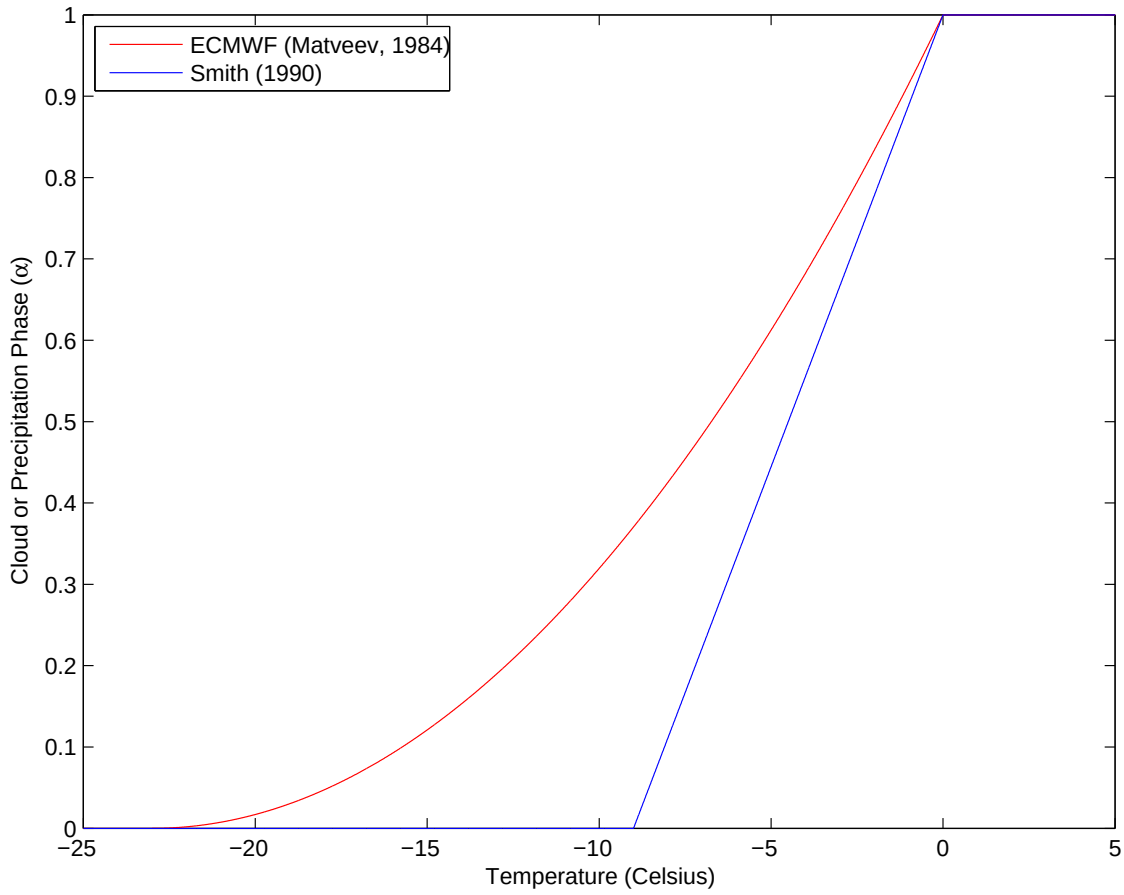

Figure 2.3: *Phase function for the Smith (1990) and Matveev (1984) schemes. A phase value of 1 implies that all of the cloud phase is liquid.*

overestimated the frequency of clouds including liquid water, especially at temperatures between 0 and -10 °C. Below -25 °C, the models tended to underestimate the liquid water fractions. Work by Bower *et al.* (1996) suggested that these results were reasonable for the mid-latitudes; most cloud contained a spread of phase from 0 to 1 at 0°C and by -25°C, all cloud phases recorded were beneath 0.1. However, similar experiments over New Mexico showed a spread of clouds with α of 0.75 or above between temperatures of 0 and -20 °C. Close to -10°C, most observations showed a phase of 0.8 or higher, which is quite different from the Smith (1990) parameterization in figure 2.3. The Smith (1990) scheme has since been replaced with a scheme by Wilson and Ballard (1999) which considers cloud in both the liquid and ice phases as separate prognostic variables; this methodology will be studied in the next section.

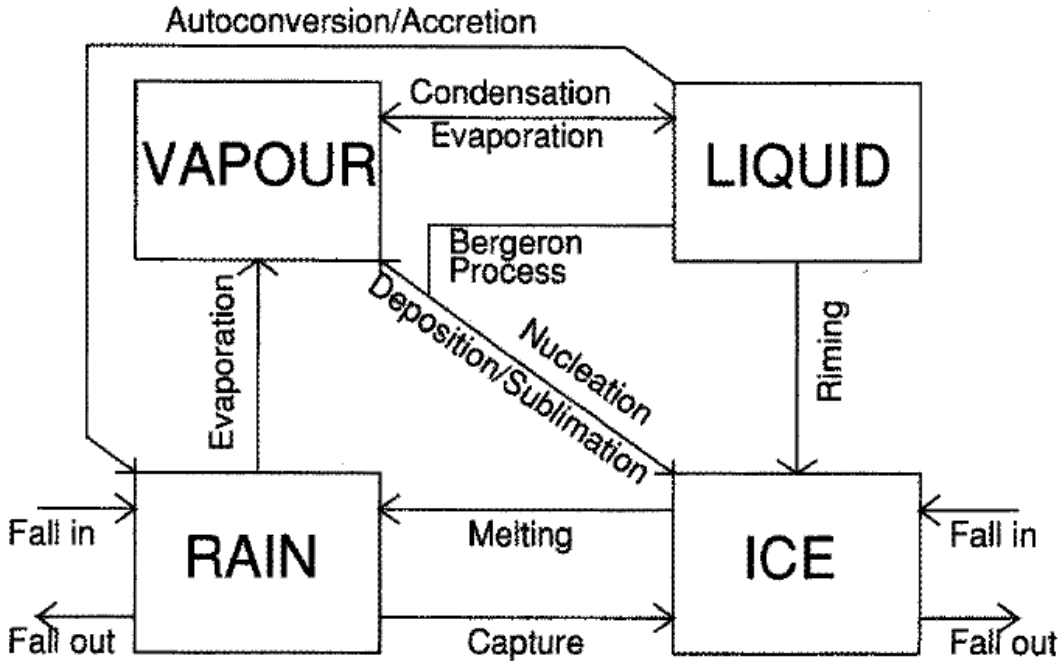

Figure 2.4: *Diagram showing the different phases and cloud phase change processes in the Met Office Unified Model (from Wilson and Ballard, 1999)*

2.4.2 Ice Water Content

So far we have only studied models with a single cloud water content variable. However, different cloud phases produce different radiative effects and hence to make improvements to cloud radiative transfer, the separation of cloud water content into phases is important. Wilson and Ballard (1999) extended the scheme of Smith (1990) to allow each grid box of the Met Office model to represent water in different phases of vapour (q), ice water content (q_i) and liquid water cloud (q_l) as shown in figure 2.4. The arrows between the grid boxes show the various different microphysical processes that are parameterized within the model. It should be noted that due to implications of model run time to produce a forecast, all ice is classified as one variable; there is no distinction between hail, snow, cloud ice or graupel.

The separation of cloud water into liquid and ice quantities has a number of advantages for a NWP such as the Met Office Unified model. Wilson and Ballard (1999) note that their method of splitting water content into ice and liquid prognostic variables has many advantages over diagnosing phase from temperature, as in Smith (1990). In particular, there are better predictions

of freezing rain and drizzle than the Smith (1990) scheme and that visibility estimates are much better due to drier boundary layers resulting from correct parameterization of rain evaporation. These are just two aspects which will be of direct benefit to forecasters. Although some of the small-scale effects such as visibility and localised precipitation are not as important in climate models, which concentrate on a much larger picture, the production of ice cloud and the differences between radiative transfer through liquid and ice clouds is significant enough to justify a separation of liquid and water clouds in most GCMs, which has been done in some cases (for example Fowler *et al.*, 1996 and Ghan *et al.*, 1997), which were designed specifically as GCMs, without being developed as part of a suite of models with different global coverages, like the Met Office Unified Model.

There is little non-radar evaluation of model ice water content; Stephens *et al.* (2002) shows some of the results of vertically integrated cloud water from different GCMs; over the polar regions where this is most likely to be ice the measurements of integrated cloud water vary as much as a factor of ten. This issue can be aided by the use of radar; this will be discussed further in section 2.5.2.

2.4.3 Cloud Fraction

Although at present most climate models and operational forecast models have a prognostic water content in at least one phase, the majority use a diagnostic cloud fraction, with just a few models having a prognostic cloud fraction. Initially, all models used a prognostic liquid water content but a diagnostic cloud fraction. For example, in Smith (1990) the cloud fraction ($\mathcal{C}_{\mathcal{F}}$) was diagnosed from relative humidity (RH), defining a critical relative humidity (RH_{crit}), at which cloud begins to form. The value of RH_{crit} is 85% for all but the two model layers closest to the Earth's surface, where RH_{crit} is 92.5%. This scheme can be expressed diagrammatically, as shown in figure 2.5. The distribution of total specific humidity (q_t) in each model grid box is assumed to be a triangular pdf, with the mean humidity corresponding to the peak of the distribution. The triangular function can move left or right on the axis, dependent on the grid box total specific water content. When the humidity exceeds (RH_{crit}), the right hand side of the triangle crosses the q_{sat} line and some of the water content is converted to liquid cloud water (q_l) or ice cloud (q_i); the cloud fraction is then simply the integral of the probability distribution of q_t that is greater than (q_{sat}), denoted by the blue triangle labelled 'CF' in figure 2.5. Figure 2.6 shows the Smith (1990) cloud fraction as

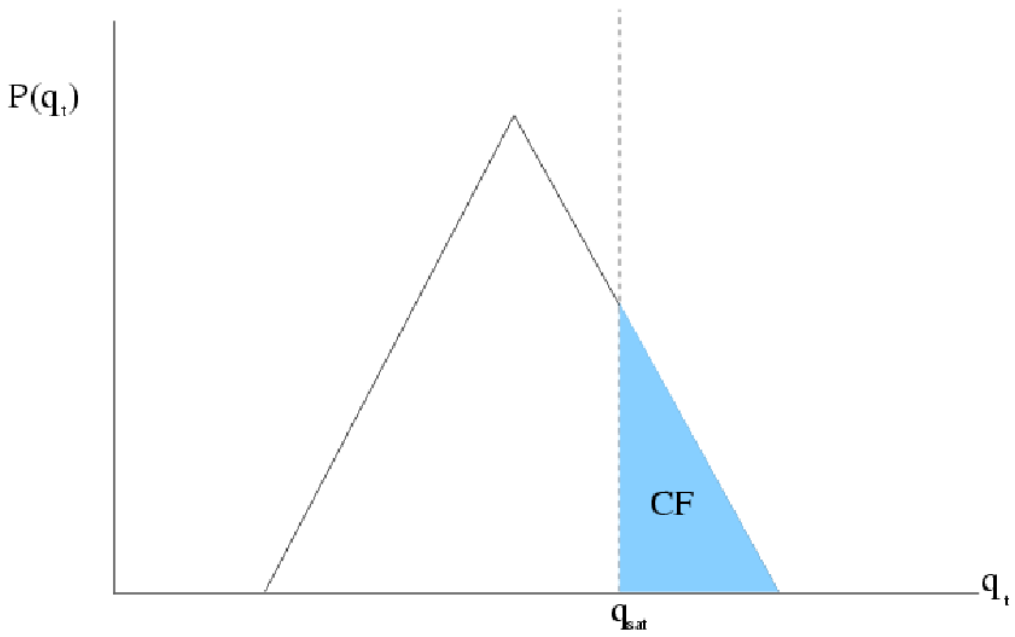

Figure 2.5: *The method of Smith (1990) for determining cloud fraction from humidity measurements. A typical triangular distribution of humidity is shown, with the blue area representing the cloud fraction.*

a function of humidity. Cloud fraction increases as the humidity exceeds its critical value, with half the grid box filled with cloud when the relative humidity is 100%. The grid box is completely cloudy once the grid box mean relative humidity reaches 115%. This process allows for sub-grid scale variability within the grid box; if the grid box mean relative humidity is 100%, it does not automatically mean that all the grid box is cloudy and by setting cloud fraction to be 1 at 115% mean relative humidity is more realistic as it does not allow the grid box to be completely cloudy until it is supersaturated.

Wood and Field (2000) compared the Smith (1990) parameterization to aircraft measurements of cloud fraction from the First ISCCP Regional Experiment (FIRE), the Atlantic Stratocumulus Transition Experiment (ASTEX), and the European Clouds and Radiation Experiment (EUCREX). They tested the parameterization in low ($0.0 < \mathcal{C}_{\mathcal{F}} < 0.3$), medium ($0.3 < \mathcal{C}_{\mathcal{F}} \leq 0.7$), and high ($0.7 < \mathcal{C}_{\mathcal{F}} \leq 1.0$) occurrences. The root-mean squared error for low cloud fraction

ranged from 9–14%, but was as high as 30% for the other categories. The Smith (1990) method was used to diagnose cloud fraction within the Met Office model until a prognostic cloud fraction was introduced (Bushell *et al.*, 2003). Wilson and Ballard (1999) used the Smith principles to diagnose both liquid cloud fraction and ice cloud fraction, assuming two distributions for cloud ice and cloud water.

Initial attempts to produce a prognostic cloud fraction were pioneered by Tiedtke (1993), who introduced a scheme for the ECMWF model. The basic equation for the rate of change of cloud fraction is similar to equation 2.13:

$$\frac{d\mathcal{C}_{\mathcal{F}}}{dt} = \left(\frac{d\mathcal{C}_{\mathcal{F}}}{dt}\right)_{ADV} + \left(\frac{d\mathcal{C}_{\mathcal{F}}}{dt}\right)_{DIFF} + \left(\frac{d\mathcal{C}_{\mathcal{F}}}{dt}\right)_{TM} + \left(\frac{d\mathcal{C}_{\mathcal{F}}}{dt}\right)_{ST} + \left(\frac{d\mathcal{C}_{\mathcal{F}}}{dt}\right)_{EV} + \left(\frac{d\mathcal{C}_{\mathcal{F}}}{dt}\right)_{CV}. \tag{2.16}$$

However, comparing the two equations we see that the precipitation generation term in equation 2.13 is replaced by a general evaporation term (subscript EV) in equation 2.16, which has to be negative by definition. It should also be noted that the stratiform term only includes cloud formation and not dissipation. Similar equations were produced by Gregory *et al.* (2002) and Bushell *et al.* (2003); the latter describes the prognostic cloud fraction currently used within the Met Office Unified Model. As noted by Bushell *et al.* (2003), sub-grid scale variations of cloud fraction are important for radiation and surface temperature calculations and the use of a prognostic cloud fraction improves the radiation calculations within their model, providing the correct overlap assumptions are used. Overlap aspects will be discussed in the next section; however, the debate about whether a prognostic cloud fraction is needed in a model still continues. While a model liquid water content is directly related to physical processes of evaporation and humidity, cloud fraction calculations are more complex and subjective. It is difficult to evaluate model cloud fraction using passive instruments and observers alone; however radar and lidar are useful tools for this purpose. A review of work in this area will be made in section 2.5.3.

2.4.4 Cloud Overlaps

In addition to the model cloud variables (such as liquid water content and cloud fraction), each model has to make assumptions about how clouds are overlapped between vertical grid boxes. The way clouds are overlapped is important for calculations of radiative transfer, cloud albedo and optical depth.

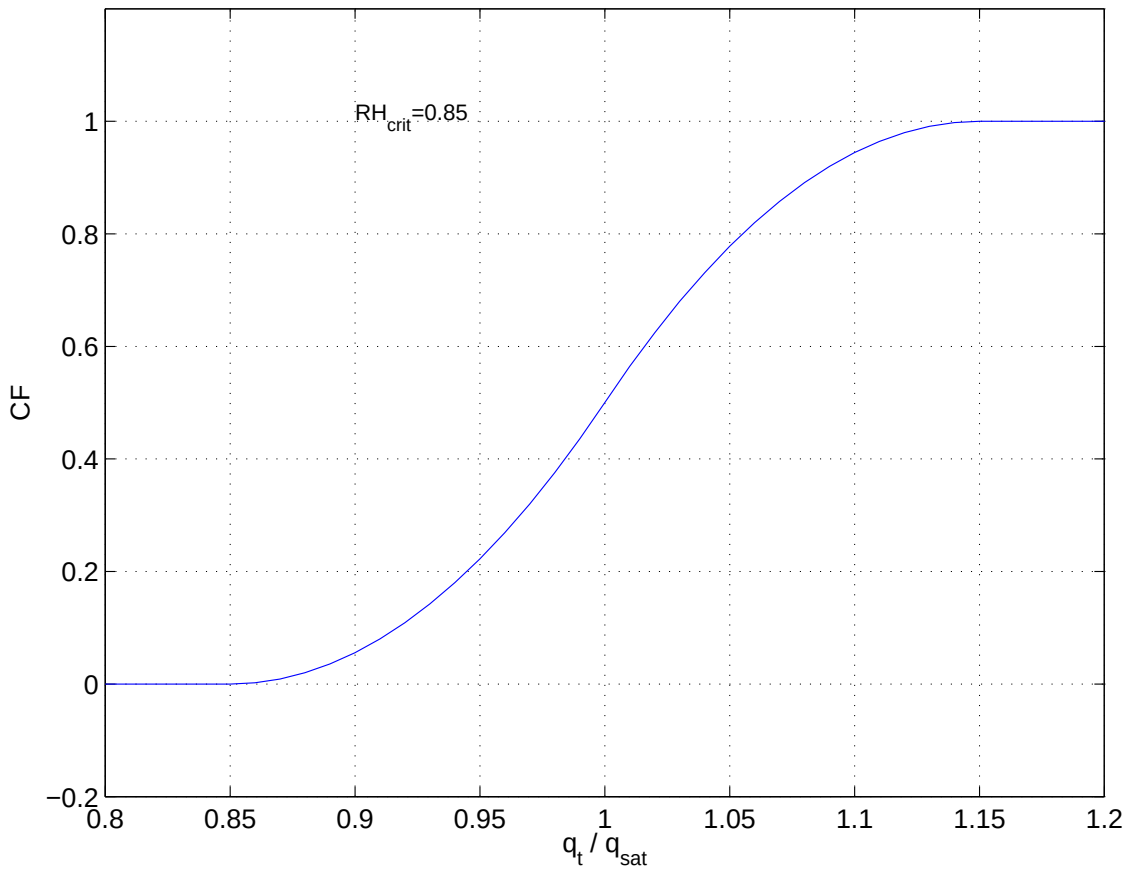

Figure 2.6: *The method of Smith (1990) for determining cloud fraction from humidity measurements. Note that once the humidity passes the critical value of 85% that cloud begins to form and the grid box is fully cloudy at relative humidity of 115%.*

The three most common model overlap assumptions are shown in figure 2.7. In the case of the maximum-random overlap (after Geleyn and Hollingsworth, 1979 and Morcrette and Fourquart, 1986), the clouds are overlapped so that neighbouring cloud in the vertical is overlapped to the maximum extent. However, where there is a completely clear grid box between two different cloud layers, random overlap takes place. In the case of the maximum overlap assumption, the clouds are arranged so that there is the maximum amount of overlap regardless of any clear layers and in the third type, random overlap occurs throughout the column.

Currently, most GCMs and NWP models (including the Met Office Unified Model and the ECMWF model) assume a maximum-random overlap between layers as it is easy to implement and the results agree with some observational studies (for example, Tian and Curry, 1989). It would seem sensible at first to have layers separated by clear sky randomly overlapped, as they

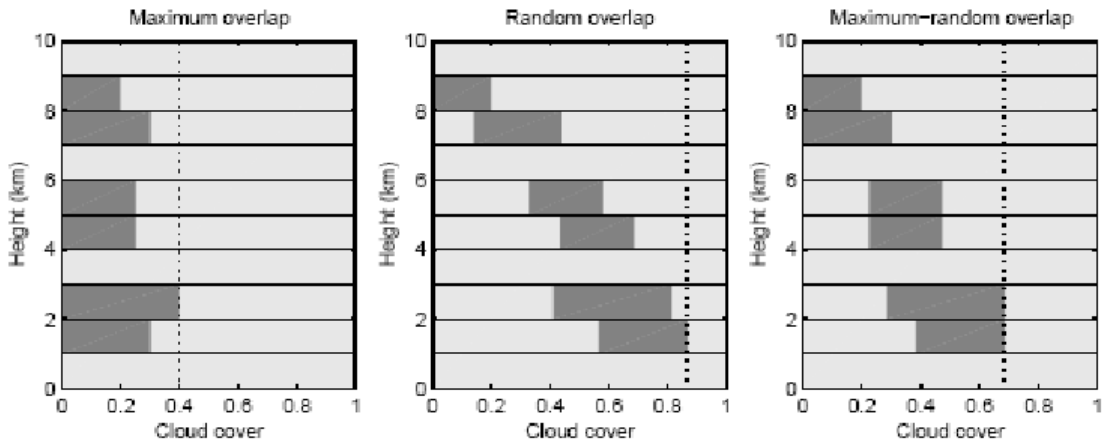

Figure 2.7: *The three main types of overlaps used in GCMs, taken from Hogan and Illingworth (2000). The dashed line shows what the total cloud cover in the column would be when viewed from above.*

may have been produced by different atmospheric conditions and to have vertically-continuous layers overlapped to their maximum extent as they may well have been produced by similar conditions such as frontal systems or deep convection.

The effects of different overlaps have been examined by several studies. Jakob and Klein (1999) used a sub-grid-scale precipitation model to examine how ECMWF cloud overlap changes affected the microphysics within the model. They found that the cloud overlap assumption is important for total column precipitation. By changing the overlap from maximum-random to random overlap within the sub-grid model, they found that the stratiform precipitation rate decreases across the whole globe. Morcrette and Jakob (2000) looked at the changes in the ECMWF model overlap assumption would bring on cloud and radiation. They found that changing model overlap assumptions in the ITCZ varied the outgoing long wave radiation by as much as 40 W m^{-2}. In addition, there were large changes in simulated global cloud cover. For the random overlap, cloud cover was as high as 71.4%, but it decreased to 60.9% when a maximum overlap was assumed. For the maximum-random overlap, a value in between these two extremes, of 63.9% is recorded.

Currently there is very little observational data available to evaluate overlap statistics in models, but radar can again be used for this purpose. This is will be examined in section 2.5.5.

2.5 Comparisons Between Radar/Lidar and Models

Although in some cases cloud parameterizations have been evaluated using cloud resolving models (e.g. Xu and Krueger, 1991), it is normal to use some form of observations to assess model performance. It is particularly useful to have observations of the three variables used in the models: cloud fraction, liquid and ice water contents. However, it is very difficult to measure directly cloud fraction or water content of a cloud. The majority of experiments previously conducted have used measurements from aircraft, plus satellite or ground-based remote sensing and cloud variables have been derived from measurements made from these instruments.

For the past ten years or so, advances in radar and lidar technology have allowed a number of new systems to start operating, such as active remote sensing from space, Doppler cloud radar systems and dual-wavelength radar. In addition, a number of methods have been developed to retrieve model variables of liquid water content, ice water content and cloud fraction directly from radar and lidar measurements of clouds. These methods will be examined in subsections 2.5.1–2.5.3. Further to the retrieval of individual model cloud variables, skill scores denoting the performance of individual forecasts of cloud location have also been developed. This will be covered in section 2.5.6.

2.5.1 Radar and Lidar Evaluation of Liquid Water Content

Measurements of liquid water content from radar reflectivity have been suggested for some time. The earliest work was by Atlas (1954), who suggested a power law relationship that related radar reflectivity and liquid water content: $Z = 0.048\mathrm{LWC}^2$. Since this study, several different forms of this power law relationship have been suggested (for example Sauvegeot and Omar, 1987; Baedi *et al.*, 1999). However, Fox and Illingworth (1997a,b) show that drizzle droplets dominate the reflectivity of a stratocumulus cloud, and can increase the radar reflectivity by between 10 and 20 dBZ, although drizzle makes little change to the liquid water content of the cloud. Since drizzle is nearly always present, this effect can cause these empirical relationships to fail.

As there has been some uncertainty in which technique to use and problems with drizzle, recently more physical approaches for estimating liquid water content have been developed. Boers *et al.* (2000) used a variety of remote sensing instruments to determine liquid water content. They first determined the cloud thickness using radar and lidar measurements, followed by estimating

the liquid water path from microwave radiometer data. By assuming the liquid water content varied linearly with height, it was then possible to determine liquid water content at any height within the cloud.

An alternative method for determining liquid water content has been suggested by Krasnov and Russchenberg (2005), which uses radar-lidar synergy to determine liquid water content of clouds. This uses the ratio of radar reflectivity to lidar extinction coefficient in order to classify every cloud range cell in the vertical radar/lidar profile as either without drizzle, with light drizzle or with heavy drizzle. They categorise a number of Z-LWC relations from previous studies (For example Atlas, 1954; Sauvegeot and Omar, 1987; Fox and Illingworth, 1997b; Baedi *et al.*, 1999) and give power law relations for cloud with no drizzle, light or heavy drizzle. Although this technique appears to give results in some conditions, there are still outstanding issues of how accurate radiometer measurements are during precipitation events, and there will be problems in the thicker clouds where the lidar signal is extinguished.

Although both techniques for liquid water retrieval are used within the Cloudnet programme, the method of Boers *et al.* (2000) is the most physically-based relationship. Although it may be argued that the assumption that LWC increases linearly with height from cloud base may be false, liquid water clouds are frequently thin (Illingworth *et al.*, 2007) and so this retrieval method is more realistic than using empirical formulae that are likely to break down given any form of drizzle precipitating from the cloud.

Illingworth *et al.* (2007) use data from three Cloudnet sites to make comparisons with 7 models (ECMWF; Met Office mesoscale and global models; Météo France; Royal Netherlands Meteorological institute (KNMI)'s regional atmosphere climate model (RACMO); Swedish Meteorological and Hydrological Institute (SMHI) Rossby Centre Regional Atmospheric Model (RCA); German weather service (DWD) Lokal Modell (LM)). The results from the Cloudnet data are shown in figure 2.8. It can be observed that the 2 Met Office models and the ECMWF model come the closest to the spread of observed liquid water content below 2 km. There are some problems with quite a number of the other models, such as the Météo France model having difficulty representing a spread of liquid water contents; this is probably due to its diagnostic liquid water content scheme, where most of the other models use a prognostic variable for liquid water content. Above 2 km, the liquid water content measurements of all models have a larger spread, due to phase changes in the models. Illingworth *et al.* (2007) present observations for the year

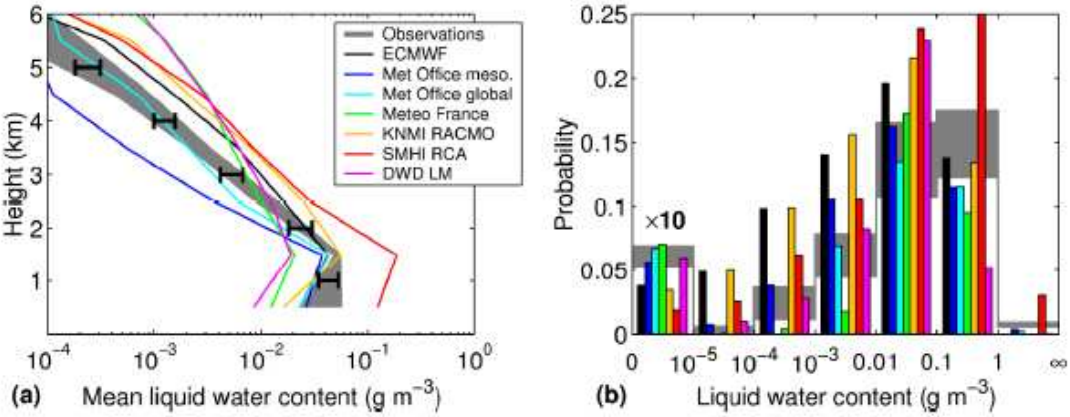

Figure 2.8: *(a) Mean liquid water content profiles from the 7 Cloudnet models and radar observations, for the whole of 2004. The error bars on the observations are due to radiometer and possibly distribution of LWC throughout the cloud. (b) Histograms showing the probability of LWC for clouds between 0 and 3 km altitude. Both figures are for all liquid clouds observed over the 3 Cloudnet sites at Chilbolton in Hampshire, Cabauw in the Netherlands and Palaiseau in France. During winter, the dominant cloud types will be frontal stratocumulus, while in Summer, the higher liquid water content values are more likely to be due to convective cumulus and cumulonimbus. From Illingworth* et al. *(2007).*

2004 with no seasonal variation; it would be interesting to see how model representation changes between summer and winter seasons with the change in the height of the freezing level. They also find that the ECMWF model overestimates the occurrence of liquid water clouds, but underestimate the water content when cloud is present.

2.5.2 Radar and Lidar Evaluation of Ice Water Content

In similar fashion to the work on liquid water content, power law relations were initially suggested for ice water content measurements from radar (e.g. Sassen, 1987; Sassen and Liao, 1996), but Matrosov (1997) questions these relations. By comparing relations from aircraft data from previous experiments (Liao and Sassen, 1994; Atlas *et al.*, 1995; Brown *et al.*, 1995), Matrosov (1997) finds that for a particular value of reflectivity there was a spread of reported IWC up to as much as one order of magnitude. However, Liu and Illingworth (2000) show that this difference is mostly due to differences in the radar frequencies used in the different campaigns and differences in how the density of ice is represented. After examining EUCREX (European Cloud Radiation Experiment) and CEPEX (Central Equatorial Pacific Ocean Experiment) data sets for particle

size distributions, Liu and Illingworth (2000) suggested that measurements of mean particle size or temperature could be used to constrain the IWC spread and give a number of relations linking ice water content to reflectivity for different temperatures. Hogan *et al.* (2006) took their work one stage further and derived the following relations for IWC at different radar frequencies using EUCREX aircraft data of the form

$$\log_{10} \mathrm{IWC} = \hat{a}ZT + \hat{b}Z + \hat{c}T + \hat{d}, \tag{2.17}$$

where $\hat{a}$, $\hat{b}$, $\hat{c}$ and $\hat{d}$ are coefficients which vary with the frequency of the radar and the units used. Using 39 hours of scanning 3-GHz radar data, Hogan *et al.* (2001) compare the mean ice water content versus mean temperature for 3-GHz radar data, and the Met Office model. They find that the mean relationships of the model and the radar between -10 and -30 °C are close, with a standard error at most of 25%. At higher temperatures, these lines diverge, possibly due to aggregation. At lower temperatures, the model underestimates the IWC; at -45 °C, this is around a factor of two. However, a close fit between -10 and -30 °C is promising for the Met Office model, as the majority of radiatively thick ice clouds do occur at these temperatures and from studying Cloudnet data, it can be seen that in fact the majority of ice clouds in the mid latitudes occur in approximately this temperature range.

In addition to the work of Liu and Illingworth (2000) and Hogan *et al.* (2006), other methods have been suggested for deriving IWC from radar and lidar measurements. Donovan and van Lammeren (2000) have developed a technique where they obtain an effective radius from the ratio of radar reflectivity to attenuation-corrected lidar backscatter and use this to obtain particle size and hence ice water content. The main drawbacks with this work is that the signal from ground-based lidars is often completely extinguished through low-altitude liquid water clouds, although this technique may have more merit with the combined CloudSat and CALIPSO data from space. Assumptions that relate the effective radius derived from the radar and lidar measurements to the true effective radius are made on the basis of ice particle habit. Uncertainties in determining the habit may lead to errors in the ice water content measurements.

An alternative to the Donovan and van Lammeren (2000) technique is to use dual wavelength radar. Hogan *et al.* (2000) used this technique to calculate particle size and hence improved IWC from the ratio of the two reflectivity values (dual wavelength ratio), assuming a gamma distribution of ice particles. However, there is limited data available at two wavelengths, although this technique shows potential for the future.

Finally, methods have been developed using Doppler velocity and reflectivity to obtain ice water contents. Matrosov *et al.* (1994, 1995) use radiometers, radar reflectivity and Doppler velocity, and Delanoë *et al.* (2007) use just radar reflectivity and Doppler velocity, and assume a particle size distribution with relations on how parameterized fall speeds vary with diameter. Delanoë *et al.* (2007) uses Doppler velocity to gain the mass of the particle from an assumed fall speed, and then uses reflectivity to get the intercept parameter of the particle spectrum. This method is useful as it only requires Doppler radar measurements, but is subject to the assumptions made on the particle fall speed. In addition, the particle terminal velocity is not directly measured by the radar; the measured velocity includes components of the air velocity, which can introduce errors into the method around the turbulent cloud base. Although not explicitly stated by Delanoë *et al.* (2007), using a clear air radar, the air velocities can be determined and particle terminal fall speed extracted.

The Cloudnet programme (Illingworth *et al.*, 2007) has used the techniques of Donovan and van Lammeren (2000), Hogan *et al.* (2006) and Delanoë *et al.* (2007) to evaluate IWC in the seven operational models. Results of this analysis are shown in figure 2.9. It can be seen that Met Office models and ECMWF model make the best representation of the mean profile of IWC and that the RCA model appears to have too large an ice water content throughout the profile, with the pdf of IWC shown in figure 2.9 (b) shows a large probability of ice water contents between 0.01 and 0.1 g m^{-3}. The German weather service's model has the closest representation of the pdf, but is very poor at representing the mean ice water content, as it underestimates the ice water content by 1 order of magnitude below 6 km, and overestimates it by roughly half an order of magnitude above 6 km.

2.5.3 Radar and Lidar Evaluation of Model Cloud Fraction and Cloud Occurrence

Having examined radar evaluation of model water contents, we now turn to look at how radar and lidar can be used to evaluate model cloud fraction. Although earlier work has been done on cloud boundaries and vertical extent using radar and lidar (for example Pal *et al.*, 1992; Uttal *et al.*, 1995), the first radar and lidar study for model comparison was conducted by Mace *et al.* (1998). In their work, cloud occurrence in the ECMWF model was compared to measurements of cloud occurrence from a 35-GHz radar operating at the Atmospheric Radiation Program (ARM), Southern Great Plains (SGP) site. A lidar ceilometer was used to determine the location of the

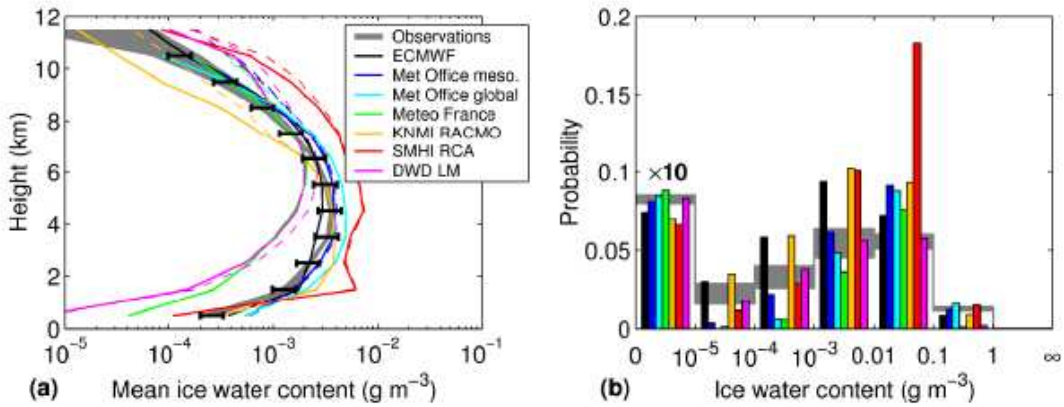

Figure 2.9: *As for figure 2.8, but for ice water content. The profiles shown include dotted lines which are the model results before filtering to remove cloud that the radar would not detect. The histograms in (b) are between 3 and 7 km altitude. From Illingworth* et al. *(2007)*

cloud base. Using a month of data, Mace *et al.* (1998) found that the model underpredicted cloud occurrence between 1 and 9 km, but overpredicted the cloud occurrence beneath 1 km and above 9 km.

Similar work by Beesley *et al.* (2000) used synergy with a 35-GHz radar and a lidar ceilometer for cloud base detection located over the Arctic. They compared hourly profiles of cloud fraction in the ECMWF model over a 24 day period in November 1997 with the same period of radar observations, and showed similar results to Mace *et al.* (1998), given Mace used a frequency of occurrence and Beesley hourly cloud fraction. Beesley *et al.* (2000) found that the model underestimates cloud from 1–5 km and overestimates it above 5 km. Due to the colder temperatures over the polar regions, the ice cloud will exist at lower altitudes in both the radar and the model. Hence the overestimate at the Artic at 5 km is probably due to the same problem with too much ice cloud above 9 km reported by Mace *et al.* (1998).

Hogan *et al.* (2001) continued the work of Mace *et al.* (1998) and Beesley *et al.* (2000) by using 35-GHz and 94-GHz radars at Chilbolton in Hampshire. Instead of comparing cloud fraction or frequency of occurrence, Hogan *et al.* (2001) examined three variables: mean cloud fraction, frequency of occurrence and amount when present. Cloud fraction was determined by assuming a model grid with one hour time resolution and the model vertical grid resolution and cloud fraction was determined by the number of pixels[1] seen by the radar in this grid box. Frequency of

[1]One pixel in data from the Chilbolton 35-GHz and 94-GHz radar data is 60 m high by 30 seconds in time.

occurrence is simply the frequency that some cloud (above a cloud fraction threshold), is observed above Chilbolton in each hourly profile, and at each model vertical grid box. A cloud fraction threshold of 0.05 was selected so that grid boxes with cloud fraction greater than this amount were defined as having cloud. Amount when present is the cloud fraction detected when cloud fraction in a grid box is above the threshold. Multiplying frequency of occurrence and amount when present together results in mean cloud fraction. Hogan *et al.* (2001) also attempt to be fair to the model by removing modelled cloud that has too low an ice water content to be detected by the radar and where, in some mid-level cases, it was difficult to distinguish between ice cloud and precipitating snow. To ensure a fair comparison, the snow-flux between vertical grid boxes is used to increase the ECMWF model cloud fraction. Hogan *et al.* (2001) find that even after these considerations have been made, the model overestimates the cloud fraction above 7 km by a factor of 2. They note that the modelled cloud tends to occur in the lowest kilometre as much as 3 hours before any cloud features are observed in reality. This is similar to Mace *et al.* (1998) who note that deep cloud events are often predicted too early, and take too long to dissipate. It should also be noted that the Mace study took place at a lower latitude than the Hogan study. This means that the ice clouds within the model and observations existed at a higher altitude. It is likely that the problems expressed by Mace *et al.* (1998), Beesley *et al.* (2000) and Hogan *et al.* (2001) are similar in nature; the ECMWF model has difficulty in correctly representing ice clouds; but the altitude difference is likely to be due purely to the latitude difference between the three data sets. Illingworth *et al.* (2007) perform cloud fraction analyses following Hogan *et al.* (2001) on the various models that take part in the Cloudnet project. The results from this work are shown in figure 2.10, where they are presented as profiles (with and without filtering to remove cloud that would not be detected by the radar) and as a pdf of cloud fraction. The results for the ECMWF model are similar to those of Hogan *et al.* (2001), with the model having difficulty in representing cloud above 7 km.

From the pdf in figure 2.10, it can be seen that the Met Office model has difficulty in representing the cloudiest grid boxes (those with cloud fraction values from 0.8 to 1). The Met Office model has some problems representing the mean cloud fraction from 0–6 km, where both the global and mesoscale models underestimate cloud fraction by around 5%. Above 6 km, the Met Office models tend to overestimate cloud fraction by 2–3%, which is in line with most of the other models. The RCA and RACMO models have problems in representing the cloud at the top of the

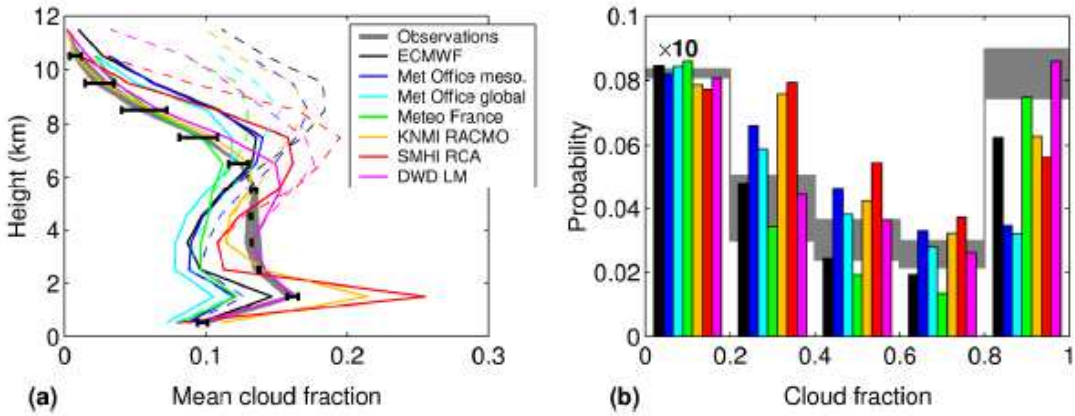

Figure 2.10: *Cloud fraction from radar observations and 7 operational models, after Illingworth* et al. *(2007). As in figure 2.9, each model profile has a dotted line, which represents the cloud fraction before filtering to remove any cloud which would not be detected by the radar.*

boundary layer; at 1.5 km, they overestimate cloud fraction between 5 and 10%. Probably the best performer is the German weather service (DWD) model, which makes a good approximation to the cloud fraction pdf and mean cloud fraction profile.

Although ground-based instruments are useful for climatological studies of the behaviour and performance of clouds within models at a single point, coverage over the whole model domain is useful. Spaceborne remote sensing has been proposed for a long time (e.g. Atlas *et al.*, 1995; Hogan and Illingworth, 1999). The Lidar In-space Technology Experiment (LITE), described by McCormick *et al.* (1993) offered the scientific community the ability to test the potential of spaceborne lidars. The lidar instrument flew on the space shuttle "Discovery" during September 1996. Miller *et al.* (1999) compared the lidar data to the ECMWF model and used the same skill scores suggested by Mace *et al.* (1998) for their ground-based study. Miller *et al.* (1999) find that the model is good at getting the cloud position correct. They give few statistics on cloud fraction, but give a percentage relating to how often cloud is detected within the model (28.9% in total) and the observations (28.4% in total) with no latitude or height variation. This does not give much information into how good the climatology of the model is in terms of cloud fraction.

In 2003, another spacebourne lidar mission, ICESat (Ice, Cloud and Land-Elevation Satellite) was launched (Zwally *et al.*, 2002). This is a platform from space, upon which a lidar instrument called the Geoscience Laser Altimeter System (GLAS) is mounted. Although its primary aims were to measure the height of the ice sheets in the polar regions, the lasers are also sensitive

enough to enable global observations of clouds. Already, data from ICESat has been used to evaluate cloud models. Palm *et al.* (2005) advanced the work of Miller *et al.* (1999) using ICESat data. In a short experiment, they average the ICESat data on to the model grid in a horizontal direction, yet interpolate the model cloud fraction on to the ICESat vertical grid. They find that over a few orbits that the model represents cloud fraction to within 3% below 10 km for a 6 hour forecast. Between 10 and 12 km, the model underestimates cloud fraction by as much as 10% and between 12 and 17 km, the model has a 10% overestimate in cloud fraction. For the 48 hour forecast, the overestimate is as large as 30%, and between 3 and 10 km the forecast overestimates the cloud fraction by 5%. However, like Miller *et al.* (1999), they make no attempt to correct for the lidar attenuation, but Palm *et al.* (2005) note that total extinction of the laser only occurs in about 10% of cases.

2.5.4 Radar and Lidar Simulation

In sections 2.5.1–2.5.2, the methods of evaluating models all involved taking radar and lidar data and transforming it to a model cloud variable. As discussed in chapter 1, it is possible to go the other way and simulate radar or lidar data from the model variables, although only a few previous examples of simulation of clouds exist within the literature. Chiriaco *et al.* (2006) were able to use the MM5 model (5th generation Pennsylvania State University-NCAR mesoscale model) to simulate observations made by radar and lidar at the SIRTA (Site Instrumental de Recherche par Télédétection Atmosphérique) observatory in France. The principle lies in using the microphysical assumptions made in the model along with the model variables to predict the radar and lidar data. An example of this is shown in figure 2.11. It can be seen that the MM5 model produces ice cloud about 3 hours too early than in the radar observations and the simulated reflectivity is too low, although the cloud is at approximately the correct height. The simulated lidar profile shows ice cloud at the right altitudes, but the model is unable to represent the two layers of cloud present. Both simulated radar and lidar signals seem very uniform in nature, with little time variation. However, Chiriaco *et al.* (2006) find that in the majority of cases, the MM5 model is able to simulate ice clouds in the mid-latitudes, but in 35% of the cases studied, the ice clouds within the model persist for too long, due to too much solid water and not enough liquid water, regardless of the parameterization scheme used.

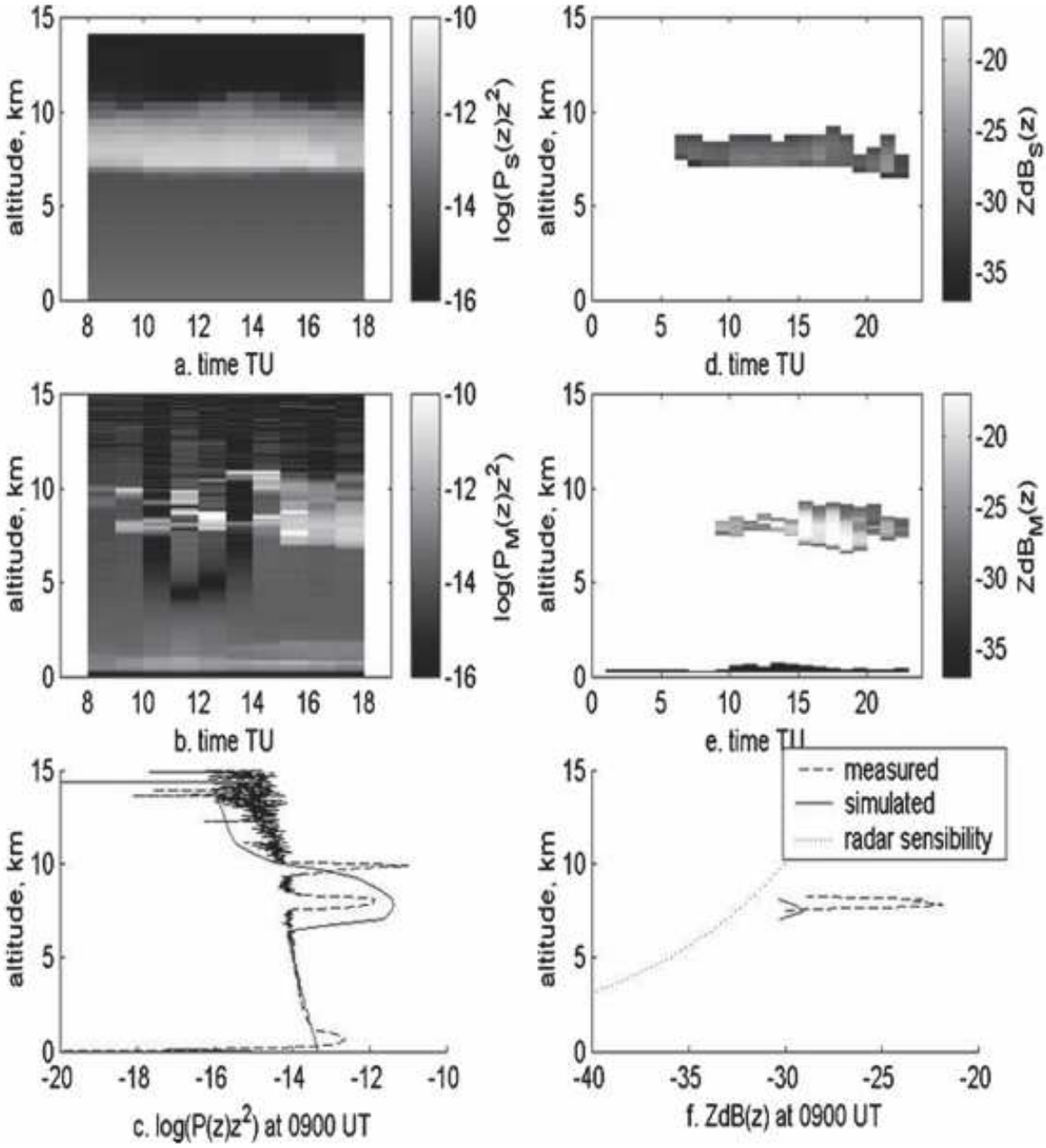

Figure 2.11: *Simulation of radar and lidar data by the MM5 model on 17 October 2003, taken from Chiriaco* et al. *(2006). (a) Simulated lidar backscatter profile; (b) Measured lidar backscatter profile; (c) Simulated and measured backscatter profiles for 0900 UTC; (d) Simulated radar reflectivity with time; (e) Measured radar reflectivity; (f): Measured and simulated profiles for 0900 UTC. The time scales in (a), (b), (d) & (e) are in UTC.*

2.5.5 Overlap Evaluation

Radar data has been used to test the validity of overlap assumptions. Hogan and Illingworth (2000) developed a method to express the overlap of different model layers numerically, with

values of an overlap parameter of zero for random overlap and one for maximum overlap. This was tested on a small amount of data from Chilbolton. Later work by Mace and Benson-Troth (2002) used a much larger data set from 4 ARM sites ranging from the tropics to Alaska, and over a much longer time period (collectively 105 months of data). Results from both papers report that the use of random overlaps for vertically non-continuous cloud (that with clear sky in between layers) is a good assumption. However, the use of maximum overlap for continuous layers is only realistic when the layer separation is small. Hogan and Illingworth (2000) show that as model level separation increases, the validity of the overlap assumption decreases from a maximum overlap at 0 separation to near-random overlap at 4 km. They propose an exponential relationship with an e-folding distance of 1.6 km to allow the overlap parameter to decay with increasing level separation, so gradually more cloud is randomly overlapped as grid spacing increases. Mace and Benson-Troth (2002) note that the cloudy layers do not easily lend themselves to a simple maximum or random overlap assumption and that for layers much greater than 1km separation, random overlap would be a better assumption.

2.5.6 Skill Scores

In addition to the climatological performance of the model, the quality of individual forecasts can be assessed using skill scores. There are many such scores around, some of which are detailed in Wilks (1995). The principle for radar evaluation consists of first transferring the radar and model data on to a common grid, as per the Cloudnet programme described in sections 2.5.1–2.5.2. Then each point in the radar data matrix is transformed into a binary score, with a cloud fraction threshold used to define whether a grid box is clear or whether it is cloudy. If the cloud fraction in the box exceeds the threshold, its binary score is set to one, otherwise the score is zero. By comparing the two data scores, each grid box can be classed as a hit, a miss, a false alarm or a correct rejection following table 2.2.

Mace *et al.* (1998) were the first to use skill scores to evaluate model cloudiness using radar and lidar measurements. They used skill scores of hit rate (HR), probability of cloud detection (POD), threat score (TS) and false alarm rate (FAR) to judge model (after Wilks, 1995):

$$HR = \frac{(A+D)}{(A+B+C+D)} \tag{2.18}$$

$$POD = \frac{(A)}{(A+C)} \tag{2.19}$$

	Radar/Lidar grid point full (score 1)	Radar/Lidar grid point empty (score 0)
Model grid point full (score 1)	Hit (A)	False Alarm (B)
Model grid point empty (score 0)	Miss (C)	Correct Rejection (D)

Table 2.2: *Definition of skill score parameters, the letters denote the symbols used to represent these variables in the skill score equations. For an accurate comparison, the two sets of data must be on the same grid (For example, Mace* et al. *(1998) used the model vertical grid and 30 minute time resolution).*

$$TS = \frac{(A)}{(A+B+C)} \tag{2.20}$$

$$FAR = \frac{(B)}{(A+B)}. \tag{2.21}$$

Mace *et al.* (1998) presented results from these skill scores without any height dependence and with a cloud fraction threshold of zero (that is any cloud amount within a grid box counts as cloud present) over a 3–month period (the same as in described in section 2.5.3) and discovered that in all scores the model performs better than a persistence forecast and climatology, both generated from radar observations. The model would be giving a perfect forecast if HR, POD, TS were equal to unity, while FAR was equal to zero.

The hit rate displays the ratio of correct forecasts to the total number of forecasts and for the model is 0.82; however, this does not reflect the amount of non-occurrence of cloud, which is easier to forecast than cloud occurrence. The model outperforms the climatology and persistence forecasts in probability of detection with values of 0.68, as compared to 0.37 for persistence and 0.23 for climatology. However, this may be biased if the model is consistently forecasting cloud occurrence all the time, so false alarm rate is used by Mace *et al.* (1998) to assess the proportion of times the modelled cloud does not have a signal in the radar measurements. Here, a lower score is better and Mace *et al.* (1998) find that the model has a mean value of 0.45, while climatology is 0.77 and persistence 0.61.The threat score, which removes non-occurrence is thought of as the probability of correctness of a cloud forecast. This has values of 0.44 for the model, nearly double the persistence value and more than 3 times the climatological value.

As part of their analysis into the performance of the ECMWF model using LITE, Miller *et al.*

(1999) used the same skill scores as Mace *et al.* (1998). In addition, they examined the same scores by allowing the model to be 'correct' in the case of it having cloud $\pm$ 1 grid box in the horizontal or $\pm$ 1 and $\pm$ 2 grid boxes in the vertical. Their analysis was carried out over night time profiles of LITE only to avoid solar contamination and over 15 orbits of data. Assuming it is night time 50% of each orbit, this equates to about 300,000 km of data. They found the hit rate to be 0.86, rising to 0.92 when the extra grid boxes were included; the threat score was 0.56 rising to 0.80; probability of detection 0.62 rising to 0.90 and false alarm rate of 0.16 falling to 0.12 with the inclusion of the extra grid boxes. These indicate that the model is very good at getting cloud in roughly the correct places, although it is far from perfect. The statistics presented are, in each case a few percent better than the Mace *et al.* (1998) results, except for the probability of detection, which is much lower. However, Miller *et al.* (1999) make no correction for lidar extinction in deriving these scores, hence the model may have accurately forecast low clouds that could not have been detected by the lidar, but this will not be obvious from the skill scores which assume where there is no lidar signal then no cloud exists.

Instead of using skill scores previously developed, Palm *et al.* (2005) introduce their own skill score (which I have denoted Palm Skill Score (PSS)) to evaluate the ECMWF model using ICESat data as follows:

$$PSS = \frac{(A - C)}{(A + B + C + D)}. \tag{2.22}$$

By definition, this skill score can go negative, should the number of hits be less than the number of misses and its range is from -1 (all data are misses) to 1 (all data are hits). It should be noted that if the model constantly forecasts no cloud (all data are misses and correct rejections), it has a negative skill score. Palm *et al.* (2005) also increase the cloud fraction threshold to 50%, only counting cloud within a grid box that is more than half full in the lidar measurements and where model cloud fraction is greater than 0.5. The results using this score for half an ICESat orbit (about 20,000 km of data) are 0.800 for the 6 hour forecast and 0.742 for the 48 hour forecast; a degradation of the forecast skill as would be expected. Due to the different nature of the score and the 50% cloud fraction constraint, it is difficult to compare their results with other ECMWF model evaluations. The 50% score may be a little unfair on the model should for example, an ICESat grid box be 51% full and the model only have a cloud fraction of 49%, this would be counted as a miss for the model but would be a hit in the scores of Mace *et al.* (1998) and Miller *et al.* (1999). Palm *et al.* (2005) note that further work on the ECMWF model is required to fully

test its performance and that their study is only an introduction into using measurements from the ICESat satellite to validate models.

Illingworth *et al.* (2007) examine the scores used by Mace *et al.* (1998), but conclude that the hit rate and false alarm rate used by Mace are not independent of the frequency of occurrence of the event. Illingworth *et al.* (2007) suggest that a random forecast should have a skill score of zero and instead use an equitable threat score (ETS) as follows:

$$ETS = \frac{(A - E)}{(A + B + C - E)} \tag{2.23}$$

where E is the number of hits given by chance, defined as

$$E = \frac{(A + B)(A + C)}{(A + B + C + D)}.$$

Illingworth *et al.* (2007) note that the equitable threat score produces the value of 1 for a perfect forecast and zero for a random forecast and note that it varies only weakly with cloud fraction threshold. Using a cloud fraction threshold of 0.05, they evaluate the score for all the Cloudnet models (detailed in section 2.5.3), as well as a persistence forecast generated by the same method of Mace *et al.* (1998). They note that the forecast skill decreases in summer as the cloud systems become more convective and stochastic. Model skill scores range from 0.1 to 0.4 and all remain above the climatology. Due to its low sensitivity to cloud fraction threshold and low scores for random forecasts, the ETS is a better method for cloud fraction detection than the scores used by Mace *et al.* (1998), Miller *et al.* (1999) and Palm *et al.* (2005).

2.6 Future Remote Sensing of Clouds and Model Comparisons

The future holds a number of possible developments in the field of clouds and how they are represented in GCMs and NWP models. As clouds are one of the largest uncertainties in future climate, one of the most important things would be to constrain how clouds interact with radiation and give better estimates of the short wave and long wave radiative forcing of clouds. This can be done with more observational campaigns and particularly with satellites. The CloudSat and CALIPSO missions (Stephens *et al.*, 2002) are the first step in establishing global long-term profiles of clouds from space. Combined radar and lidar measurements can be used to constrain ice particle spectrum size (as in Intrieri *et al.*, 1993), and ice water content (as in Donovan and

van Lammeren, 2001). Eventually these are planned to be carried on the same platform as part of the EarthCARE mission. Dual Wavelength Ratio (Hogan *et al.*, 2000) would be useful in estimating particle size and constraining ice water content and it would be hoped that one day dual wavelength radars could be operated from space.

Simulation of radar and lidar data has been discussed and many ideas brought forward (Bony-Lena, 2006; Stephens, 2006). In the presence of thick liquid clouds, attenuation of lidar signals and some radar signals occur. In this case, simulation can allow a fairer comparison of modelled cloud to be produced. In the case of lidar operating at visible wavelengths, simulation is particularly useful as it shows how model clouds would affect incoming solar radiation. Simulation is very useful in providing a model equivalent of the measured radar or lidar signal, which allows data assimilation of the measured signals to take place.

In parameterization the sub-grid scale representation of clouds is becoming more important. Already there has been some work into expressing cloud vapour and fraction as a pdf over the grid box (e.g. Tompkins, 2002, 2006) and the treatment of cloud on a sub-grid scale is important for radiation. Improvements to the maximum-random overlap scheme seem possible given the results of Hogan and Illingworth (2000) and Mace and Benson-Troth (2002), allowing cloud layers with grid spacing closer together to have maximum overlap, but layers that are further apart to be semi-randomly overlapped, dependent on the grid spacing.

From the poorer performance of the diagnostic Météo France model in representing liquid water content (Illingworth *et al.*, 2007), the need for prognostic liquid water content is important for correct cloud representation. Splitting of cloud into different phases produces good results in the Met Office models and should continue, although work is required to make the distribution of water contents closer to the observed pdf without compensating with a loss of mean cloud fraction.

CHAPTER THREE

Doppler Radar Evaluation of Evaporating Ice in Operational Models

3.1 Introduction

The representation of ice clouds in operational weather and climate models is not only crucial to radiative transfer (e.g. Stephens *et al.*, 1990; Senior and Mitchell, 1993; Lohmann and Roeckner, 1995), but can have several implications for both the dynamics and the thermodynamics of the model. Clough and Franks (1991) suggested that the dynamics of operational models can be altered significantly by the evaporation of ice beneath warm frontal surfaces. Using simple numerical models, studies such as Clough and Franks (1991), Harris (1977) and Hall and Pruppacher (1976) suggested that due to the low bulk density and fall velocity the evaporation should, in theory, take place in a shallow layer. This rapid cooling (on the order of 1 K hour^{-1}) in a shallow layer leads to alteration of the thermal structure of warm fronts, affecting thermal advection and hence the dynamics of the front. Forbes (2002) and Forbes and Hogan (2006) examined this problem using Chilbolton 94-GHz radar observations of approaching warm fronts. They found that in the radar observations, ice crystals evaporated at the bottom of the frontal surface in a layer that was 500 m deep on average, with no evaporation layer greater than a depth of 1 km. When they examined the corresponding Met Office Unified Model data, they observed that this "evaporation zone" was 2 to 3 times the depth shown in the observations. The mis-representation of this layer means that the model does not accurately represent the cooling around the base of the ice clouds and they then showed that this can lead to the front developing incorrectly within the model. This can eventually lead to the incorrect position of the front and its associated rainbands.

Forbes (2002) re-ran several experiments using the Met Office model and suggested several candidates that may cause the poor representation of this layer in the model. These are as follows:

- The model vertical grid resolution may be too low at cirrus altitudes, and so does not allow for a sharp decrease in prognostic variables such as ice water content. The current Met

Office operational model has a vertical grid spacing between 500 and 700m in the mid-troposphere and so it is not possible to resolve depth scales less than this at ice cloud altitudes.

- The relative humidity in the model may be too great beneath the evaporating ice cloud. This incorrect representation of the humidity gradient in the model would lead to an ice particle evaporation rate that is much too low, and hence the particles falling further before they completely evaporate.
- The model's ice particle terminal fall speed may be much too high or the numerics in the model much too diffusive. A higher fall speed will lead to the ice crystals falling further before they have evaporated. This may also be due to numerical problems with the ice sedimentation term.
- The model's parameterized ice evaporation rate may be much too low, due to other micro-physical assumptions, leading to greater evaporation depth scales.

In addition to these reasons, the effect of turbulence on the evaporation zone has not been examined. The Met Office model only contains turbulence within the boundary layer. However, at the base of thick ice cloud, the air can be very turbulent (Harris, 1977; Bouniol *et al.*, 2003). As the ice crystals evaporate from the base of the ice cloud into drier air, there is some significant cooling that occurs, which can trigger convective instability and lead to turbulence. This turbulence will increase the amount of entrainment of clear, dry air that could increase the evaporation rate of the crystals. As this effect is not represented in the model, the model may underestimate the parameterized evaporation rate and overestimate the depth of the evaporation zone. Therefore one additional candidate for the increased evaporation zone depth can be added to the list:

- The model does not account for the increased evaporation rate caused by vigorous turbulence generated by the ice crystals evaporating from the ice cloud into the dry air beneath.

Forbes (2002) performed a sensitivity study by modelling a front in one dimension (height). Part of this experiment involved decreasing the model vertical grid spacing to test whether the model vertical grid resolution was adequate. Starting with a model with an increased vertical resolution of 70 layers, he re-ran the model and then gradually decreased the number of levels down to the operational level of 38. The results from various resolutions could then be compared.

He noted that there was only a 30% increase in the depth of the evaporation zone. Therefore, some process in the microphysics of evaporating ice is not being accounted for in the model.

Forbes also compared the humidity profiles in the model with those obtained from radiosonde launches from the nearby Larkhill radiosonde station. His studies showed that on average, the relative humidity in the model appeared to be too high just below the frontal surface. He noted that this would have a large impact on the evaporation depth scales, but could not say categorically whether the increased evaporation zone depth was due entirely to this factor or whether another factor in the microphysics was also important.

Since the study, the 94-GHz radar at Chilbolton has been updated to measure the vertical Doppler velocity parameters as well as standard radar reflectivity (Z). These extra parameters include the Doppler fall velocity, which can be used to examine the fall velocity of the evaporating ice crystals and the standard deviation of mean Doppler velocity, from which the turbulent kinetic energy dissipation rate can be inferred, using the method of Bouniol *et al.* (2003). Thus, other candidates for the deeper model evaporation depth scale, such as incorrect parameterized fall velocity and levels of turbulence can be examined in order to try and find the reason why the evaporation of ice beneath ice clouds is poorly represented in the Met Office model. This extra information has also been of value in studies of ice clouds and in particular the boundary between the ice cloud and clear, dry air beneath.

In addition to the work covered by Forbes (2002), the existence of a 94-GHz radar and model data can be used to develop our knowledge of ice cloud. Several cloud products have now become available as part of the Cloudnet project. This enables an examination of various properties of ice clouds, such as the variance in ice water content and the change in turbulent kinetic energy through the ice clouds. Not only can this data further our knowledge of ice clouds, but it can be used to study how operational models other than the Met Office represent the evaporation zone, and find out if the problems discussed are limited only to the Met Office model or are common between all models.

In this chapter, the various candidates for the increased evaporation zone depth in the model are examined. Section 3.1.1 contains details about the structure of a warm front. Section 3.2 discusses the basic principles and equations used in the Met Office parameterization scheme. Section 3.3 is an introduction to the radar and model data and their capabilities, while section 3.4 describes the method that was used to compare the two different sets of data. In section 3.5,

the ice crystal fall velocity and its representation in the Met Office model is studied. In section 3.6, the role of turbulence on evaporation zone depth is examined, to see if this is the reason for the increased evaporation zone depth in the Met Office model. In section 3.7 the role that density plays within the model, is looked at by re-running the model parameterization scheme with several different density functions. In section 3.8 the representation of humidity in the model is studied, in order to see if the model can correctly represent the sharp drop in relative humidity that occurs beneath the evaporating ice cloud. The model's evaporation rate is also critically analysed— how does it react to a sharp change in humidity over one grid box? Section 3.9 presents results of the depth of the evaporation zone for other models— do other European operational models all suffer from an artificially increased evaporation zone depth? A summary of the results from all sections is provided in section 3.10.

3.1.1 Structure of a Warm Front

Warm fronts occur as part of mid-latitude cyclones, and both have been studied extensively for many years (e.g. Wexler and Atlas, 1958; Harris, 1977; Browning and Monk, 1982; Browning, 1983; Browning *et al.*, 1995; Clough *et al.*, 2000). The flow of cold, dry air beneath the warm frontal surface has been illustrated many times (e.g. Browning and Monk, 1982; Browning, 1985). Figure 3.1 shows a conceptual model of a mid-latitude cyclone from Browning and Monk (1982). Plot (a) shows the plan view of the cyclone and the location of the major flows of moist and dry air through the cyclone can be seen, including the warm conveyor belt, which flows along the cold front and then down the surface of the warm front. The location of the warm and cold fronts, as well as the upper cold front are shown. Looking at the cross-sections in plots (b) and (c), the warm conveyor belt can be seen rising along the slope of the warm front, and is shown by the highest values of wet bulb potential temperature (θ_w). There is a sharp change in θ_w across the frontal surface and dry, cold air can be seen to flow from ahead of the warm front towards the frontal surface. Using radiosonde measurements, Taylor *et al.* (1983) show that the warm front is indeed a very sharp boundary between cold, dry air beneath the front and warm, moist air above the frontal surface. Browning (1985) show that precipitation occurs across most of the warm front. At warmer temperatures, this precipitation will be liquid, but at higher altitudes, the air will be much cooler. This is the level at which ice will fall and sublimate into the dry layer beneath. This sublimation of ice beneath approaching warm fronts has been studied many times

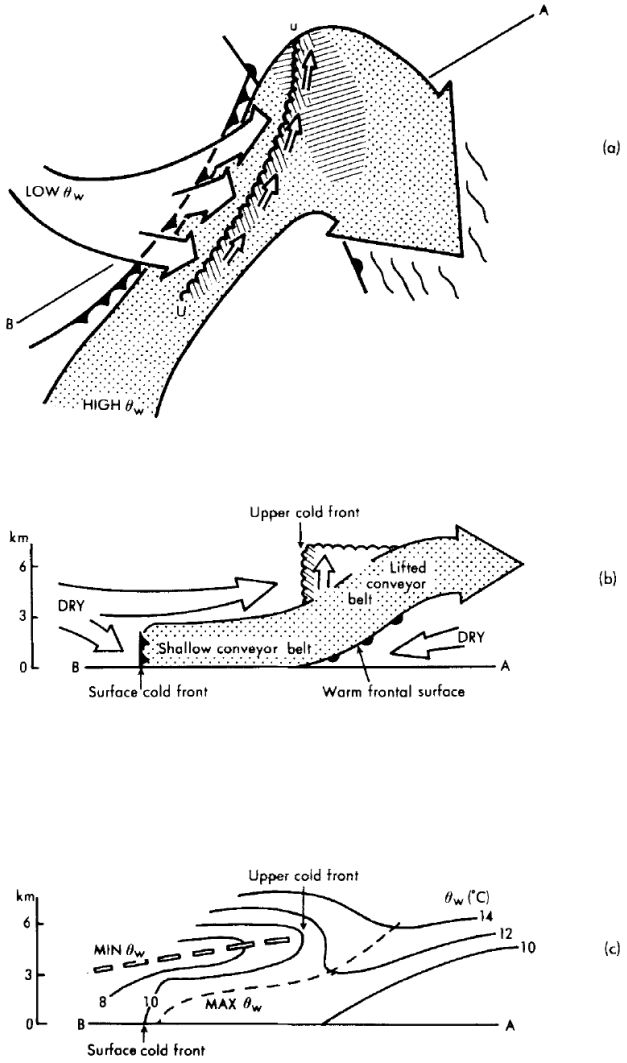

Figure 3.1: *(a): Plan view of a conceptual mid-latitude cyclone showing the location of the warm and cold fronts, upper level cold front and low wet bulb potential temperature (θ_w) air passing through the cold front. (b) Cross section through the fronts, showing the inflow of dry air ahead of the warm front. (c) Cross section of wet bulb potential temperature, with high values of θ_w corresponding to moist air. From Browning and Monk (1982).*

before (e.g. Harris, 1977; Clough and Franks, 1991). Clough and Franks (1991) hypothesise that the evaporation will take place in a shallow layer. They envisage that as the frontal surface is a boundary between dry air and moist air, there will be rapid ice sublimation, and this will lead to air descending beneath the front. This process is illustrated in figure 3.2. From this "Clough and Franks" mechanism shown in figure 3.2, localised circulations within the vicinity of the front have

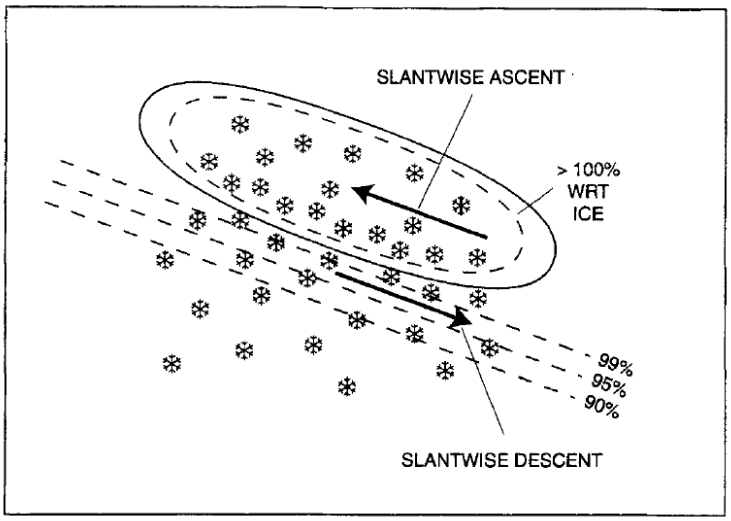

Figure 3.2: *Schematic figure showing the slantwise ascent and descent mechanism suggested by Clough and Franks (1991). Dashed contours show relative humidity with respect to ice. From Clough* et al. *(2000).*

been suggested to occur. This has been supported by observational evidence (Clough and Franks, 1991; Thorpe and Clough, 1991). In addition, Bouniol *et al.* (2003) show that the boundaries of clouds can be very turbulent, which is possibly caused by sharp cooling of the air as ice particles evaporate. They derive a method for measuring the turbulent kinetic energy dissipation rate within clouds, which shall be used later in this chapter.

3.2 Model Parameterization Scheme

In order to see how well the Met Office model is representing the ice evaporation zone, the assumptions made in the ice parameterization scheme will be used (whether they are right or wrong) to simulate radar reflectivity (Z) and Doppler velocity (V_{Dop}) from model ice water content. If the model parameterization scheme is wrong, and this is the cause of the deeper evaporation zone in the model, then this will show in the analysis.

The ice parameterization scheme used in the Met Office Unified Model is detailed in full in Wilson and Ballard (1999). The model carries IWC as a prognostic variable, using an exponential ice particle distribution as follows:

$$N(D) = N_0 e^{-0.122T} e^{-\Lambda D} = N(T) e^{-\Lambda D}, \tag{3.1}$$

where $N(D)$, the number concentration is a function of D, the particle diameter, T in °C and $\Lambda = \frac{3.67}{D_0}$, where D_0 is the equivolumetric median diameter. The model assumes that $N_0 = 2\times10^6$ m^{-4} and the mass of an ice particle is parameterized as

$$m(D) = aD^b, \tag{3.2}$$

where $a = 0.069$ kg m^{-2} and $b = 2.0$. All particles in the model are assumed to be spheres. Ice particles can have a variety of habits, which generally depend on air temperature. However, for evaporation studies which take place at the base of the cloud, there is evidence (Field and Heymsfield, 2003; Westbrook *et al.*, 2007b) that in this region, the dominant particle type are aggregates. Hence, a spherical particle approximation can be seen to be reasonable. Using equation 3.2, the density of the crystals in the model can be defined as

$$\rho_i = 0.13D^{-1} \tag{3.3}$$

where ρ_i is the crystal density in kg m^{-3} and D is in m. This equation is very similar in form to that proposed by Brown and Francis (1995): $\rho_i = 0.07D^{-1.1}$, but there is a factor of two difference in the resulting density. In this simulation, ice density is capped at the density of solid ice, which prevents the formation of superdense ice. Section 3.7 examines the effects of the depth of the evaporation zone and the quantities Z and V_{Dop} by changing the density function in equation 3.3. The model parameterization for the mass of ice is also given as a function of D. Thus, ice water content (IWC) can be expressed as

$$\mathrm{IWC} = \int_0^\infty N(D)m(D)dD. \tag{3.4}$$

The information obtained from equations 3.1 & 3.3 can be used to simulate the radar reflectivity, (Z), using equation 2.8, and Doppler Velocity of the crystals, (V_{Dop}), as follows:

$$Z = \int_0^\infty \frac{|K_{ice}|^2}{0.93}\gamma(D)N(D)D^6dD, \tag{3.5}$$

$$V_{\mathrm{Dop}} = \frac{\int_0^\infty |K_{ice}|^2N(D)\gamma(D)v_c(D)D^6dD}{\int_0^\infty |K|^2N(D)\gamma(D)D^6dD}. \tag{3.6}$$

The term γ in equations 3.5 & 3.6 represents the Mie to Rayleigh ratio and is a function of diameter, with values ranging from 0 to 1. For small ice crystals ($D \leq 0.1$mm), Rayleigh scattering is

assumed, but the value of γ drops sharply from 1 to 0 as diameter increases, oscillating just above zero for diameters of 2 mm or larger. Despite the values of Z and V_{Dop} being much smaller for these larger diameters when compared to Rayleigh scattering, there may still be some important contribution via the D^6 term in both equations. $|K_{ice}|^2$ is the dielectric factor of the ice particle, which is proportional to its density squared. The value of 0.93 is the dielectric factor for liquid water.

The term $v_c(D)$ in equation 3.6 refers to the fall-speed of an ice particle of diameter D, parameterized as

$$v_c(D, \rho_a) = \alpha D^{\beta} \left(\frac{\rho_0}{\rho_a}\right)^{0.4} \tag{3.7}$$

where $\alpha = 25.2$ m$^{0.473}$s^{-1} and $\beta = 0.527$. Since the air density is not always constant at 1 kg m^{-3}, the correction used in Wilson and Ballard (1999) is incorporated into 3.7. The air density calculated from the model's pressure and temperature fields is ρ_a, while ρ_0 is a density of 1 kg m^{-3}. The form of equation 3.7 originates from Locatelli and Hobbs (1974), who found it to be a reasonable approximation for a variety of different single particle habits. In a study modelling precipitation in frontal rainbands, Cox (1988) took α to be 16.8 m$^{0.473}$s^{-1} and β to be 0.527 for ice particles as when integrated over the whole particle spectrum the relation agreed with fall-speeds for ice observed by Heymsfield (1977). Also, the fall velocity used within the model tends to be a favourite tuning parameter. By varying the values of α, and in some cases β, the lifetime of the model cloud can be controlled. The values of α and in equation 3.7 was increased from the Cox (1988) value to allow the lifetime of clouds in corresponding climate model simulations to be roughly correct and as the velocities produced at different temperatures agreed better with observed values after the air density correction was applied (R. M. Forbes, Personal Communication). The method used to calculate Z and V_{Dop} from IWC is straightforward. At each grid box, the model value of IWC is calculated from the ice water mixing ratio (q_i) according to

$$\mathrm{IWC} = \frac{pq_i}{RT}, \tag{3.8}$$

where p is the pressure, R is the gas constant for dry air and T is the temperature. The variation in Z and V_{Dop} with IWC and temperature for Rayleigh scattering is shown in figure 3.3 while the variation of these quantities assuming Mie scattering at 94-GHz is shown in figure 3.4. Using values of D from 0 to 20 mm, which represent the full spectrum of ice crystals observed in nature, equations 3.4, 3.5 and 3.6 are used to calculate values of IWC, Z and V_{Dop} for values of

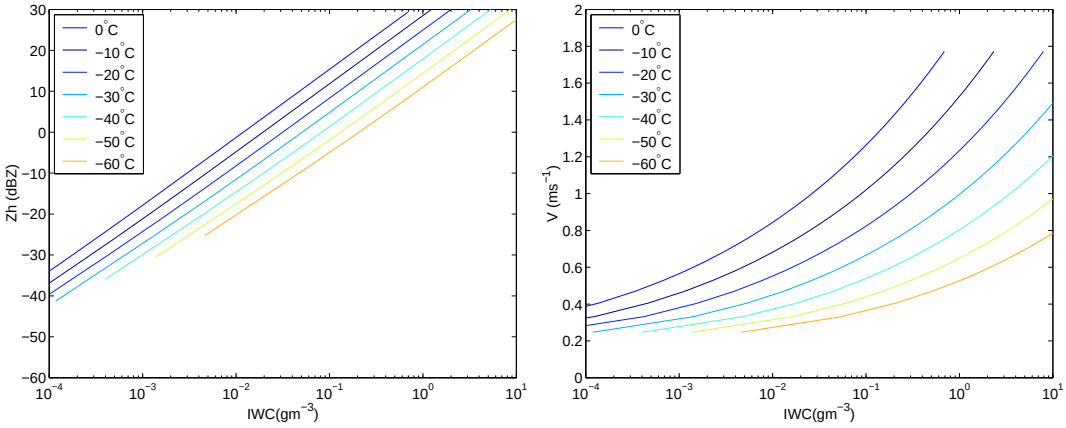

Figure 3.3: *Variation of Z (left) and V_{Dop} (right) with IWC and temperature for Rayleigh scattering at 94 GHz with D_0 ranging from 0 to 5mm. Ice water content increases with D_0, so that a given temperature, the lowest IWC values correspond to the smallest values of D_0. In these figures, Rayleigh scattering is assumed by setting the value of γ to 1 in equations 3.5 and 3.6.*

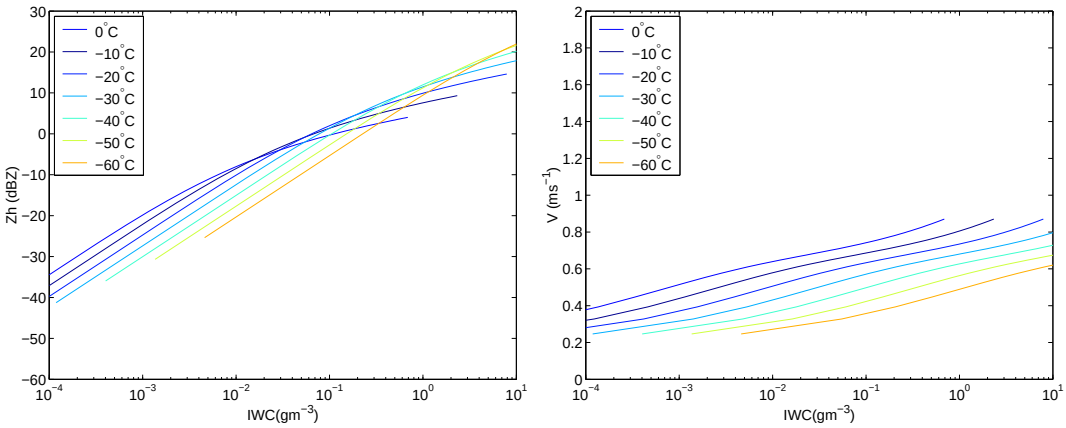

Figure 3.4: *Variation of Z (left) and V_{Dop} (right) with IWC and temperature for Mie scattering at 94-GHz with D_0 ranging from 0 to 5mm. As in figure 3.3, the lowest values of IWC correspond to the smallest values of D_0. Mie scattering has been simulated by reducing the value of γ from 1 towards zero, dependent on particle diameter.*

D_0 between 0 and 5mm, and for a temperature of 0°C. There is some modification to both Z and V_{Dop} when Mie scattering is assumed, and in particular it is worthwhile noting that Mie scattering actually reduces the velocity by as much as 50% at a given temperature. Mie scattering affects the calculation of Z at higher temperatures. Analytical solutions are available to relate Z to IWC for Rayleigh scattering; Z is roughly proportional to IWC$^{5/3}$ and V_{Dop} is roughly proportional to $\Lambda^{0.527}$, but when Mie scattering is included , only numerical solutions are possible.

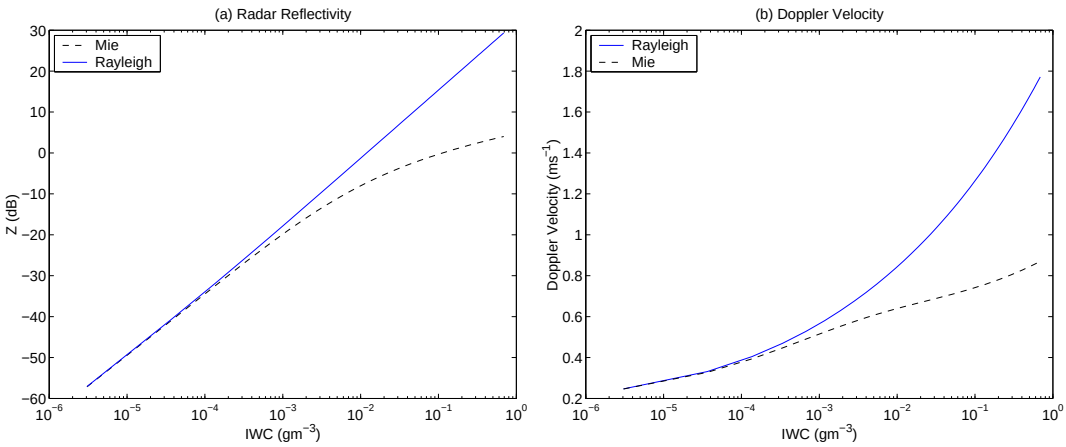

Figure 3.5: *Plots of the model parameterization results of IWC versus Z (left) & V_{Dop} (right) for a temperature of 0° C.*

As the wavelength of the 94-GHz radar is roughly 3 mm and D_0 ranges from 0 to 5 mm, the assumption used for Rayleigh scattering that the wavelength is much bigger than the mean particle size is no longer valid. Hence all calculations of Z and V_{Dop} from now on include Mie scattering. In order to calculate Z and V_{Dop} from the model without needing 2D interpolation, the values of IWC for a given temperature that have been obtained from model data are then scaled to the equivalent value of IWC at 0°C (IWC$_{T=0}$) by dividing by a scaling factor, s ($= \exp(-0.122T)$), where T is in °C. The plots of IWC versus Z and IWC versus V_{Dop} for 0°C are shown in figure 3.5. The obtained value of IWC$_{T=0}$ for each grid box can then be converted into a value of $Z_{T=0}$ and a value of V_{Dop} using 1D interpolation and assuming Mie scattering. Since the radar reflectivity factor is temperature dependent, the value of $Z_{T=0}$ must be converted to a value of Z by s. Since equation 3.6 has the $N(D)$ terms on both the top and bottom of the equation, it is independent of temperature and hence the V_{Dop} value does not need to be scaled by the temperature factor. Thus, values of Z and V_{Dop} are obtained and can be compared with the radar measurements as described in section 3.4.

3.3 Description of the Radar and Model Data

3.3.1 94-GHz Radar Data

The instrument used for this study is the vertically-pointing 94-GHz radar at the Chilbolton Observatory in Hampshire. Since July 2001, it has been able to measure Doppler parameters in addition to the standard radar reflectivity (Z). It operated continuously (apart from short periods of occasional maintenance) between January 2003 and March 2004, and thus provides a long data set of the presence and microphysical properties of ice cloud; the data for this chapter is taken from this period. The three parameters used in this study are:

- **Radar Reflectivity (Z)**

  This parameter is the intensity of the echo returned to the radar after backscatter from the ice particles. It is defined as in equation 3.5. High values of reflectivity (values of Z greater than 5 dBZ in this example) occur in rain, or melting ice, while typical ice cloud only has reflectivity values of around -10 dBZ in the example shown in figure 3.6; it should be noted that these values vary between cases. It is possible to obtain estimates of IWC from Z and temperature, using analytical formulae as suggested by Liu and Illingworth (2000) and taken further by Hogan *et al.* (2006); this is the reverse of the model parameterization scheme, which takes IWC and simulates Z as described in section 3.2. Figure 3.6 shows the image of Z taken through an approaching warm front on 23 January 2004. The descending cloud base associated with the warm front can be seen, and the rain associated with this front is shown from 17.00 UTC onwards. The highest reflectivity values between 1100 and 1700 UTC indicate the position of the ice particles which are evaporating into dry air beneath.

- **Doppler Velocity (V_{Dop})**

  This is a measure of the reflectivity-weighted vertical velocity of the crystals as they fall from the cloud. However, the Doppler fall velocity measured by the radar (V_{Dop}) is a sum of the vertical air velocity and the actual ice particles' terminal velocity. This means that in the presence of strong updraughts or downdraughts, such as in the turbulent evaporation zone, there is an error on the measured terminal velocity due to movement of air. Figure 3.6 shows the Doppler velocity of the 23 January 2004 case. This shows that the particles

have low velocities within the ice cloud, but the fluctuation of the velocity increases in the evaporation zone. The heavy rain from 17:00 UTC onwards has the highest fall velocity. As well as showing the velocities of the falling ice crystals, V_{Dop} can be used to distinguish rain from falling ice and thus any data with very high fall velocities and high reflectivity values can be rejected as rain.

- **Standard Deviation of Mean Doppler Velocity ($\sigma_{\bar{\mathrm{v}}}$).**

  This is an indication of the turbulence of the air. It is the 30-second standard deviation of 1 second mean Doppler velocities. As the pulse repetition frequency of the radar is 6520 Hz, in each second 6520 samples are used to calculate the mean Doppler velocity and then 30 samples of mean Doppler velocity are used to calculate the standard deviation of mean Doppler velocity at the 30-second radar time resolution. The values of $\sigma_{\bar{\mathrm{v}}}$can be converted into a turbulent kinetic energy dissipation rate (ϵ) by the method of Bouniol *et al.* (2003). This method consists of taking measurements of $\sigma_{\bar{\mathrm{v}}}$, and large-scale horizontal model wind to work out the intensity and size of the eddies being sampled, which then in turn can be related to the turbulent kinetic energy (TKE) dissipation rate (ϵ), using a Kolmogorov spectrum. Figure 3.6 shows a plot of $\sigma_{\bar{\mathrm{v}}}$ for the 23 January 2004 case. The red colours show the very turbulent air within the evaporation zone, while the blue colours within the ice cloud show that the eddies of a particular size have less energy and thus less velocity variance associated with them. Hence there is less dissipation of TKE. This data can be used to test the theory that the mis-representation of turbulence in the Met Office Unified Model is the cause of the deeper evaporation zone within the model. This will be discussed in section 3.6, where the relationship between the depth of the evaporation zone and ϵ will be examined. Although there are alternative methods of deriving turbulence from Doppler spectral width (Chapman and Browning, 2001; Kollias *et al.*, 2001), another parameter available from the 94-GHz Chilbolton cloud radar, the results obtained from this method may be biased due to the contribution from the spread of terminal velocities in the particle size distribution. Hence the method of Bouniol *et al.* (2003) is used in the study.

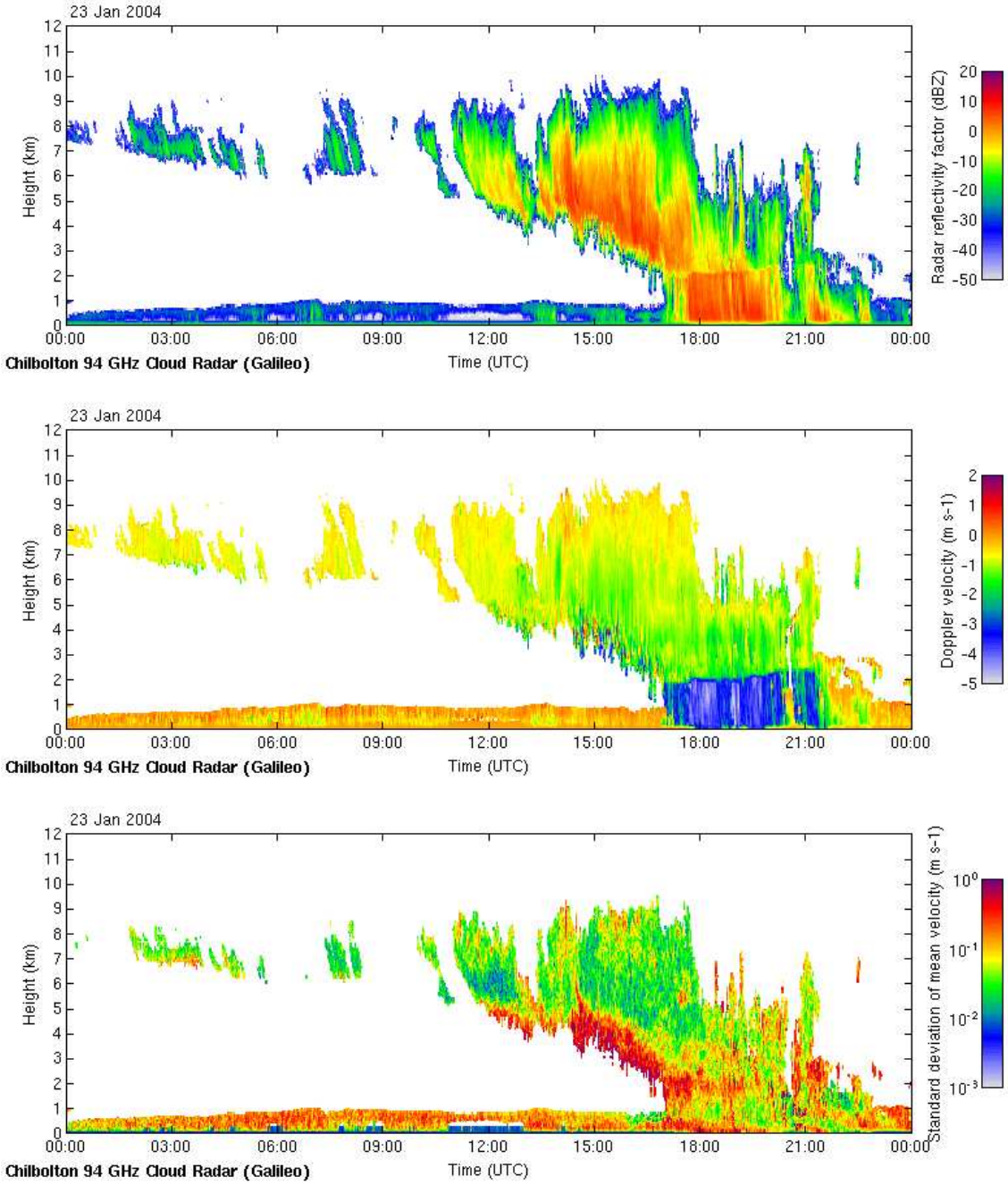

Figure 3.6: *Radar Parameters on 23 January 2004. Top is radar reflectivity, middle is Doppler Velocity and bottom is standard deviation of mean Doppler velocity. A very comprehensive database of warm fronts and other cloud occurrences is available as quicklooks on the Cloudnet website. Go to http://www.cloud-net.org/ for more details. Also available are the corresponding model data and selected products, such as ice and liquid water contents, particle size and turbulent kinetic energy dissipation rate*

3.3.2 Met Office Model Data

The model used in this study is the Met Office Unified Model at mesoscale resolution (approximately 12 km). The model time series is generated by taking hourly vertical profiles of the grid boxes that lie above Chilbolton, from 6–11 hour forecasts. These hourly snapshots give values of model wind, temperature, relative humidity and ice water content (IWC). The microphysical cloud parameterizations used in Wilson and Ballard (1999), which have been discussed in detail in section 3.2, are used to obtain radar reflectivity (Z) and Doppler velocity V_{Dop} from the Met Office data, so that they can be compared with the radar data.

3.3.3 Selection of Data

The data are selected from a variety of cases of evaporating ice taken over a one-year period from January to March 2004. Each day was examined by eye and the following criteria were used to select cases used in this study:

- **Ice cloud thickness and duration**

  Cases were divided into individual hours of data, and for an hour to be retained for analysis, it had to show ice cloud with ice evaporating into the layer below. The duration of the ice clouds had to be at least 2 hours and the cloud had to be at least 2 km thick. Any period with no ice cloud, or ice cloud that was less than 2 km thick or did not last for more than 2 hours were rejected from the study.

- **Absence of Rain**

  Any hours that contained any rain amongst the ice data were rejected, even if there was ice present above the falling rain. This is because the radar signal is significantly attenuated by the falling rain (see figure 2.2 and associated discussion in chapter 2) and any ice data above the rainfall were usually of poor quality and not reliable enough to analyse. Also, in the cases where there is rain reaching the ground, as from 17.00 UTC in the example shown in figure 3.6, there will be no evaporation of ice into dry air.

- **Ice data only**

  The temperature in each ice water content profile should remain below 0°C so that the measurements from the radar are indeed ice and not liquid water cloud. Mixed phase cloud

is also rejected using data from the Chilbolton 905-nm lidar ceilometer to locate the presence of liquid water in the radar data. This shows as strong lines of attenuated backscatter superimposed within the ice cloud. Any data suspected to contain supercooled water was removed.

3.3.4 Definition of an Evaporation Zone

The depth of the evaporation zone is defined by the same method as Forbes (2002). The evaporation zone is said to be the region between the maximum IWC and the height below where the IWC had decreased to 10% of this maximum (i.e. 90% of the ice had evaporated from the profile). In each profile, the ice should completely evaporate just below the bottom of the evaporation zone, and profiles where there is liquid water cloud (where the temperature rises above 0°C before the bottom of the evaporation zone is reached) were rejected.

3.4 Methodology

To compare radar data, (which has a 30 second time resolution and 60 m vertical resolution), with model data, (which has a one hour time resolution and a vertical resolution that varies from 500 m to 750 m in the mid-troposphere), would be rather difficult due to the large difference between the two grids. To overcome this problem, it is necessary to perform some sort of averaging that allows a justified and fair comparison between the data obtained from the radar and the model. However, performing long temporal averages through sloping ice cloud causes problems. An average at constant height will average clear air ahead of the approaching front, and as the cloud base descends, the average will include the cloud base and evaporation zone as well as the mid-cloud regions and possibly even clear air above the descending cloud. This means that the end result is somewhat biased, tending to overestimate the depth of the evaporation zone. Since this is the quantity of interest, it is important that correct measurements of this are made. To solve this problem, adjustment of each radar and model profile takes place after the averaging of the radar data on to the hourly model grid has taken place. The process is described in detail below:

1. The radar data are averaged to a one-hour resolution, consisting of 120 radar profiles of 30 seconds duration. The vertical grid resolution remains the same. This horizontal averaging

removes some of the effects of updraughts and downdraughts on the vertical velocity within the cloud.

2. The model data are linearly interpolated on to the radar height grid. This sets the model data and radar data to the same vertical resolution which allows a fair comparison.

3. The profiles of both radar and model are adjusted vertically to account for the slope in approaching warm fronts. This is done by finding the height of the maximum reflectivity value in each hourly radar or model profile and shifting it up or down, so that the maximum value occurs at an adjusted altitude (z_{adj}) of zero.

The entire process is shown in figure 3.7. As well as adjusting the reflectivity (Z), all the other measured and derived quantities such as Doppler fall velocity, turbulent kinetic energy dissipation rate, ice water content, and model crystal fall velocity are averaged and adjusted. However, each profile is adjusted using the maximum reflectivity only, and not each individual quantity maximum. So for example, the V_{Dop} measurement that lies at z_{adj} of zero in each profile is not the maximum value of V_{Dop} in that profile. Instead, it is the value of V_{Dop} that is at the same altitude as the maximum value of Z in that profile.

Once this procedure is complete, it is possible to time-average the entire data set and produce a profile of the mean radar reflectivity and fall velocities versus height relative to the peak in Z.

3.5 Profiles of Radar Reflectivity and Fall Velocity

As mentioned in section 3.4, a comparison can be made between the radar and model reflectivity (Z). Also, a similar comparison can be made between the Doppler fall velocity (V_{Dop}) obtained from radar measurements with the Z-weighted fall velocity obtained from the model parameterization. Looking at the profile of radar and model reflectivity over the 89 hour period (figure 3.8), it can be seen that the values of Z from the model are about 30% (3 dBZ) too large on average. This could be a result of wrong values of ice water content in the model or could be due to an incorrect parameterization within the model. The larger density function noted earlier could be the cause; this shall be examined later in section 3.7.

The key result that is shown in figure 3.8 is that the model crystal fall velocity is 30% lower than the Doppler fall velocity (V_{Dop}) measured by the radar. This could be due to an incorrect

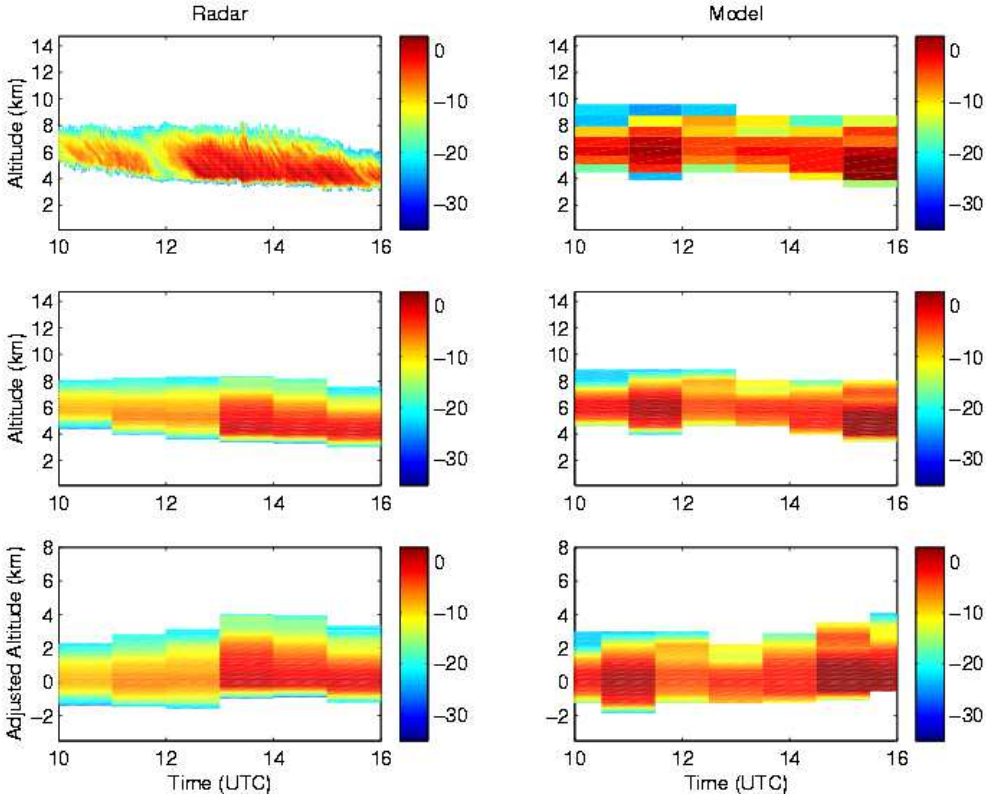

Figure 3.7: *Transformation of radar and model reflectivity (Z) data from 4 March 2004 to allow fair comparison. Radar data are shown in the left column, model data on the right. The raw data is on the top row. The centre row shows the result of averaging the radar data to a 1 hour resolution, while the model data was interpolated over a radar height grid. The bottom row shows the result of the adjusting of both data sets. Each profile is set with maximum Z at z_{adj} of zero.*

model parameterization, but in order to see if this is the case, we need to eliminate the effects of updraughts and downdraughts that are present in the data. This is discussed in section 3.5.1.

3.5.1 Preferential Sampling of Updraughts and Downdraughts within the Radar Data

When making a comparison between radar and model Doppler velocity, it is important to note the effects of vertical wind on the radar data. The Doppler fall velocity measured by the radar can be broken down into two components:

$$V_{\mathrm{Dop}} = v_a + v_t. \tag{3.9}$$

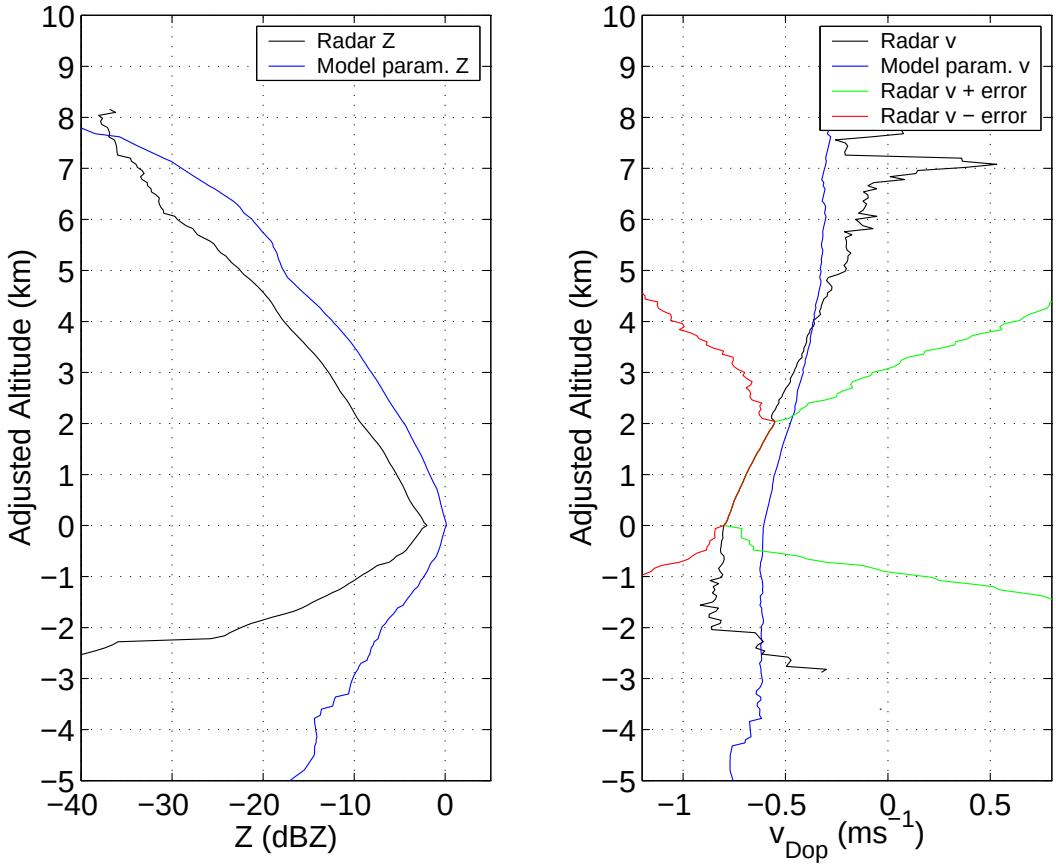

Figure 3.8: *Profiles of Z (left) and V_{Dop} (right) averaged over 89 hours. The red and green lines on the Doppler fall velocity plot give an estimate of the error on the radar fall velocity due to preferential sampling of updraughts and downdraughts throughout the cloud, discussed in section 3.5.1.*

The components are due to the vertical air velocity (v_a), and the Z-weighted mean ice particle terminal fall velocity (v_t). The air velocity within ice cloud can vary from a few cm s^{-1} to 2 m s^{-1}. A typical ice particle terminal fall velocity is on the order of 1 m s^{-1}. Although initially it may appear that updraughts and downdraughts present a large error in the data, it is possible to study an area of the ice cloud where the air vertical velocity is small, or where the updraughts and downdraughts will average out over a long period of time so the mean vertical velocity is small. This last statement is true for the middle of the cloud. The radar V_{Dop} data has been averaged over one-hour periods. By doing this, it is assumed that in the middle of the cloud, the vertical air velocity is entirely due to the ascent rate of the air in the warm front, which is typically of the order of a few cm s^{-1} (Browning, 1983), so that $\bar{v_a} << \bar{v_t}$.

In the future, it may be possible to obtain measurements of v_a directly by using a clear air

radar, pointing at zenith. Although such a radar exists at the Chilbolton observatory, it is only used on an event basis and therefore no data of this type was available during the year-long 94-GHz radar data set used in this study.

Figure 3.9 shows Doppler velocity measurements of an ice cloud on 23 January 2004. In the evaporation zone there are areas of high downdraughts and one or two updraughts. Fingers of strong downdraughts can be observed extending below the base of the ice cloud. In between these downdraughts, there are dry, clear areas, with no radar echo. Since the 94-GHz radar can only detect velocities of particles and not of clear air, this area shows up as being empty and free of updraught. By taking a horizontal average through this area means that only the downdraughts which are visible to the radar will be included in the average and so an average will tend to overestimate the ice particle fall velocity in this area. In the middle of the cloud, there are no clear pockets and so the updraughts and downdraughts will average out over time. To see where the data are reliable, in addition to showing an average of just the cloudy region, any clear areas within the cloud were filled with Doppler velocities of +2 m s^{-1} and -2 m s^{-1} before each set of data is averaged. The results are the red and green lines in figure 3.8. Where these two lines agree exactly with the radar velocity curve, the data are reliable and where there are biasing areas of clear sky, the red and green lines diverge from the mean radar velocity. Data from the areas where the red and green lines agree is defined as the mid-cloud region. This exists as a result of the condition set in section 3.3.3 that the ice cloud must be at least 2 km thick. Section 3.5.2 examines the differences between the model parameterized fall velocities and radar fall velocities in the middle of the cloud and within the evaporation zone.

3.5.2 Using Velocity Measurements in the Middle of the Cloud to Test the Accuracy of the Model Parameterization

In order to test the accuracy of the Met Office parameterization scheme, model and radar Doppler velocities have been compared for grid boxes (1 hour in time versus 60 m vertical) within the middle of the ice cloud and within the evaporation zone. In order to see how well the model parameterization performs with different particle sizes, the velocity values have been plotted against the reflectivity values. Due to the large amount of data, the fall velocities have been binned into 1-dBZ bins, with the mean, standard deviation and range of the data shown. Figure 3.10 shows the results for the middle of the cloud, and the results for the evaporation zone. By examining

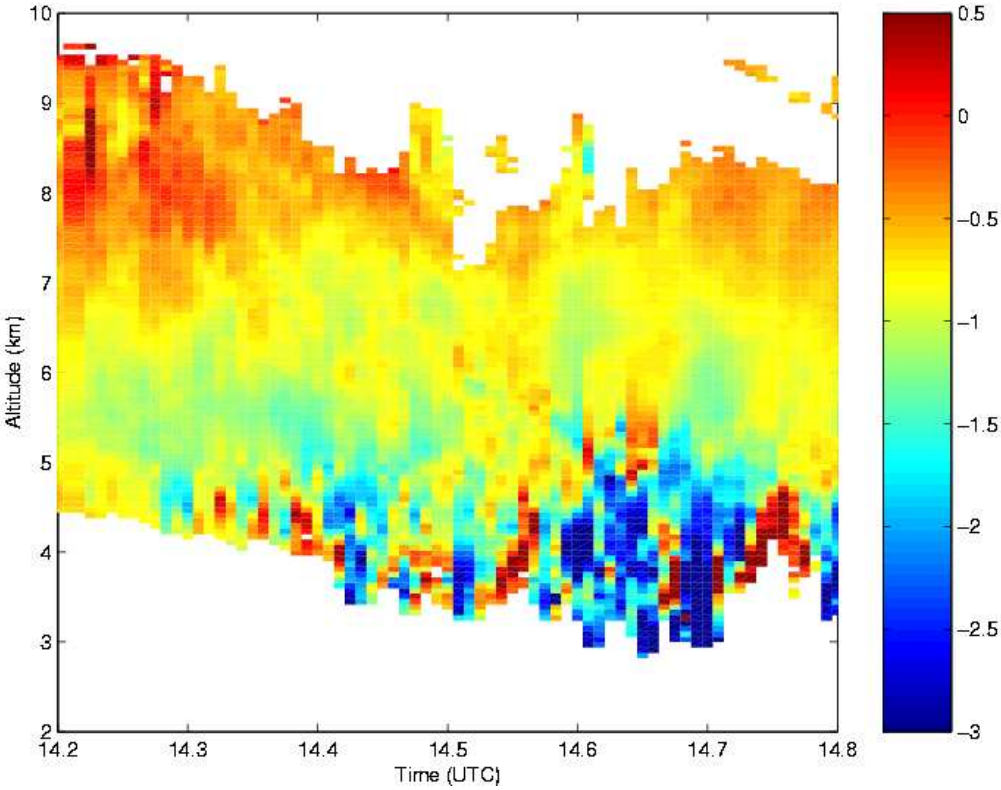

Figure 3.9: *The structure of Doppler velocity (V_{Dop}) in a ice cloud, observed on 23 January 2004. Around the base of the ice cloud and in the evaporation zone, there are large vertical velocities. In the middle of the cloud, the vertical velocity of the particles is much less, due to the absence of strong updraughts or downdraughts. The Doppler velocity in these areas is very close to the terminal fall speed of the ice particles, and so data from the mid cloud region can be used to test the performance of the model's ice crystal fall velocity parameterization. Where there is clear sky close to the edge of the ice cloud, any averaging will be biased.*

the plot for the middle of the cloud, it can be seen that for low values of Z (small particles), the model accurately predicts the observed values of V_{Dop} . Above Z values of -15 dBZ, the model crystal fall velocities are up to 50% less than those observed by the radar. Thus, the difference in radar and model fall velocity above z_{adj} of zero in figure 3.8 appears to be entirely due to the model poorly representing the larger particles.

Looking at figure 3.10b, which shows the comparison between model and radar fall velocities in the evaporation zone, it can be seen that the radar fall velocities are always much greater than the model values. This is due to the preferential sampling of downdraughts when averaging radar data to a one hour horizontal resolution.

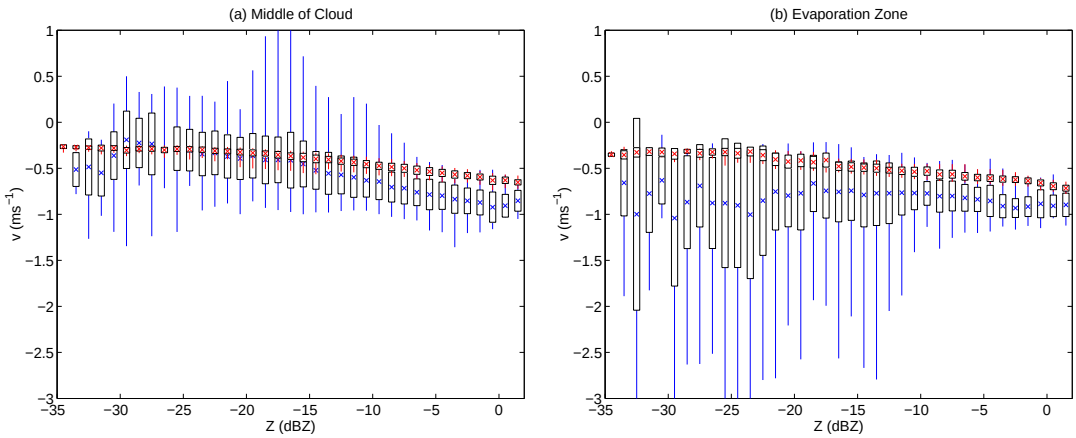

Figure 3.10: *Hourly averaged Z and V plots for (a) the middle of the cloud and (b) the evaporation zone. The data are binned into 1 dBZ bins, with the model data in red and the radar data in blue. The mean Doppler velocity in each bin is shown with a cross, the standard deviation about the mean in each bin is shown by the edge of each box. The whiskers show the range of the data.*

From the comparison made for the middle of the cloud, it appeared that the model parameterization was making a reasonable job of representing the radar Doppler fall velocity. If one assumes it behaves in the same way within the evaporation zone before the effects of the vertical air velocity were included, then it would appear that the model does not have the ice particles falling out too fast. In fact, as can be seen in figures 3.8 & 3.10 the model parameterization generally has the ice particles falling out too slowly. Forbes (2002) suggested that the evaporation zone depth would scale linearly with ice particle fall velocity— so to have an evaporation zone in the model with a depth of 2 to 3 times that in the radar data, a model ice particle fall velocity of 2–3 times the radar fall velocity would be required. Even with a strong downdraught present in the radar data shown on the right hand plot in figure 3.10, there is no way that a velocity of 2–3 times the radar fall velocity could occur. It is very unlikely that large-scale updraughts and downdraughts in ice cloud would be larger than 20 cm s^{-1}, so the model parameterized particle fall velocity can be ruled out as the reason for the deep evaporation zone within the model. In fact, if the model's parameterized fall velocity were increased to match the radar measurements, this would increase the depth of the evaporation zone and make the model's error even bigger. So one can conclude that some other factor than fall velocity is causing the error in the depth of the evaporation zone.

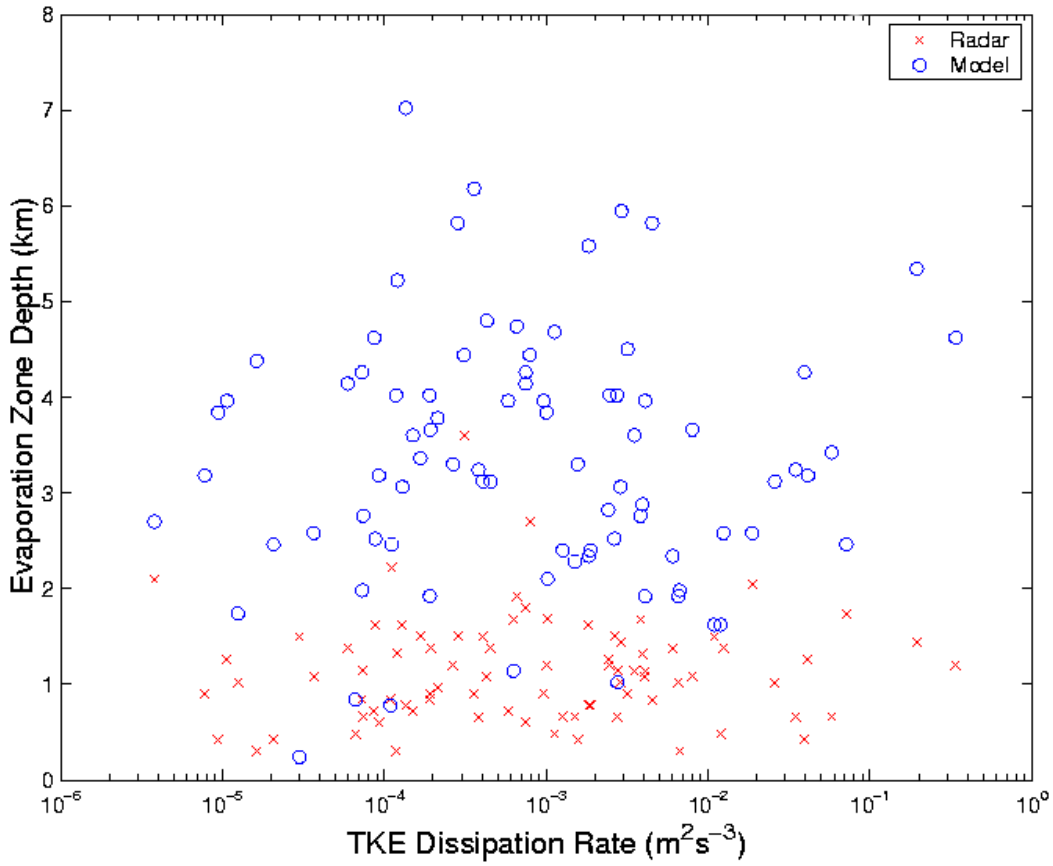

Figure 3.11: *Hourly-averaged evaporation zone depth scales against maximum hourly-averaged turbulent kinetic energy dissipation rate, (ϵ), in each profile for the model and radar data. The model evaporation zone depth is 2–3 times the depth of the radar in the majority of cases, but there is no clear relation between evaporation zone depth and turbulence. Red crosses show the radar points and blue circles show the model points.*

3.6 Examining the Effects of Turbulence

In section 3.1 it was hypothesised that the deeper evaporation zone depth in the model is due to the model not accounting for the increased evaporation rate caused by vigorous turbulence generated by the ice particles evaporating from the ice cloud into the dry air beneath. Since the model does not account for any turbulence above the boundary layer, this may be the cause of the deeper evaporation zone in the model.

Turbulent kinetic energy (TKE) dissipation rate (ϵ) have been estimated from radar observations of standard deviation of mean Doppler velocity ($\sigma_{\bar{v}}$), according to the method described in

Bouniol *et al.* (2003). The maximum value of ϵ in each profile has been plotted against the depth of the evaporation zone for both radar and model data. If the mis-representation of turbulence is the cause of the deeper evaporation zone in the model, then we should see a decrease in the radar evaporation zone depth as ϵ increases, but no change in the model evaporation zone depth with ϵ. Figure 3.11 shows the plot of maximum ϵ in each hourly averaged profile against evaporation zone depth for the 89 hours of study. In the vast majority of the cases shown in figure 3.11, the model evaporation zone depth is much greater than the radar, and in most cases, it is 2–3 times this depth. However, there is no change in radar evaporation zone depth as turbulence increases, which means that the amount of turbulence released does not affect the evaporation depth scales of the ice. Thus, it can be concluded that the absence of turbulence in the model cloud parameterization scheme is not the cause of the deeper evaporation zone within the model.

3.7 The Effect of Ice Particle Density

In section 3.1 it was also hypothesised that the model's deeper evaporation zone could be due to the model parameterization scheme having an incorrect density function, which would affect the parameterized fall velocity and thus increase the evaporation zone depth. Currently the function used is given in equation 3.3. This differs slightly from the Brown and Francis (1995) $\rho_i = 0.07D^{-1.1}$ and is completely different from the relationship Francis *et al.* (1998) $\rho_i = 0.175D_a^{-0.66}$. The differences in the relationships occur due to whether the diameter, D is defined by maximum dimension (Brown and Francis, 1995) or by area (D_a, Francis *et al.*, 1998). In both cases the mass of ice is the same. It is not clear from Wilson and Ballard (1999) whether the Met Office density function given in equation 3.3 is defined by maximum dimension or area.

In order to test whether incorrect parameterized ice particle density is the cause of the deeper evaporation zone in the model, a sensitivity test on the data set was performed. The current parameterization, given in equation 3.3 was altered as follows. First, the value of the 0.13 constant was doubled and halved to form two new relationships:

$$\rho_i = 0.26D^{-1}, \tag{3.10}$$

$$\rho_i = 0.065D^{-1}. \tag{3.11}$$

Equation 3.11 is very similar to the Brown and Francis (1995) relationship and thus is of use when

comparing the results of the current model parameterization to that which would be achieved using the Brown and Francis (1995) relationship. Finally, the Francis *et al.* (1998) relationship was inserted into the parameterization as another check to see how valid the current model parameterization was. The results of performing these tests are shown in section 3.7.1.

3.7.1 The Effects of Changing the Density Relationship

The results for all four tests described in section 3.7 are shown in figure 3.12. Equation 3.4 relates ice water content to particle mass, and therefore density. To completely test whether the evaporation zone depth would be affected by changes in density, we would need to re-run the model and allow the density to affect the ice water content. However, the results do show how changing the particle density alters the parameterized fall velocity and the model reflectivity values. As these tests have not re-run the model, there was no detectable change in evaporation zone depth in any of the tests.

Looking back at figure 3.8, which shows the run with the original model density ($\rho_i = 0.13D^{-1}$), it can be seen that the reflectivity values predicted with the model parameterizations are too high by about 3 dB. This means that the model IWC is also too large due to the density function being too large. When the Brown & Francis density function is used or the density function in the model is halved, as shown in the top right and bottom left plots of figure 3.12, the model and radar reflectivity values agree in the 3 km above the evaporation zone. Doubling the density function in the model makes the reflectivity 6 dB too large above the evaporation zone. Using the Francis *et al.* (1998) relationship makes the reflectivity 4 dB too large above the evaporation zone. This means that the density function in the Met Office model is too large, and should be closer to half the value. Since the Brown & Francis relationship agrees better than the Francis *et al.*, one can conclude that the diameter, D, in the model is most likely defined by maximum dimension, not by area. There is good evidence (Hogan *et al.*, 2006) for the Brown & Francis relationship and since radar and model reflectivity agree very well when this relationship is used this would suggest that the inputs used to simulate reflectivity are roughly correct. Hence, it can be suggested that the agreement between radar and model reflectivity above the evaporation zone gives evidence that the ice water mixing ratio is well represented in the model in these regions.

Looking now at fall velocity, it can be seen that altering the density in the model parameterization has little effect on the profile of model Doppler velocity. It changes in total by about 10%

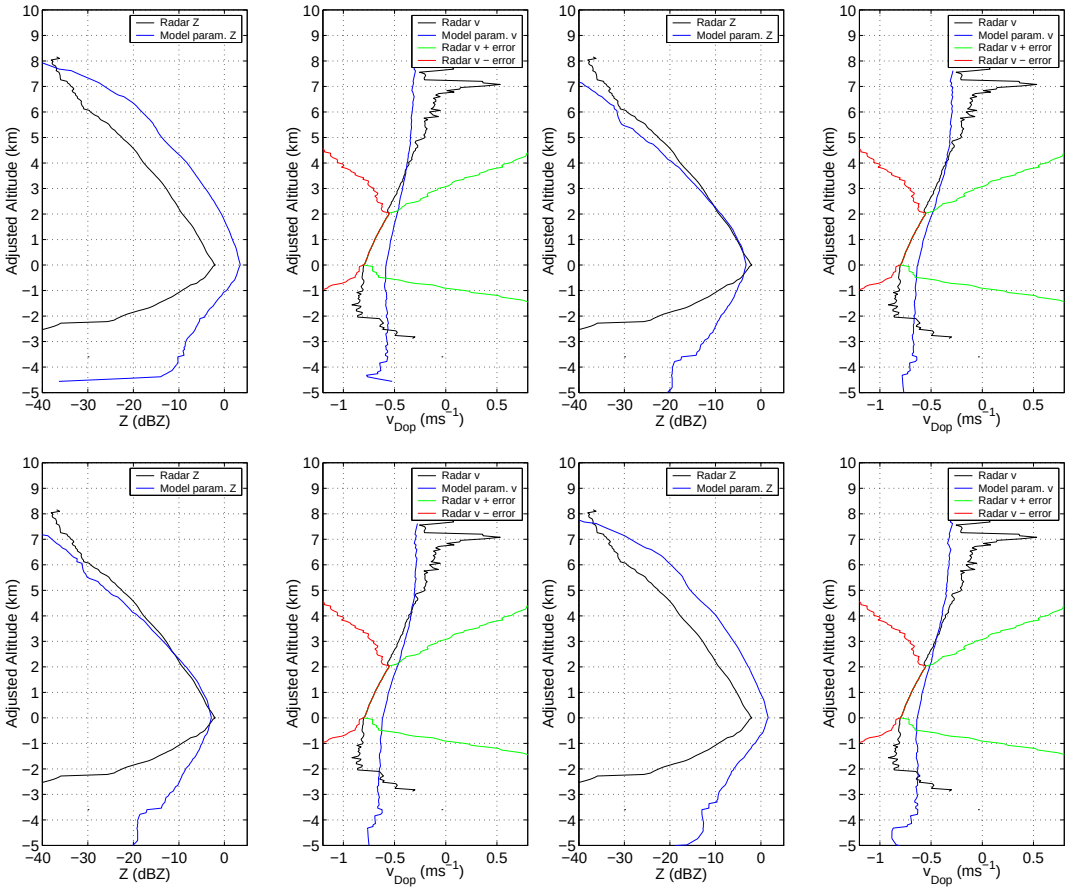

Figure 3.12: *Profiles of Z and V_{Dop} when the density in the Met Office Model is doubled (top left), halved (top right), changed to Brown and Francis (1995) (bottom left) and changed to Francis* et al. *(1998) (bottom right).*

between the cases shown in figure 3.8. Changing the density affects the weighting of the large and small particles towards the contribution in Doppler velocity, and this is not significant enough to make the parameterized Doppler velocity greater than the radar Doppler velocity. Hence the incorrect particle density does not change the parameterized fall velocity enough for it to cause the deep evaporation zone in the model.

3.8 Humidity and Evaporation Rate Studies

So far, several candidates for the increased depth of the evaporation zone have been examined, including ice particle terminal fall velocity, ice particle density and the effects of turbulence. One remaining candidate is the role of humidity. Forbes (2002) partially addressed this problem. He

studied several sonde profiles through evaporating ice cloud, and found that the model relative humidity was on average 7% too moist beneath the frontal surface, where the ice particles were evaporating. He also studied several sonde profiles from Larkhill radiosonde station for the time period corresponding to the year-long 94-GHz radar data set at Chilbolton. Forbes found that in some of the individual sonde profiles, the relative humidity dropped sharply beneath the evaporation zone, a change that was not accurately represented by the model, which still had a moist bias beneath the evaporation zone. Having eliminated most of the other candidates from being the likely cause of the deep evaporation zone in the model, this factor looks very likely to be the cause. In section 3.8.1, several sonde humidity profiles are studied to try and see how the model represents the drop in humidity beneath the evaporating ice cloud. In section 3.8.2, the equations set out in Wilson and Ballard (1999) are used to estimate the evaporation rate beneath the evaporating ice cloud, to see if the model's evaporation rate calculations are correct.

3.8.1 Model Representation of Sonde Humidity Profiles

In order to see whether humidity is really the cause of the deeper evaporation zone within the model, profiles from the Larkhill radiosonde were compared with the model profiles of relative humidity. The Larkhill radiosonde station is 25 km to the west of Chilbolton and is the closest radiosonde station to the radar that was available at the time of study. However, as Larkhill is not an operational radiosonde station, there were only a limited number of sonde profiles available at the same time as there was evaporating ice cloud present. One case that illustrates the argument for how the model represents the humidity profile occurred on 4 March 2004. Figure 3.13 shows the radar reflectivity profile for this case study. During the day, a thick ice cloud developed, which did not descend to the ground, nor was it part of a system that later produced precipitation at Chilbolton. However, a sonde was launched from Larkhill at 13 UTC that was analysed. The results of this analysis are shown in figure 3.14. Similar sonde ascents through warm fronts were produced by Taylor *et al.* (1983) and Forbes (2002) and showed that humidity tends to increase sharply around the cloud base.

Two points can immediately be raised from figure 3.14. The first is that there is a substantial decrease in IWC predicted by the radar reflectivity values. The peak value of the model's IWC is a full order of magnitude less than the radar's peak IWC. The model does not have high enough values of Z beneath 5 km, caused by the values of IWC being much too low. Thus the model has

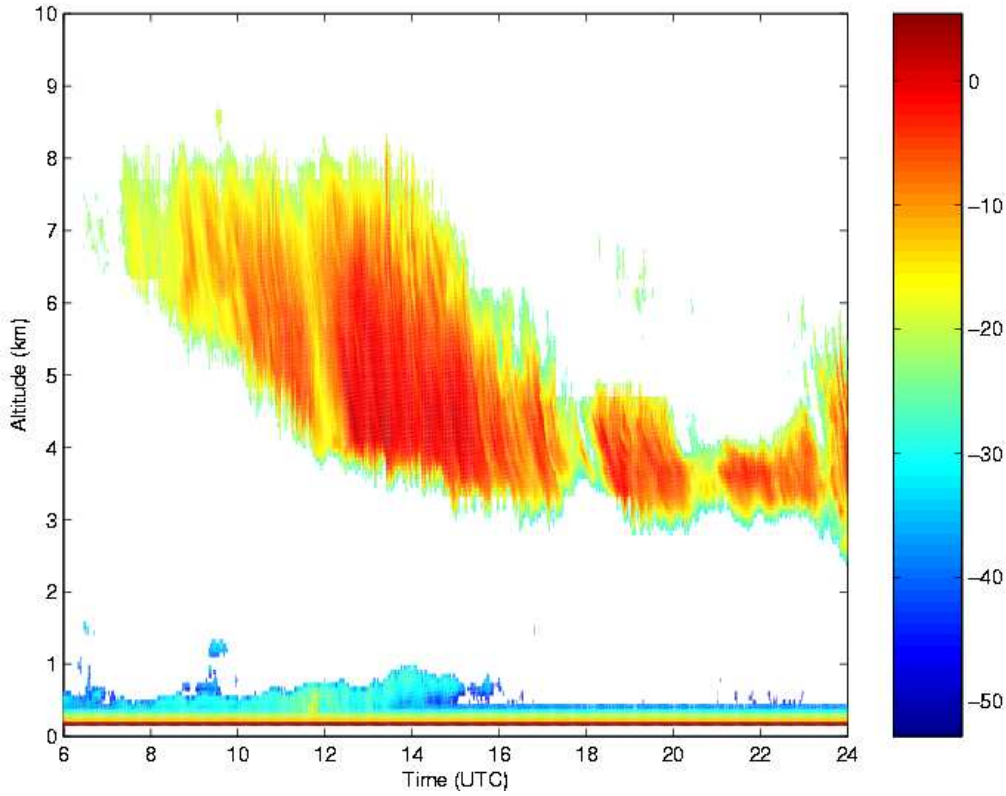

Figure 3.13: *Radar reflectivity data from 4 March 2004. A thick ice cloud was detected over Chilbolton for most of the day, starting at around 07 UTC and remaining very thick until 16 UTC. The cloud then remained until 24 UTC but was substantially thinner than before.*

not accurately represented this particular ice cloud.

The second point that can be seen is that the model does not accurately represent the gradient of relative humidity beneath the evaporating ice cloud. The model's peak relative humidity value starts at 6 km, and it does not decrease to 20% relative humidity until an altitude of 3 km. The sonde profile shows the relative humidity actually decreasing from 100% to 20% in a layer about 200 m deep, and at an altitude of 4 km, which agrees with the position of the cloud base from the radar measurements and the findings of Clough and Franks (1991). This appears to be the cause of the deeper evaporation zone in the model on this particular day.

In this case, the model has not correctly represented the IWC and thus the high Z values at the base of the ice cloud. Its humidity profile suggests that the evaporation should start a lot further up at 6 km, and the model evaporation zone extends from 6 km down to 3.5 km. This

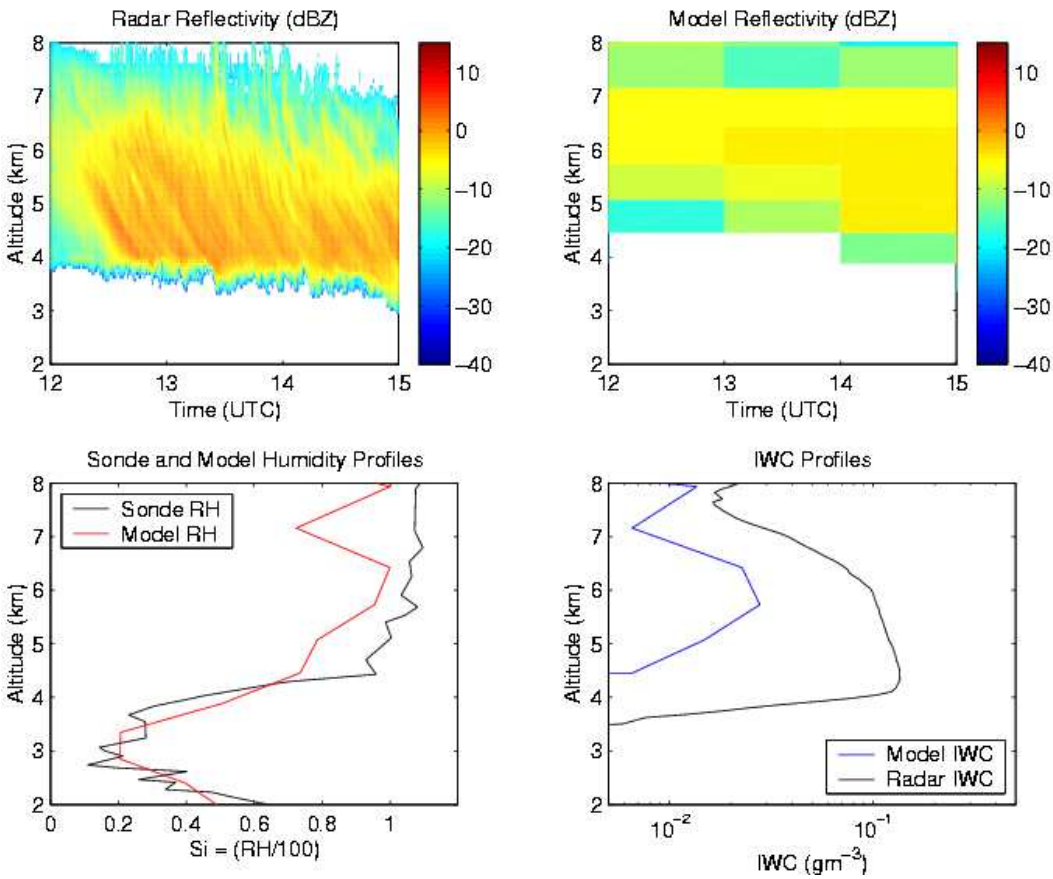

Figure 3.14: *Analysed data from radar, model and 13Z UTC Larkhill radiosonde on 4 March 2004. Radar ice water content was estimated using equation 14 of Hogan* et al. *(2006). All humidity values shown are with respect to ice. There is a sharp drop in both relative humidity and IWC at the cloud base, but the model does not represent the maximum IWC. The gradient in humidity is much steeper in the observations than in the model.*

would mean an evaporation zone depth of 2.5 km; much deeper than that shown in the sonde relative humidity profile. But does this actually apply to all cases? In order to see what happens for various humidity profiles during the period of study, several sonde cases were selected, and profiles of both model and sonde relative humidity were plotted. However, since Larkhill is not an operational radiosonde station, sondes were only released on an event basis, and not at regular intervals, as occurs at operational radiosonde stations. Also, in not all cases is the decrease in humidity so clear cut as in the case in figure 3.13; in some cases there is a layer of more moist air immediately beneath the evaporation zone. What can be seen in some profiles is that the relative humidity from the sonde measurements decreases in the evaporation zone as the ice particles evaporate into dry air, but there can be a moist area beneath this layer, associated with, say low

cloud which causes a sharp increase in the humidity profile. Therefore it is not always easy to pick clear-cut cases where the humidity gradient in the sonde profile decreases, which can be noisy when comparing it to the model gradient of humidity which is often smooth. However, it is not too difficult to pick out the sharpest drop in humidity in each case.

In order to attempt a fair test of model humidity against sonde humidity, sonde profiles were selected that occurred during the year long period. These profiles were taken when evaporating ice cloud coincided with an ascent from the Larkhill radiosonde station. Several of the sonde profiles were very noisy and it was quite difficult to compare these to the model profiles of relative humidity. Thus many of the sonde profiles were rejected for one of several criteria:

- There was no corresponding ice cloud in the model, and therefore there was no IWC or RH profile from which to calculate an evaporation rate.
- The sonde profile had only a few points and these points did not give a reliable estimate of humidity or humidity gradient.
- The sonde profile showed some layers of moist air close to the base of the evaporation zone and therefore relative humidity actually increased beneath the evaporation zone.

It is, however, worth noting that relative humidity is reasonable when measured from radiosondes. Ferrare *et al.* (1995) noted a systematic dry bias in Vaisala radiosonde measurements when compared to Raman lidar, of the order of 3–5%. Heymsfield and Miloshevich (1995) found that the observed humidity from radiosondes was sub-saturated when simultaneous crystal measurements showed pristine crystals growing in ice-supersaturated measurements, hence suggesting that the radiosonde humidity had a dry-bias. Miloshevich *et al.* (2004) also noted the lags of radiosonde humidity sensors. For the Vaisala radiosondes, this lag varies from a couple of seconds at $-10°$C to twenty seconds at $-35°$C, which is the range of temperatures ice was found to evaporate in this study. Despite these biases, relative humidity can be measured to within 5% and the humidity gradient derived from sondes is fairly accurate.

After the above criteria had been applied to the sonde profiles, twelve profiles were left. These profiles are shown in figure 3.15.

In almost all of these profiles, it can be seen that the model does not make a very good representation of the humidity gradient beneath the ice cloud. The model tends to diagnose a

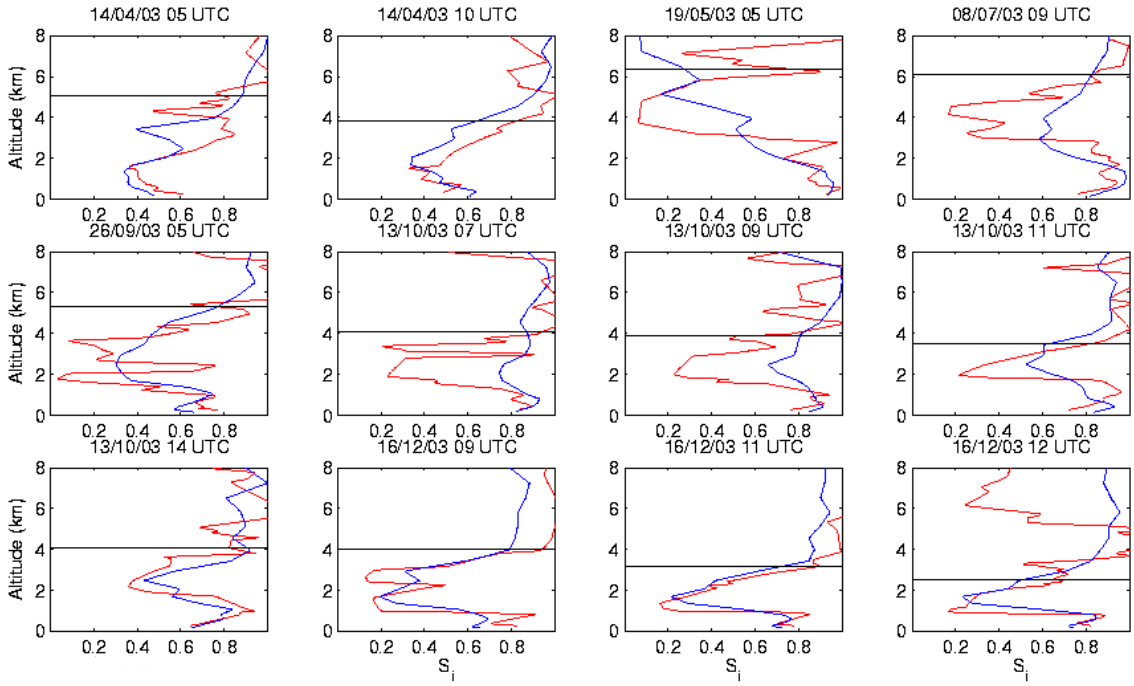

Figure 3.15: *Profiles of saturation ratio with respect to ice (S_i) taken from twelve sondes from the Larkhill radiosonde station (plotted in red) and the corresponding model relative humidity profile (plotted in blue). The black line indicates of the top of the observed evaporation zone, defined by taking the maximum value of the radar-derived ice water content.*

smoothed version of the sonde humidity profile, and it takes an increased depth for the humidity to drop to its first minimum value beneath the top of the evaporation zone. The most likely explanation is that the numerics of the model are diffusive, so sharp gradients in humidity cannot be maintained within the evaporation zone. However, it is also important to check the validity of the model's evaporation rate. This is tested in section 3.8.2, and the correlation between the humidity gradient through the evaporation zone and the evaporation zone depth is shown in figure 3.16. It can be seen that the sonde-and-radar derived evaporation zone depth decreases with increasing relative humidity gradient and that the model data appears to be following the same curve as the radar data. So it would appear that the two sets of measurements obey the same laws of physics. However, the model has smaller humidity gradients, and deeper evaporation zones as a result. This provides quite conclusive evidence that an incorrect humidity gradient is the cause of the deeper evaporation zone in the model. The next section compares radar and model humidity to see if the incorrect representation of the humidity gradient changes the model's evaporation

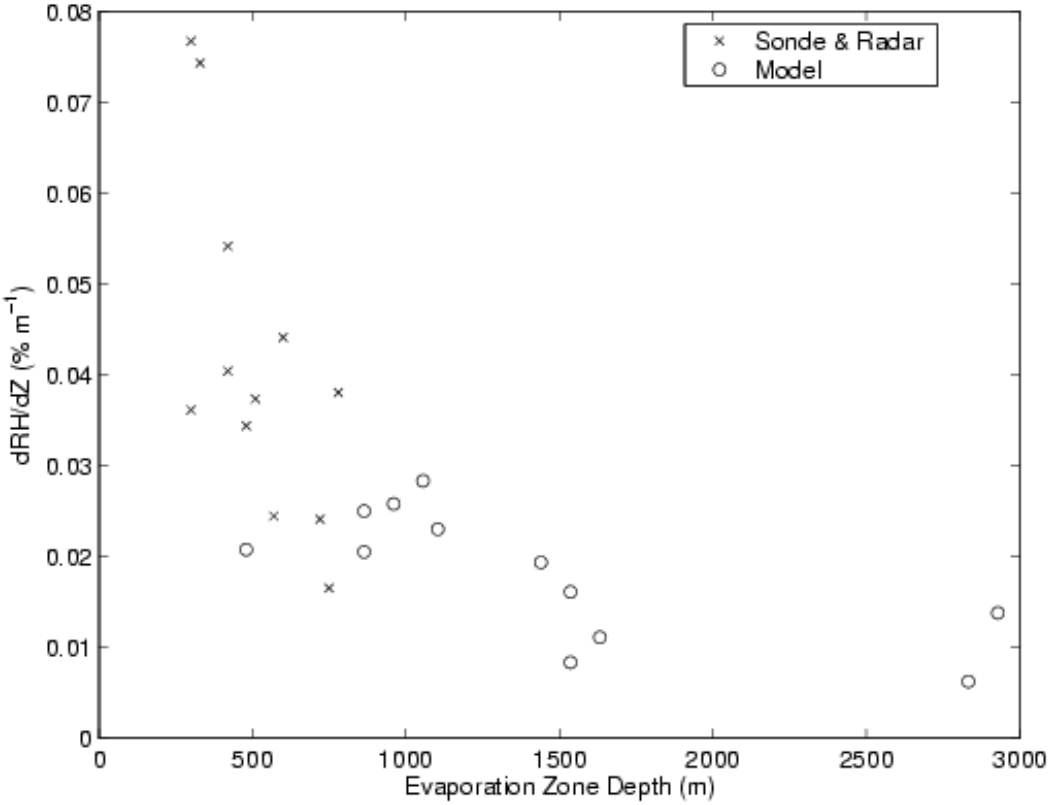

Figure 3.16: *Plots of the depth of the evaporation zone versus the humidity gradient for each of the sonde/radar and model profiles shown in figure 3.15.*

rate.

3.8.2 Comparison Between Radar and Model Evaporation Rates

In section 3.8.1, evidence was examined that suggested the model's deeper evaporation zone was due to the model incorrectly representing a sharp drop in humidity within the evaporation zone. This section compares the radar and model evaporation rates, to see if they vary, and examines the evaporation rate equation used by the model, to see how it depends on humidity and whether the incorrect humidity gradient suggested in section 3.8.1 would significantly change the evaporation rate.

The formula used by the Met Office model to calculate evaporation or deposition of ice is

given by Wilson and Ballard (1999) as:

$$\frac{dm}{dt} = \frac{4\pi C(S_i - 1)F}{\left(\frac{L_s}{RT} - 1\right)\frac{L_s}{k_a T} + \frac{RT}{X e_{satice}}}. \tag{3.12}$$

Here, $\frac{dm}{dt}$ is the rate of change of the mass of the particle due to the supersaturation with respect to ice ($S_i - 1$). The gas constant for water vapour, R is 461.5 J kg^{-1} K^{-1}, k_a is the thermal conductivity of air at temperature T, X is the diffusivity of water vapour in air at temperature T and a given air pressure. The capacitance term is represented by C and since all ice particles in the model are assumed to be spheres, C is equal to $\frac{D}{2}$, while e_{satice} is the saturated vapour pressure over ice and L_s is the latent heat of sublimation of ice. The factor F is a ventilation coefficient, given by Pruppacher and Klett (1978) for spheres to be $F = 0.65 + 0.44Sc^{1/3}Re^{1/2}$, where Sc is the Schmidt number, equal to 0.6 and Re is the Reynolds number, equal to $v(D)\rho D/\mu$, where $v(D)$ is the fall speed of the ice particle and μ is the dynamic viscosity of the air. This equation is similar to the forms of Pruppacher and Klett (1978) and Mason (1971) and is based on well-established cloud physics, so the increased depth in the evaporation zone should not be caused by an incorrect parameterization of the evaporation rate. However, the values of the variables used in equation 3.12 may still be wrong and hence cause the deep evaporation zone.

To see if the model evaporation rate is correct, it is necessary to compare radar and model evaporation rates. This can be done by studying each hourly average profile of V_{Dop} and IWC in both the radar data and model output. The flux density in kg m^{-2} s^{-1} at the top and bottom of the evaporation zone can be estimated by multiplying the radar IWC at the top or bottom of the evaporation zone by the mean radar V_{Dop} at the same point. The same procedure can then be followed for the data obtained from the model output. The difference in flux between the top and bottom of the evaporation zone can then be divided by the depth of the evaporation zone to give an estimate of layer-mean evaporation rate. The differences in radar and model evaporation rate for the 89-hour period of study are shown in figure 3.17. It should be noted that the model velocity used is V_{Dop} which is Z-weighted. Ideally, we should use the IWC-weighted velocity. However, the two do not differ significantly so use of V_{Dop} is justified.

Figure 3.17 shows that the model's layer-mean evaporation rate is only one third of that derived from the radar data. Since the equation used by the Met Office model is based on well-established cloud physics, it is unlikely that the parameterization is wrong by such a large amount. Hence, the lower model evaporation rate must be caused by incorrect values of one or more vari-

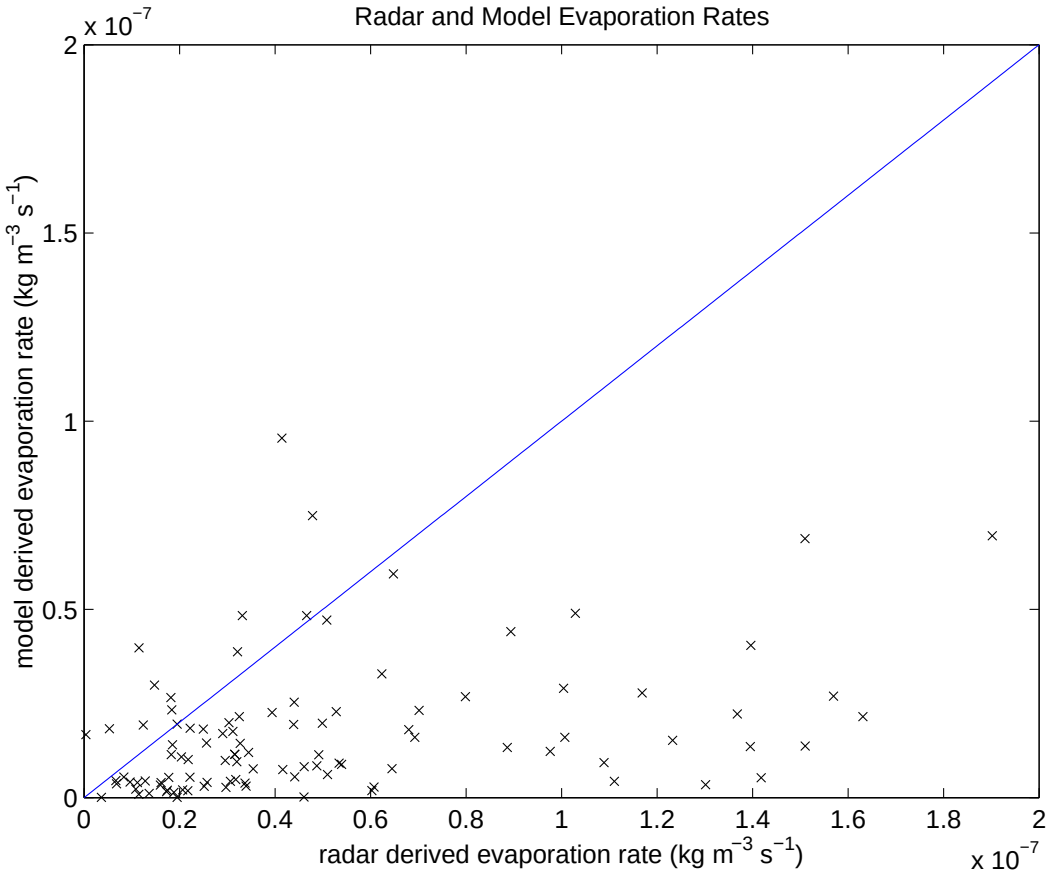

Figure 3.17: *The correlation of the radar layer-mean evaporation rate versus the model's parameterized layer-mean evaporation rate calculated for the model and radar evaporation zones, calculated using the IWC flux density difference and the evaporation zone depth. The blue line is the line y=x.*

ables being inserted into equation 3.12. Looking again at this equation, we can see that although it is a function of several factors; these can quickly be attributed to changes in four variables. The terms on the bottom half of the equation are functions of temperature and pressure only. The capacitance term, C is a function of particle diameter only, the supersaturation ratio $(Si - 1)$ is a function of relative humidity only and the ventilation coefficient, F varies with temperature, pressure and particle diameter. Hence the entire equation is a weak function of temperature and pressure, but strongly dependent on particle diameter and relative humidity. This suggests that the either the relative humidity in the equation is wrong, or the parameterized particle diameter is wrong. If the particle diameter, given in equation 3.1 was wrong, then the model would produce incorrect values of reflectivity, IWC and V_{Dop} which would have been identified in sections 3.5

and 3.7. The evidence from section 3.8.1 suggests the humidity gradient is wrong by up to a factor of three and this increases the model's evaporation zone depth. This incorrect humidity gradient would also reduce the evaporation rate to one third of its true value, which agrees with figure 3.17.

3.8.3 Summary of Humidity and Evaporation Rate Studies

The evidence shown in figures 3.14 and 3.15 show that the model's humidity gradient is much shallower than in the observations taken from the sondes released at Larkhill. In the observations there is often a drop from around 100% relative humidity with respect to ice to as little as 20% in the evaporation zone, which is typically about 500 m deep. At ice cloud altitudes, the model's grid resolution is between 500 and 750 m, which means that this change in relative humidity would be represented as a step function. Due to the numerics in the model being artificially diffusive, this sharp change in humidity cannot be maintained. The model's incorrect humidity gradient means that the supersaturation with respect to ice in equation 3.12, which governs the evaporation rate is too high, and hence the evaporation rate is too low, causing a deeper evaporation zone in the model output. This agrees with Forbes (2002), who noted a sharp drop in humidity around the evaporation zone. The theory of the humidity gradient being 2–3 times shallower and hence causing a slower evaporation rate and eventually an evaporation depth of 2–3 times that seen in the observations would agree with the results presented by Forbes (2002) and Forbes and Hogan (2006). However, when Forbes (2002) increased the model grid resolution, there was only 10% observed change in the evaporation zone depth. This is most likely due to the fact the grid resolution was still not enough within the model to achieve an accurate representation of the humidity gradient within the evaporation zone.

3.9 Other Operational Models

In addition to studying the Met Office model, it is interesting to see if other operational models have an increased evaporation zone depth. If one or more of the other operational models do not suffer from this problem, then there is something in these models that could be adapted and used in the Met Office model. If the models all suffered from this common condition, then it may be an intrinsic numerical problem which could be difficult to resolve. As part of the Cloudnet project, corresponding ECMWF, Météo-France and RACMO (Regional Atmosphere

Climate Model, produced by KNMI) model output was available for Chilbolton at the time of this study, and in sections 3.9.1, 3.9.2 and 3.9.3 each of the individual models will be studied in turn. In each study, the Met Office model parameterization scheme has been used. This is because the equations used to relate Z and V_{Dop} to IWC are unlikely to change significantly despite changes in the cloud scheme between models. However, in section 3.7 it was hypothesised that the density function used in the Met Office model, given in equation 3.3 may be too large and the Brown and Francis (1995) density function was thought to be more realistic. In order to account for this, each model has been tested using the Brown and Francis (1995) density function and the density function used in the Met Office model, shown in equation 3.3 and taken from Wilson and Ballard (1999).

3.9.1 Comparison with the ECMWF Model

The ECMWF model uses a prognostic cloud scheme based on Tiedtke (1993). This means that cloud liquid content (either vapour or ice) and cloud fraction are carried as prognostic variables. Evaporation is parameterized as a simple change in saturation water vapour pressure with time, which can be related to a change in the ice water content of the model. The model has 60 levels in the vertical compared to the Met Office's 38, which translates to the ECMWF model having a vertical grid resolution of 529 m at 5 km, which is less than the Met Office's grid resolution of 615 m. However, when Forbes (2002) increased the number of levels in the Met Office model, he found out that there was only a 20% decrease in the depth of the Met Office evaporation zone. Will the ECMWF model show the same result? The results for the model with the Met Office parameterization scheme and density function are shown in figure 3.18.

The results show that the ECMWF model does indeed have a much deeper evaporation zone than in the radar observations. The results are comparable to the Met Office model shown in figure 3.8. The mean depth of the evaporation zone is defined as before, using the model profile of IWC. In the ECMWF model, this depth is on average, 1334m which is 2.10 times the observations. Looking at the profiles of Z and V_{Dop}, the results are similar to those from the Met Office model. The ECMWF does underestimate the fall velocity of the ice particles, but this result is probably less reliable as the parameterization for particle velocity is not necessarily the same in both the Met Office and the ECMWF models. The Z profile obtained via the ECMWF output is very close to the observations, less than 1 dBZ in the region above the evaporation zone. This means that the

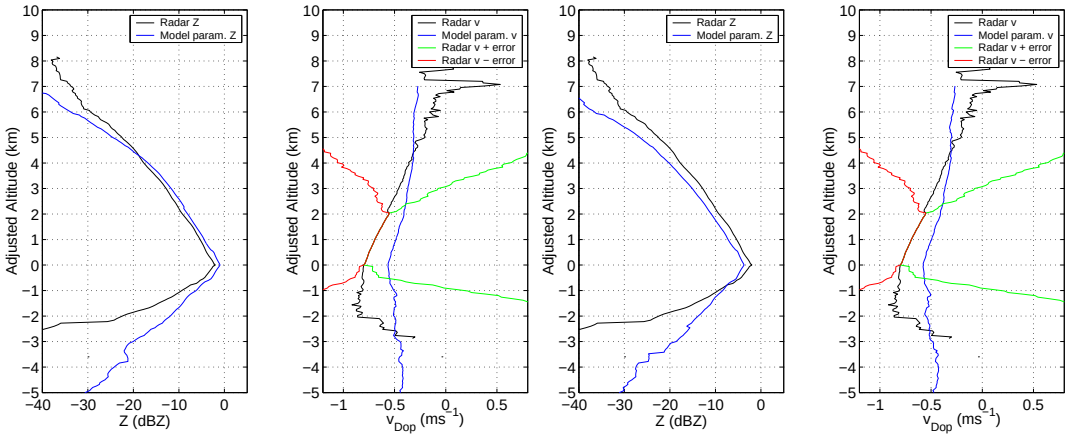

Figure 3.18: *Z and V_{Dop} profiles (left) for the ECMWF model values using the Met Office model parameterization scheme (left) and the Brown & Francis density function (right). The data used is the same as that used to study the Met Office model earlier in the chapter.*

ECMWF does a better job of representing the IWC in the cloud above the evaporation zone, but performs just as poorly as the Met Office model in the representation of the evaporation layer.

When comparing the results shown in figure 3.18 it can be seen that there is little difference in the profiles of Z and V_{Dop} . When the Met Office density function is included, the model slightly overestimates the Z values above the evaporation zone. If the Brown & Francis density function is included, then the model slightly underestimates the Z values. Since there is little difference between the two profiles of Z, it can be concluded that the ECMWF model gets accurate mean Z values and therefore predicts mean IWC very well. The depths of the evaporation zone do not change when the density function changes, the same result as for the Met Office model and what was expected after analysing the Met Office data.

3.9.2 Comparison with the Météo-France Model

The Météo-France model differs from the Met Office and ECMWF models as it uses a diagnostic, rather than a prognostic cloud scheme. This means that it uses the model's relative humidity to diagnose the cloud amount and ice water content in the model. How does this differ in the representation of the evaporation zone?

At 41 levels, the Météo-France model has slightly higher resolution in the vertical than the Met Office model. The grid resolution at 5 km is 502 m, over 100 m smaller than the Met Office's

615 m. The results for using the Met Office density function and Brown and Francis (1995) density function are shown in figure 3.19.

The Météo-France model has difficulty getting close to the correct values of Z above the evaporation zone. At the closest point the difference is 5 dBZ. This means that the model is underestimating the IWC by quite a significant amount. The evaporation zone depth is also poorly represented. The mean depth of the evaporation zone is 912 m, which is 1.44 times that of the radar observations. If we were to judge the model on evaporation depth alone, this would appear to be a much better result than the ECMWF and Met Office models. This is probably due to the model's ability to diagnose lower values of IWC using the lower humidity values, but it still will have difficulty in representing the sharp humidity gradient, leading to a slightly deeper evaporation zone than normal. However, despite the evaporation depth being lower than the other models, the representation of Z and hence IWC is quite low, the worst result from all of the models studied in this chapter. This is most likely due to the use of a diagnostic, rather than prognostic scheme.

The profile of V_{Dop} is similar to the Met Office and ECMWF models, on average 30% lower than the radar observations. However, once again this result is subject to differences in particle fall velocity between the parameterizations.

Inclusion of the Brown and Francis density function causes the model to underestimate the mean value of Z and therefore the values of IWC by 8 dBZ, an even larger amount than before. The depths of the evaporation zone are unchanged and the V_{Dop} are unchanged. This means that although the Météo-France model makes the best model representation of evaporation zone depth, it has serious problems in getting the correct mean values of IWC.

3.9.3 Comparison with the RACMO Model

The RACMO (Regional Atmosphere Climate Model) is produced by KNMI, the Dutch meteorological service. The model has 40 levels in the vertical and a resolution of 532 m at 5 km, very similar to the ECMWF model, with the same cloud scheme used (Illingworth *et al.*, 2007). The results for this model are shown in figure 3.20.

When using the Met Office model density function, the RACMO model represents the peak value of Z at the top of the evaporation zone to within less than 1 dBZ. However, the evaporation

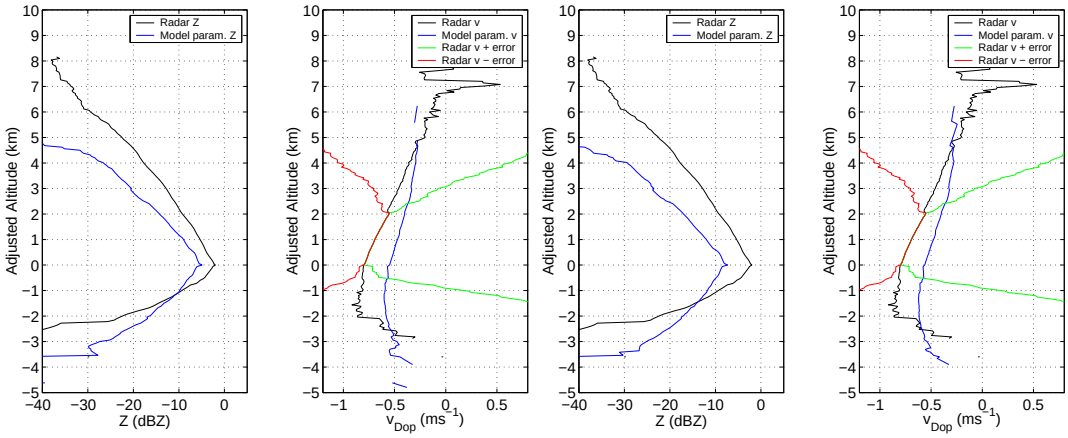

Figure 3.19: *Z and V_{Dop} profiles for the Météo-France model values using the Met Office model parameterization scheme (left) and the Brown & Francis density function (right). The data used is the same as that used to study the Met Office model earlier in the chapter.*

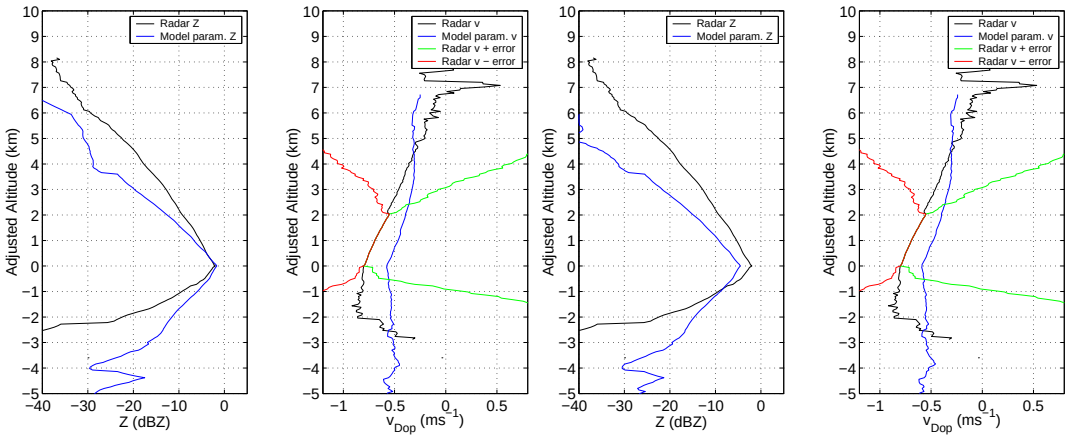

Figure 3.20: *Z and V_{Dop} profiles (left) for the RACMO model, using the Met Office model parameterization scheme (left) and the Brown & Francis density function (right). The data is the same as that used for the Met Office study earlier in the chapter.*

zone is not represented well and Z values in the middle of the ice cloud are about 5 dBZ lower than in the radar observations. When the Brown & Francis density is used, the Z values decrease even more and thus this model will underestimate the values of IWC within the ice cloud. The profile of V_{Dop} is similar to the other models and it is underestimated by 30%, although this result will depend on the model crystal terminal velocity parameterization. The depth of the evaporation zone in this model is on average 1317 m, 2.08 times the observations and very similar to the result

from the ECMWF model. The model is able to accurately represent the mean value of the peak IWC in the profile, but performance is not as good in the depth of the cloud, or at lower IWC. Factors within the model cause the ice mixing ratio to fall off too rapidly with height, as this discrepancy is observed with both Met Office and Brown and Francis (1995) density functions.

3.9.4 Summary of Results from the Other Models

From the results for each of the above models, shown in table 3.1, it can be seen that the evaporation zone depth is much deeper in each model than in the radar observations, thus demonstrating that the Met Office model's problems are not unique. In section 3.8 the step function in humidity was discussed and it was suggested that the model is artificially diffusive and unable to maintain a sharp gradient in humidity, hence affecting the evaporation rate and deepening the model evaporation zone. Perhaps such a numerical problem is the cause of the deep evaporation zone in all of these models.

The Météo-France and RACMO models have problems representing the values of Z, and therefore IWC accurately in the cloud above the evaporation zone. Thus this is something that should be looked into further, clearly the representation of the IWC field needs to be improved. The differences in the Météo-France model could be due to IWC being a diagnostic variable, while in other models (e.g. ECMWF, Met Office, RACMO) it is a prognostic variable.

3.10 Conclusions and Summary

This chapter has studied 94-GHz cloud radar measurements with the aim to see how well the evaporation zone beneath ice cloud is represented in the Met Office model. The depth of the evaporation zone in the Met Office model is on average, 2.55 times that observed by IWC measurements calculated using radar reflectivity and model temperature. Various candidates for the increased depth of the evaporation zone have been considered and the following conclusions can be drawn:

- The parameterized fall velocity in the model is around 30% too low. In order to examine the fall velocity in the evaporation zone, the effects of the vertical air velocity need to be taken

Model	Cloud Scheme	Vertical Grid Resolution at 5 km	Mean Evaporation Zone Depth	Standard Deviation of Evaporation Zone Depth	Depth Factor
Met Office	Prognostic	615 m	1614 m	630 m	2.55
ECMWF	Prognostic	529 m	1334 m	865 m	2.10
Météo-France	Diagnostic	502 m	912 m	452 m	1.44
RACMO	Prognostic	532 m	1317 m	714 m	2.08

Table 3.1: *Summary of evaporation zone depths, cloud schemes and grid resolution from the models. The depth factor is the ratio of model and radar mean evaporation zone depths, so a depth factor of two would imply that the mean model evaporation zone depth is twice the radar observations.*

into consideration. There is confidence in the result above the the point where evaporation starts, as the vertical winds will average to zero over a long time period. However, the parameterized fall velocity still remains too small in this area and thus will tend to make the depth of the evaporation zone less in the model than in the observations. Therefore the parameterized fall velocity is not the cause of the erroneously high depth of the evaporation zone in the Met Office model.

- The representation of turbulence in the model has no effect on the depth of the evaporation zone. The depths of the evaporation zone in the model are always 2–3 times the observed depth, despite significant changes in the turbulence.

- Using a wide variety of density functions suggested by recent studies, the depth of the evaporation zone within the Met Office model changes less than 10%. This implies that the parameterized density of the ice particles is not increasing the parameterized fall velocity enough to cause a deeper evaporation zone within the model. Using the Brown and Francis (1995) density function in the model allows the best representation of model reflectivity and therefore ice water content. Without re-running the model, it is not possible to see whether the density changes would affect the IWC and change the evaporation zone depth.

- The humidity gradient within the evaporation zone or immediately beneath the ice cloud is much smaller in several model profiles than in radiosonde ascents from Larkhill. The drop from moist air with 100% relative humidity to dry air with 20–30% relative humidity

is observed to take place in a shallow layer. Studies of the layer mean evaporation rate show that the model's parameterized evaporation rate is about 30% of that observed by the radar. The parameterized evaporation rate equation used in the parameterization scheme is based on well-established cloud physics and is dependent on four fundamental variables: temperature, humidity, particle diameter and pressure. The error in evaporation rate can be attributed to incorrect humidity as unrealistic changes in the other parameters would be required. The sharp drop in humidity would take place over the space of one model grid box and would be represented as a step function, but the numerics of the model are too diffusive and so the sharp humidity gradient cannot be maintained.

- The problems seen in the Met Office model are not unique and apply to all other models tested from a variety of institutes and forecast centres across Europe.

CHAPTER FOUR

A 1D Explicit Microphysics Model of Ice Evaporation

4.1 Introduction

Several studies (Hall and Pruppacher, 1976; Harris, 1977; Clough and Franks, 1991) have attempted to theoretically calculate the survival distance of ice crystals and masses of solid ice evaporating into dry air. However, all of these studies have produced a mean depth scale of evaporation, rather than attempting to accurately calculate evaporation depth. Often many simplifying assumptions, such as using a single particle, assuming constant temperature, constant pressure and constant relative humidity are made. In the real atmosphere, things are more complex, and this study attempts to calculate evaporation depth as accurately as possible, using a spectrum of particles and a profile of variable temperature, humidity and pressure, intended to represent the real atmosphere as closely as possible.

In the previous chapter, data from the 94–GHz radar at Chilbolton was compared with output from the Met Office model. In the model, the evaporation zone depth was found to be between two and three times that observed in the radar data. It was found that when radiosonde and model humidity profiles were compared, the model humidity gradient tended to be much lower in the evaporation zone than the sonde observations. Due to the height resolution of the model at this altitude and problems with numerical diffusion, the model will not be able to represent this sharp humidity gradient. Instead the humidity gradient will be much shallower, as the results from chapter 3 have shown. If the Met Office model was able to accurately represent this gradient of humidity, for example, with a much higher resolution grid, would it be able to correctly define the evaporation zone observed by the radar? Forbes (2002) looked into this and in his experiments he doubled the number of levels in the Met Office model. This would have meant that at ice evaporation levels, the model grid spacing would be between 250 and 375 m. His results showed that the evaporation-zone depth would decrease by 10% in the Met Office model. However, taking

a typical evaporation-zone depth to be 500 m, there would only be two model grid points in the evaporation zone, which I believe is not nearly enough to accurately represent the model humidity gradient.

Thus, in this chapter, I shall write the assumptions used in the Met Office model into a high resolution 1D model, which studies Evaporation Level Physics and Numerical ice Transport (ELePhANT). In particular, the same mass-size and fall speed assumptions as the Met Office model are used, but in addition, the particle size distribution is resolved. A description of the physics used in the ELePhANT model is given in section 4.2 and experiments to examine the sensitivity of the evaporation depth scale are described in section 4.3. Sonde data from the Larkhill station are inserted into the ELePhANT model in section 4.4, to see how well the model represents the evaporation zone observed in the radar, using nearby sonde data. An important aspect in the study to to ensure the model has the correct parameterization of capacitance; recent work in this field is discussed in section 4.5. Conclusions are drawn in section 4.6 and future work in section 4.7.

4.2 Description of the Model

The evaporation rate equation is given in Wilson and Ballard (1999), following the work of Mason (1953):

$$\frac{dm}{dt} = \frac{4\pi C(S_i - 1)F}{\left(\frac{L_s}{RT} - 1\right)\frac{L_s}{k_a T} + \frac{RT}{X e_{satice}}}, \tag{4.1}$$

where m is the mass of an individual ice particle, t is time, C is the capacitance of the particle, which for spheres is $\frac{D}{2}$, where D is the particle diameter, S_i is the saturation ratio $\left(\frac{RH}{100}\right)$, T is the temperature (K), R is the gas constant for water vapour (461.5 J Kg^{-1} K^{-1}), L_s is the latent heat of sublimation of ice to vapour, X is the diffusivity, e_{satice} is the saturation vapour pressure with respect to ice and k_a is the thermal conductivity of air. F is the ventilation coefficient, given for spheres as

$$F = 0.65 + 0.44\mathrm{Sc}^{1/3}\mathrm{Re}^{1/2}, \tag{4.2}$$

where Sc is the Schmidt number, equal to 0.6 and Re is the Reynolds number $\frac{v(D)\rho D}{\mu}$, where ρ is the air density, $v(D)$ is the fall velocity of the crystal and μ is the dynamic viscosity of the air. The physical meaning of the ventilation coefficient is the effect of the air rushing past the evaporating ice particle and hence increasing the rate of evaporation (Mason, 1971; Pruppacher and Klett, 1978). The more turbulent the air, the higher the Reynolds number in equation 4.2

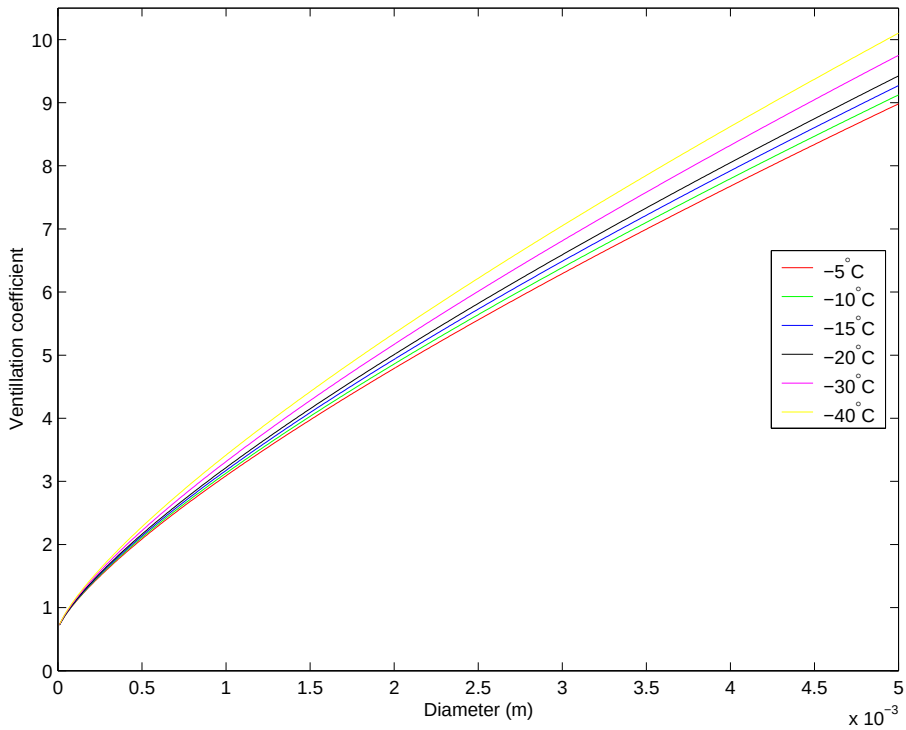

Figure 4.1: *The variation of ventilation coefficient from Wilson and Ballard (1999) with particle diameter and temperature. The ice particles are assumed to be spherical.*

and the faster the evaporation rate. Figure 4.1 shows the variation of ventilation coefficient with diameter and temperature. As can be seen, the ventilation for the largest particles approaches 10, hence the rate of evaporation for these largest particles is much greater. Since ice water content is dominated by these largest particles, it is important that the ventilation coefficient is represented accurately to ensure the correct evaporation depth occurs.

Although equation 4.1 may look complicated, the terms L_s, X, e_{satice}, k_a are functions of temperature and pressure. With the exception of e_{satice}, all these variables are weak functions of temperature and pressure. The capacitance, C is a function of diameter, D and F is a function of D, temperature and pressure. Thus, the evaporation equation could be expressed as a function of just a few variables, as in equation 4.3.

$$\frac{dm}{dt} = f(D, RH, T, p) \tag{4.3}$$

In section 4.3, this expression shall be evaluated to see which of these four variables the evaporation rate, and hence evaporation zone depth, is most sensitive to.

The mass of an ice crystal (kg) and its fall speed (m s^{-1}) in the Met Office model is given as

a function of its diameter in metres as follows:

$$m(D) = 0.069D^2, \tag{4.4}$$

$$v(D) = 25.2D^{0.527}. \tag{4.5}$$

These equations are based on Cox (1988) and Locatelli and Hobbs (1974). The values used in equation 4.4 were selected by Cox (1988) to give a sensible variation of particle density with size. This results in a roughly double the mass and double the density than the Brown and Francis (1995) relationship, which was used to accurately measure ice water content in clouds. Despite the difference, this study retained the Met Office model values to try and make the ELePhANT model as close to the Met Office model parameterization scheme as possible. The values used in equation 4.5 are larger than those given by Cox (1988), who used $v(D) = 16.8D^{0.527}$.

In order to obtain the distance an individual particle falls before it completely evaporates, we must first convert equation 4.1 to an expression for the change in diameter of a particle over time and then use the fall speed to convert this to a fall distance (z). This can be done using equations 4.4 and 4.5 and the chain rule:

$$\frac{dD}{dz} = \frac{dm}{dt} \times \frac{1}{dm/dD} \times \frac{1}{dz/dt}. \tag{4.6}$$

Once this information is known, the survival distance of an individual particle can be calculated numerically by integration. It is difficult to find an analytical solution to equation 4.6 due to the nature of the ventilation term, which cannot be integrated analytically when incorporated into equation 4.6. The number concentration of ice particles in the Met Office model is given as follows:

$$N(D) = N_0 e^{(-0.122T)} e^{(-\Lambda D)}, \tag{4.7}$$

where T is the temperature in degrees Celsius and $\Lambda = \frac{3.67}{D_0}$, where D_0 is the equivolumetric mean diameter and N_0 is 2 $\times 10^6$ m^{-4}. This expression can be used to determine ice water content (IWC) at the start of evaporation and at any layer in the model.

$$IWC = \int_0^\infty m(D)N(D)dD, \tag{4.8}$$

where $m(D)$ is the obtained from equation 4.4. The Met Office model resets the distribution back to the form in equation 4.7 at every vertical step, but in this explicit model, the smallest particles

evaporate first. As the Met Office model resets the distribution to its initial form, it automatically adds more small particles in place of a few large ones. Since evaporation depth depends on ice water content, which is proportional to the cube of diameter, this will mean that in the Met Office scheme the IWC will artificially reduce and the evaporation zone depth will decrease. However, the Met Office model vertical resolution at ice cloud altitudes ranges from 500m to 750m, so this resetting process will have little effect on the evaporation depth, if the correct humidity gradient were maintained.

4.2.1 Model Constraints and Simplifications

The 1D ELePhANT model was set up with a vertical grid with a 5 m resolution and 6 km domain. In the first experiment, a simple linear humidity gradient was used. In all cases, the humidity was set as 100% at the top of the domain and was not allowed to fall below 20% at any point in the profile.

In a similar nature, the temperature profile was set to be dry adiabatic with different starting temperatures at the top of the domain. Unrealistic runs, where the temperature increased above 273 K and therefore the ice would melt, rather than evaporate were removed from the study.

The profile of pressure decreased with height using a simple exponential distribution with a scale height of 8 km. As with temperature, the user is able to define the pressure at the top of the profile. The pressure in each profile is capped at 1040 mb.

The initial value of Ice Water Content (IWC) is a function of temperature and the particle median diameter (D_0) as expressed in equation 4.8. However, once the temperature at the top of the profile is known, equations 4.7 and 4.8 can be inverted to obtain D_0. So, the user can decide on a particular IWC to use at the top of the profile. This is then converted to give the corresponding value of D_0 at that temperature, which the model then uses to set up the particle size distribution as given in equation 4.7.

4.3 Evaporation Depth Sensitivity to Temperature, Pressure, Humidity and Initial Ice Water Content

With the model set up, a simple sensitivity study was performed to see how the evaporation depth changed with relative humidity gradient and one of the other variables (IWC, temperature and pressure). The model was initially run with a control experiment where the humidity gradient was altered over a range of values from 0.001 to 0.08% m^{-1}, but the values of the other variables remained fixed as follows: Initial temperature $-20°$C, initial pressure 850 mb, and an initial D_0 of 0.5 mm (which at this temperature is equivalent to an initial IWC of 7.7 $\times$ 10^{-3} g m^{-3}). The model was used to calculate a series of evaporation zone depths using these data. Then a set of four experiments were run to test the sensitivity of the model to various parameters as follows:

1. **Sensitivity to initial temperature.** The ELePhANT model was run exactly as the control run, but with the initial temperature being varied from $-30°$C to $-5°$C. This range spans the profiles of temperature in the Met Office model at ice cloud altitudes above Chilbolton.

2. **Sensitivity to initial IWC.** The value of D_0 was altered within the model, from 0.25 mm to 1.5 mm. This represented a change in IWC between 9 $\times$ 10^{-4} g m^{-3} and 0.21 g m^{-3} at this temperature, which is representative of the range of values observed over Chilbolton during the studies made in chapter 3. No changes were made to the ice water content by altering the number concentration of the particles, as in the ELePhANT model it is assumed that all particles of the same size evaporate at the same rate and take the same distance to evaporate. Therefore increasing the number of particles of any given size would not have any effect on the evaporation zone depth.

3. **Sensitivity to initial pressure.** The model was run with variations made in initial pressure, ranging from 500 mb to 1000 mb, but with the other parameters exactly as in the control run. The range of pressures used spanned the observed pressure levels at which evaporation started in the radiosonde profiles.

4. **Sensitivity to temperature gradient.** Lastly, we ran the model with constant temperature throughout the domain to see how this would affect the evaporation depth. In this experiment, the ELePhANT model was set as the control run, with the exception of the temperature gradient being replaced with an isothermal layer with temperature of $-20°$C.

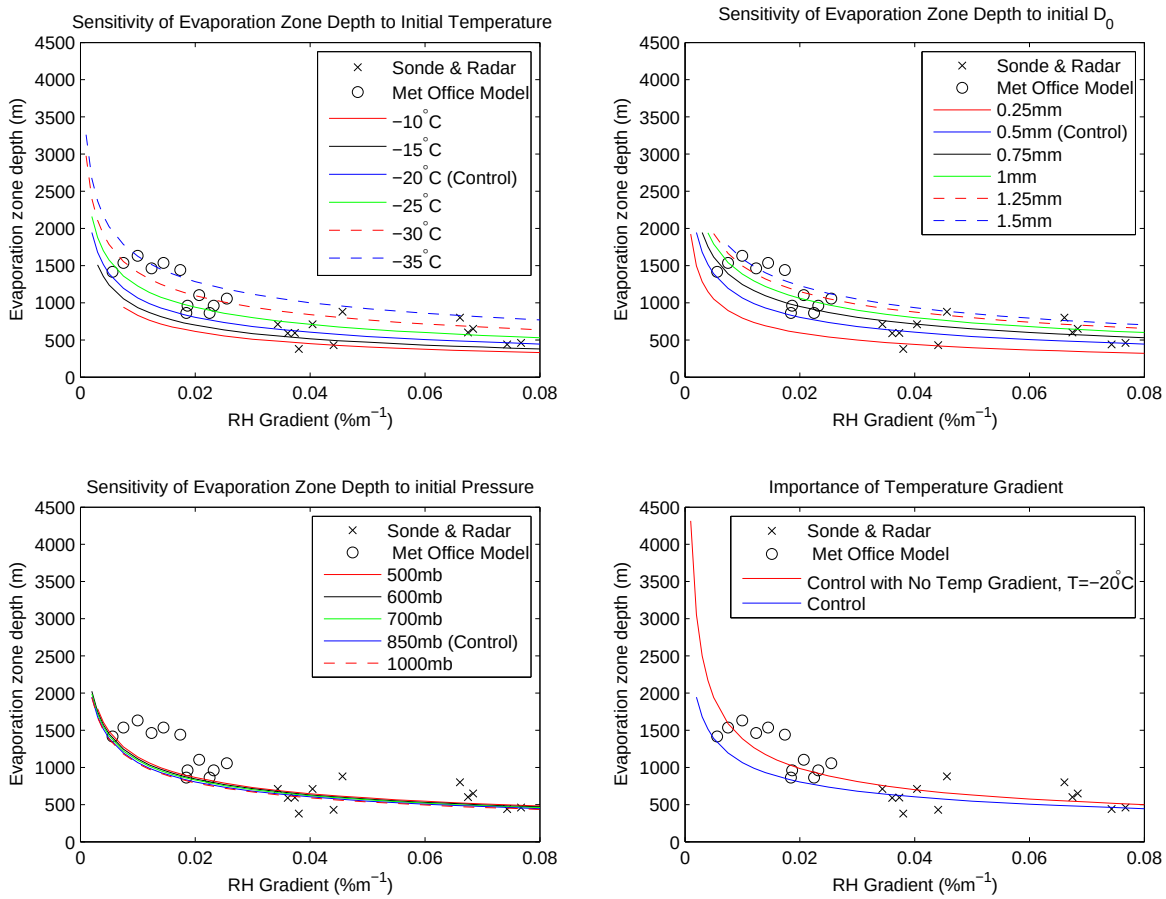

Figure 4.2: *Changes in evaporation zone depth with changes in initial temperature, initial D_0, initial pressure and when the linear temperature gradient in the model is replaced with an isothermal layer. The circles represent the points taken from model data and the crosses represent the evaporation depths from the radar data and humidity gradients from sonde measurements. Although the model was run on a domain of 6 km, only realistic solutions (where the temperature remains below zero degrees Celsius) are shown.*

The results of all four experiments are shown in figure 4.2. From these plots, we can see that the evaporation depth changes quite rapidly as humidity gradient increases, in all cases. Hence, humidity gradient is the single most important variable that we need to consider in determining the evaporation depth. In section 3.8.1, it was noted that sonde profiles can be measured to an accuracy of around 5%, after examining work by Ferrare *et al.* (1995), Heymsfield and Miloshevich (1995) and Miloshevich *et al.* (2004). Hence we can conclude that the humidity gradients derived from sondes are reasonably accurate.

However, the top left plot of figure 4.2 shows that the sensitivity to evaporation zone temperature is also an important factor in determining evaporation zone depth. The temperature fields within the model are accurate to within a couple of degrees Celsius and so this is not likely to be the cause of the model's deep evaporation zone, but nonetheless, any model which wants to accurately measure evaporation depth scales must include a temperature effect. The bottom right plot shows the effect of including a humidity gradient, but no temperature gradient in the model. This isothermal layer means that although the relative humidity decreases within the profile, the specific humidity is much greater at each individual point in the profile. Since evaporation is sensitive to specific humidity, this means that deeper evaporation zones will occur. The overall conclusion from this study is that the variable controlling evaporation rate and evaporation depth is specific humidity and that whenever a gradient in relative humidity is present, a gradient in temperature should also be used to ensure accurate evaporation within the model. Previous studies (Hall and Pruppacher, 1976; Harris, 1977) did not make this assumption. However, if we want to know what is causing the deep evaporation zone within the Met Office model, we must deal with the sensitivity to each variable individually.

The top right plot shows the effect of changing the value of D_0 on the evaporation depth, over a sensible range of values. The results show that changing the value of D_0 has a large effect on the ice evaporation depth and therefore it is important that the model has a particle size and ice water content reasonably accurate, but if we examine the top right plot of figure 4.2, we can see that to cause a doubling in evaporation zone depth, the model's D_0 would have to be double the value seen in nature, which would mean an ice water content of about one order of magnitude larger. If such an error were present in the mean particle size, we would have seen a much larger radar reflectivity factor when we examined this in chapter 3.

The bottom left plot shows the sensitivity to pressure variations within the model. Generally pressure is measured quite accurately within the model and as can be seen from the plot, evaporation depth is not sensitive to significant pressure changes. Changing pressure only changes the ventilation coefficient by a small amount and this is not enough to change the evaporation depth by more than a few metres and hence we can conclude that incorrect pressure is not a cause of a deep evaporation zone within the model.

There may also be effects due to the particle shape and distribution used within the Met Office model. However, the Met Office model follows an exponential distribution, which is used

by many other general circulation models. The evaporation depth may also be sensitive to the fall speed parameterization. However, for the purposes of this experiment, we have not decided to show any changes in particle size or distribution in order to try and prove that Met Office model could accurately represent evaporation with the present scheme and a high grid resolution.

4.4 Evaporation Depth Experiments Using Radiosonde Data

Once we know that the ELePhANT model works well with the profiles of temperature, relative humidity and pressure of an idealised atmosphere, the next step is to find out how well the model can represent an accurate profile of Ice Water Content derived from the 94-GHz radar at Chilbolton, using sonde temperature, pressure and humidity data from the nearby station at Larkhill.

The ELePhANT model was initiated with data from the sonde profiles in chapter 3. In each case, the start of the evaporation was defined by examining the humidity profile from each sonde and locating the sharpest drop in humidity closest to the height at which the radar data showed maximum values of ice water content. In practice, it was not too difficult to pick subjectively the sharpest drop in humidity for each case. The top of the evaporation zone was defined as the maximum point in humidity immediately above the sharp drop in humidity. The sonde profile from the ground to this evaporation start point was used. The ELePhANT model was run on each of the 12 sonde cases in turn, along with the corresponding Met Office model data for these cases. Figure 4.3 shows the results for the best case study, 4 March 2004, where the ELePhANT and radar profiles agreed through most of the evaporation zone. The radar data for this case can be seen in figure 3.13, which shows an almost constant cloud base with time and therefore the sonde data from the 13 UTC sonde was quite likely to be representative of the radar data above Chilbolton. The start of the evaporation, defined by the start of the fall in the observed sonde humidity profile, does not always occur at the same height as the maximum in radar-derived ice water content, which was used to define the start of the evaporation zone. So, in figure 4.3, the ice water content profiles have been shifted vertically upwards by 280 m to ensure the evaporation started at the same point in each profile and a fair comparison can be made. Not all cases agree as well as the one presented in figure 4.3, but it shows that the ELePhANT model can produce an accurate estimate of evaporation depth given a good sample of data.

Figure 4.4 shows one of the cases where the ELePhANT model doesn't perform quite as

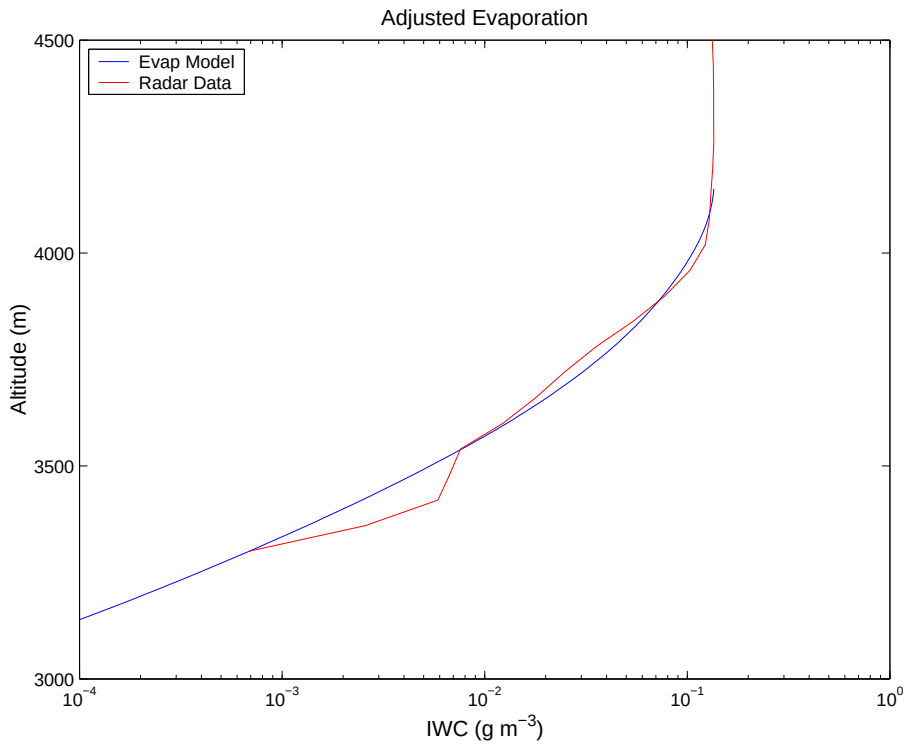

Figure 4.3: *Profiles of ice water content for the best result, the case of 4 March 2004 at 13 UTC.*

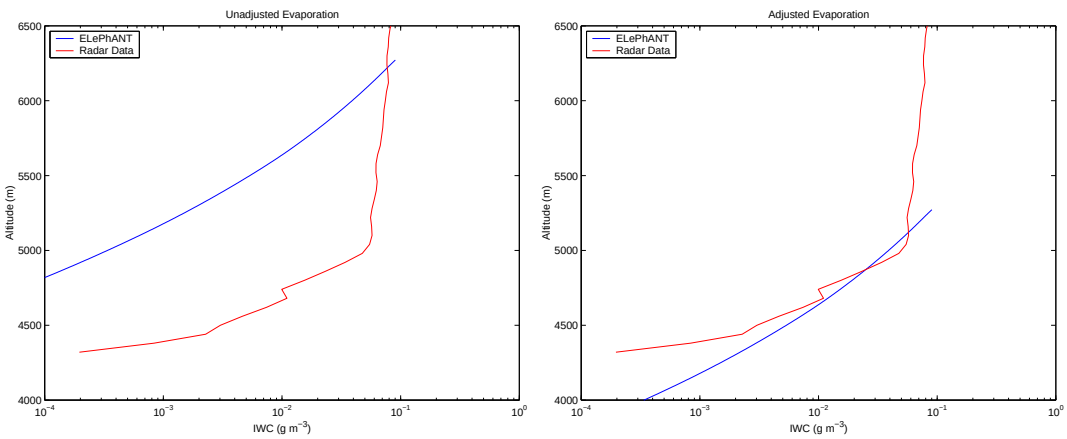

Figure 4.4: *Case study of 14 April 2003 at 05 UTC, where the ELePhANT model doesn't perform too well. On the left, we see a plot of evaporation set with the ELePhANT model evaporation starting at the same point as the maximum IWC observed by the radar. The right hand plot shows the result when the IWC profiles are adjusted so that the evaporation starts at the same point in each profile.*

well. From the plot on the right, it is obvious that the ELePhANT model has the wrong humidity gradient and the evaporation decreases much shallower with height then expected and hence the

evaporation zone is 200m deeper in the ELePhANT model than in the observations. It appears that the modelled evaporation follows the decrease in ice water content quite well, but that further down the profile, the humidity gradient changes and is much steeper, hence the evaporation is much greater and the overall evaporation depth is decreased in reality. The ELePhANT model takes the radiosonde data to calculate the evaporation, but if the sudden change in humidity was not represented in the sonde data, for example if it passed through a different section of cloud as it had drifted away from the location of the radar, then the model would incorrectly represent the humidity gradient and the evaporation depth.

The results for all 12 sonde cases used are shown in figure 4.5. This shows that the points generated for each of the twelve runs of the ELePhANT model with radiosonde data and each of the twelve runs of the ELePhANT model with Met Office model data appear to lie on the same line. When the ELePhANT model is initiated with radar and sonde data, the results predict evaporation zone depths on the same scale as those observed by the radar. This implies that the Met Office model is obeying the same evaporation physics as in nature, but the inputs of humidity into the Met Office model are wrong, causing deeper evaporation zone depths within the Met Office model.

It should also be noted that not all points lie perfectly on the straight line in figure 4.5. There is a random difference in both model and radar data which may be due to measurement noise. This is particularly true for radar-derived values of ice water content, which has been observed by Hogan *et al.* (2006) to have as much as a 55% error when calculated from radar and temperature measurements. It should also be noted that there are slight differences in parameterization between the ELePhANT and Met Office models. The ELePhANT model does not set its distribution back to the form of equation 4.7 at each time step but the Met Office model does. The grid spacing of the ELePhANT model is much finer than the Met Office model, which would create a systematic difference in the evaporation depth. The Met Office model applies a correction on the fall speed due to variations in the air density, but the ELePhANT model does not have this correction. This would mean that the fall speed within the ELePhANT model is too fast at lower pressures. Also, there is the possibility of a lag in the sonde's humidity measurements as it passes from dry air to saturated air as discussed in Miloshevich *et al.* (2004). They found that at the temperatures evaporation was observed to start at in this study, typical Vaisala radiosonde lags in humidity are at maximum twenty seconds. Unfortunately, the sonde data did not include the

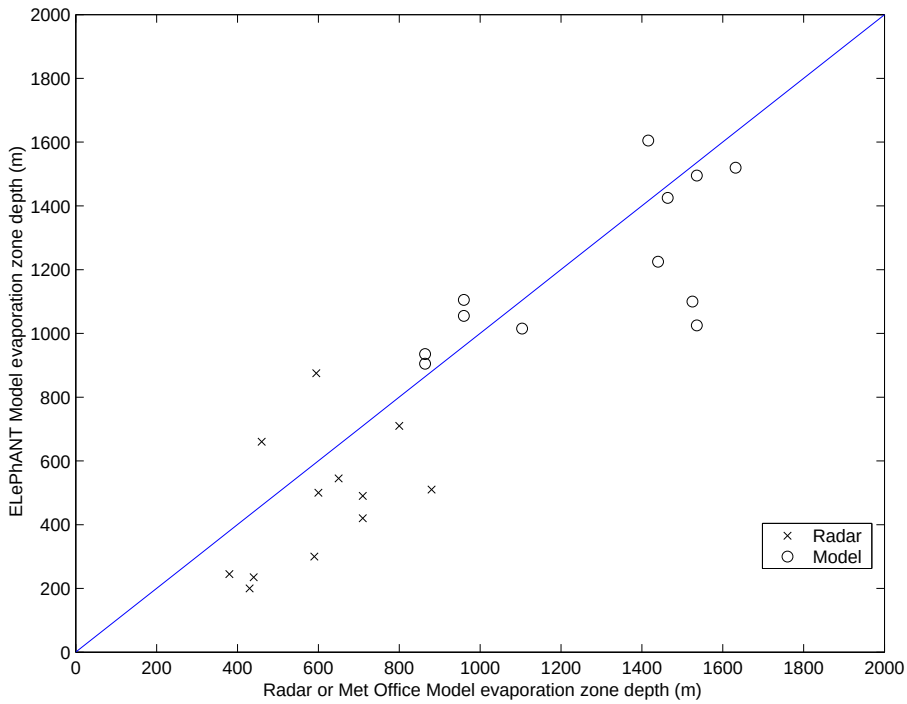

Figure 4.5: *Scatter plot of evaporation depths for the ELePhANT model using the humidity profiles generated for each of the twelve sonde (crosses) and model (circles) cases and the actual radar or Met Office model evaporation depth.*

ascent rate, but for the Vaisala RS80 radiosonde used, the ascent rate is roughly 5 m s^{-1} (Miloshevich *et al.*, 2004), which would lead to a vertical lag of 100 m and roughly 20% overestimate in evaporation depth.

4.5 Issues with Modelled Capacitance

So far, all experiments with the Met Office model have assumed that the capacitance of the particle, C is correct. Currently, the models use the value of spheres ($C = D/2$), which has been adopted for use in the ELePhANT model. However, this assumption should be relaxed in light of evidence (Field and Heymsfield, 2003; Westbrook *et al.*, 2007b) that aggregates are the dominant particle habit in thick non-precipitating ice clouds such as those studied in chapter 3. Numerical experiments by Westbrook *et al.* (2007a) have shown that for aggregates, the value of capacitance is roughly half the value for spheres ($D/4$), which will lead to a reduction of the evaporation rate.

In order to test how the Met Office model would respond if the capacitance were lowered,

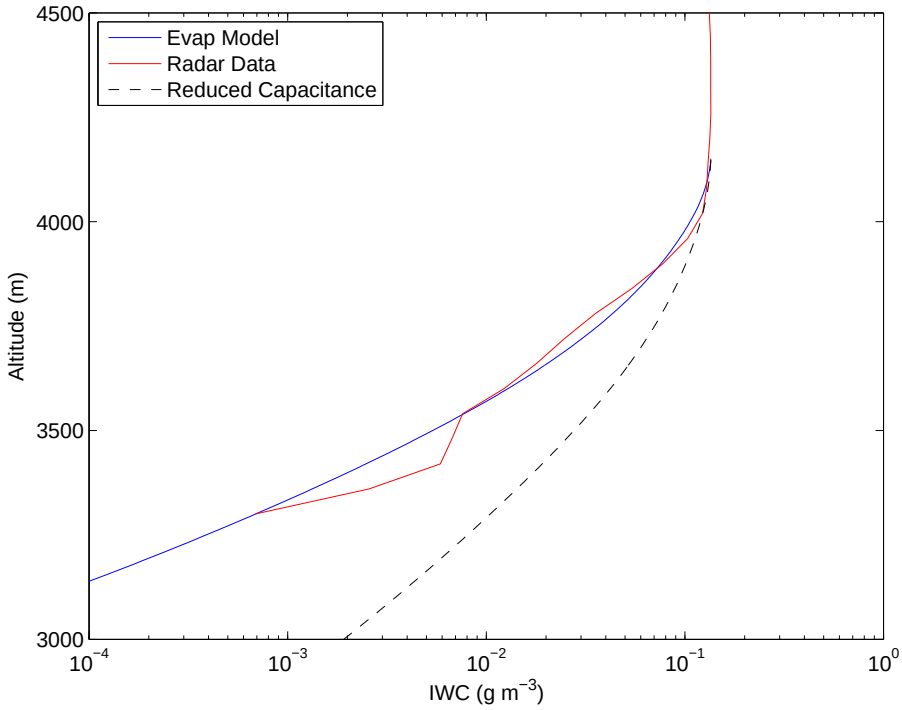

Figure 4.6: *Rerun of the Case of 4 March 2004 (as in figure 4.3) with the previous work displayed and the reduced capacitance (assuming particles are aggregates and after the work of Westbrook* et al.*, 2007a) shown as a black dashed line. The ventilation is assumed to be the same as for spheres.*

a value of $C = D/4$ was inserted into the ELePhANT model and the case study of 4 March 2004 repeated. All other factors, including the ventilation coefficient were kept constant. Figure 4.6 shows the results. It should be noted that the evaporation depth zone of the ELePhANT model when run with the reduced capacitance increases for this case from 545 m to 805 m. From this short experiment it should be noted that firstly the Met Office model assumption of spheres combined with the correct humidity profile will produce an accurate evaporation depth. However, concerns must be raised if the particles being observed at the base of evaporating ice are indeed aggregates; the reduce capacitance would lead to an increased evaporation depth within the Met Office model and could suggest that the model still has problems accurately representing the humidity profile properly. However, in this simple experiment, the ventilation coefficient has remained the same as for spheres. An accurate value of ventilation coefficient for aggregates has yet to be determined (Westbrook, personal communication). Should the value of ventilation coefficient be greater for aggregates than for spheres, then the reduced capacitance evaporation curve in figure 4.6 will move closer to the sonde-and-radar derived curve. Further work should

be done to assess the sensitivity to different capacitances and how accurate the humidity profile is within a number of cases of capacitance and ventilation coefficient.

4.6 Conclusions and Summary

This chapter has introduced the ELePhANT model which has tested the hypothesis made in chapter 3, that the deeper evaporation zone depth in the operational models were due to the models incorrectly representing the sharp drop in humidity within the evaporation zone. The ELePhANT model is a simple numerical model which has also been used to examine the sensitivity of the evaporation zone depth to several different atmospheric variables. The following conclusions can be drawn:

- The evaporation zone depth is most sensitive to changes in the humidity gradient. If the humidity gradient increases from 0.02 % m^{-1} then the evaporation zone depth decreases from 1 km to 500 m. Evaporation depth is also sensitive to changes in the temperature profile. A change in temperature from -10 to -20°C increases the evaporation depth by 200 m. Changes in the initial ice water content, made by changing the equivolumetric mean diameter of the ice particles are also important. Doubling the value of D_0 leads to an increase in the evaporation depth by 200 m.

- The evaporation zone depth is not sensitive to changes in pressure or changes in ice water content made by changing particle number concentration. Changing the starting pressure from 500 to 1000 mb changed the depth of the evaporation zone by less than 100 m.

- The ELePhANT model can predict evaporation depths for both radar and model profiles of ice water content to within 200 m of those observed by the radar. Systematic inaccuracies occur from the differences in grid spacing between the models, the parameterization scheme differences and that the sonde may have a lag when it passes from dry to moist air. Random inaccuracies may occur when the profiles of humidity may not be from the same cloud the radar is seeing over Chilbolton, depending on the direction of the wind and the sonde drift. Random measurement noise, particularly from radar measurements of ice water content may create random errors in the results.

- The results from the ELePhANT model shows that if the Met Office model had the correct

humidity gradient it could accurately represent evaporation zone depths. The evaporation zone depth is more sensitive to humidity gradient changes than changes in any other variable and hence the results from the ELePhANT model give strong evidence that the shallow humidity gradient within the evaporation zone in the Met Office model causes the deeper evaporation zone in this model.

4.7 Future Work

Although this chapter has shown that the Met Office model could potentially represent the correct evaporation depth scale, given enough grid resolution to represent the humidity profile accurately, there is still further work that could be done in this field. Firstly, the parameterization schemes of other models could be used to simulate evaporation and examine whether the humidity gradient is also a factor in their deeper evaporation depths and it would be interesting to see whether the schemes which incorporate two cloud water phases (e.g. Met Office, Wilson and Ballard, 1999) would perform better than the schemes which diagnose cloud phase, assuming one water content (e.g. ECMWF, Tiedtke, 1993, modified by Jakob, 1994). It would be worthwhile to see if the diagnostic Météo France model would represent the humidity drop accurately.

In addition, particle size should be examined with the model. Results in this chapter have shown that using the capacitance proposed for aggregates (Westbrook *et al.*, 2007a) would reduce the evaporation rate and lead to an even deeper evaporation zone within the Met Office model. Work needs to be continued to see if this really is the case that the aggregate assumptions should be made and if so, is there a larger problem than previously thought with the Met Office model, or would a ventilation coefficient for aggregates cancel out this effect?

Finally, the issue of wind drift should be considered with sonde profiles: more radiosondes should be launched and a critical distance away from Chilbolton should be set using the synoptic situation and satellite pictures to include only sondes for evaluation of the models that do not drift too far away. This is of particular relevance to a frontal system, where the front may only be tens of kilometres thick, a fast moving sonde could drift into clearer air and produce misleading results.

CHAPTER FIVE

A Lidar Forward Model for Comparisons Between ICESat and the ECMWF Model

5.1 Introduction

In chapter 1, it was noted that clouds are an important component of the climate system and that it is important for clouds to be accurately represented in both general circulation models (GCMs) for forecasts of future climate, and operational numerical weather prediction (NWP) models for precipitation and surface temperature forecasts. The ECMWF model is used for operational NWP forecasts and is capable of forecasting cloud and precipitation across the globe.

There have been a number of previous studies assessing the clouds within the ECMWF model. Jakob (1999) compared ECMWF reanalysis (ERA) data to data from the International Satellite Cloud Climatology Project (ISCCP) for the period July 1983 to December 1990. The reanalysis used the prognostic ECMWF cloud scheme (Tiedtke, 1993, modified by Jakob, 1994) and found that the ERA data tended to have underestimates of cloud cover in the extra-tropical oceans, the trade wind cumulus, the stratocumulus sheets off the west coast of subtropical continents and the summertime convective cloud over Eurasia. Similarly, Karlsson (1996) compared ECMWF model cloud cover with 2 months of advanced very high resolution radiometer (AVHRR) data over Scandinavia, and found that the ECMWF model had an underestimate of cloud by as much as 13%. However, these techniques are based only on passive observations and can give very little information on the vertical distribution of cloud. As noted in chapters 1 and 2, active remote sensing techniques are necessary to evaluate a model cloud scheme throughout the depth of the atmosphere.

Previous active ground-based studies have also assessed the performance of clouds in the ECMWF model. In chapter 2, we examined results from a number of radar evaluations of the

ECMWF model (Mace *et al.*, 1998; Beesley *et al.*, 2000; Hogan *et al.*, 2001; Illingworth *et al.*, 2007). In general, these showed that model cloud layers were generally too deep, with the ice cloud occurring more often than in the radar observations. Hogan *et al.* (2001) found there was a tendency for the ECMWF model to produce low cloud features up to 3 hours before they were observed. It is unknown why this effect occurs, but Hogan *et al.* (2001) suggested it may be due to an incorrect represented diurnal cycle. The boundary layer within the model was hypothesised to change from a nocturnal, stable profile to a daytime, well-mixed stratocumulus topped boundary layer too rapidly after sunrise. In addition, an assessment of ECMWF model cloud and surface radiation fields by Morcrette (2002) showed that above the ARM southern great plains site, the ECMWF model was able to get the position of ice and liquid water clouds roughly correct. Estimates of the reflectivity of ice and liquid clouds showed that the ice clouds within the model had roughly the correct reflectivity values, but liquid water clouds gave too low a reflectivity. However, power law relations were used to determine LWC from reflectivity factor and as shown in chapter 2, these may be unreliable.

The use of active instruments in space was discussed in section 2.5, with introductions to the Lidar In-space Technology Experiment (LITE; McCormick *et al.*, 1993), and ICESat (Zwally *et al.*, 2002). LITE data was used by Miller *et al.* (1999) to evaluate the ECMWF model and ICESat data was used in a similar ECMWF model evaluation study by Palm *et al.* (2005). In this chapter, we shall use ICESat data to evaluate the cloud parameterization scheme within the ECMWF model. The data from ICESat have been available long enough for some cloud studies to already have been undertaken. In particular, the satellite lidar data can be used to observe clouds in locations where passive instruments have difficulty making observations. Spinhirne *et al.* (2005) showed that ICESat lidar measurements get around the problem of the high surface reflectance of ice and snow that causes a positive bias in passive retrievals of cloud fraction. Comparing data from MODIS (MODerate resolution Imaging Spectrometer) to the ICESat lidar, they found that ICESat lidar measurements recorded cloud fractions around 0.4 to 0.6 at $-87°$ latitude while MODIS gave a cloud fraction close to 0.9. Although there may be some attenuation from thick ice clouds at these latitudes, the ICESat measurements are likely closer to the truth as unlike the MODIS observations, they are not contaminated by the large albedo of the polar surface. Comparisons of cloud top height made between MODIS and SEVIRI (Spinning Enhanced Visible and Infra-Red Imager) data and ICESat were also made by Naud *et al.* (2005). They found that

MODIS and SEVIRI overestimated the cloud top heights by 300–400 m when the clouds were low and opaque, but overestimated the cloud top height for high and thinnest clouds. For low cloud, Naud *et al.* (2005) state that this is most likely to be due to contributions of water vapour above the cloud-top contaminating the MODIS retrieval or to poorly resolved temperature inversions in reanalysis profiles. For high clouds, it is suggested that the part of the cloud where the most interactions with radiation take place is closer to cloud base and that this affects the cloud top retrievals.

Palm *et al.* (2005), took one orbit of ICESat data and compared it to the cloud fraction from the ECMWF model. By making direct comparisons between cloud fraction and using skill scores from Miller *et al.* (1999), they deduced that the ECMWF model was capable of representing low clouds quite well, but often produced too much high cloud, particularly evident from long (48 hour) forecasts. Model skill scores also decreased with increasing time. However, one must be very careful when comparing observations made by lidar instruments directly to clouds as there will be a loss of signal power (attenuation) as the beam passes through clouds, and often there will be a total extinction of the signal in liquid water clouds. Palm *et al.* (2005) estimated that this occurs around 10% of the time. However, to achieve a fair comparison between lidar and model, a method of accounting for the attenuation of the signal must be found.

This study attempts to make a fair comparison between the ICESat lidar and the ECMWF model. We follow a similar method to that used by Chiriaco *et al.* (2006), where model variables are used to predict the lidar signal, rather than try and use the lidar observations to retrieve model variables. This means that we account for the attenuation that occurs as the lidar passes through thick cloud, allowing a much fairer comparison with the model.

Section 5.2 describes the methodology used to derive the lidar signal from the ECMWF model variables. Processing of the ICESat lidar signal is necessary to remove noise and to place the data upon the ECMWF model grid; this is described in section 5.3. Once processing is complete, various statistical tests can be performed to judge the model's performance across the globe. These are described in section 5.4, with the associated results. A summary of the findings is presented in section 5.5.

5.2 Processing of Model Data

In this section we shall use a lidar forward model to predict the backscatter received by the ICESat lidar, given model variables of liquid water content and ice water content. This method is able to account for the attenuation of the ICESat signal as it passes through cloud.

Following the method of Platt (1973), and using equation 2.11, the lidar equation may be written as follows:

$$\beta'(z) = \frac{\alpha(z)}{s} \exp\left(-2\eta \int_{z}^{z_{lid}} \alpha(z')dz'\right), \tag{5.1}$$

where $\beta'(z)$ is the attenuated backscatter at altitude z above the Earth's surface and z_{lid} is the orbit altitude of the ICESat. The extinction-to-backscatter ratio or "lidar ratio" is shown by s and multiple-scattering is approximately represented by η. The visible extinction coefficient is α. Collectively the $\alpha(z)/s$ term represents the unattenuated backscatter while the terms within the exponential represent the attenuation of the lidar signal, sometimes referred to as the 'transmission term'.

The principle of the lidar forward model is to first use ECMWF model variables to predict the value of the visible extinction coefficient, α, at each vertical grid box within the model; this is explained below. If we can obtain an estimate of the lidar ratio, s, and the multiple-scattering factor, η, then the attenuated backscatter can be predicted at each level of the model and then compared to ICESat data.

5.2.1 Converting Model Variables to Extinction Coefficient

To calculate the value of the visible extinction coefficient, α from model variables at each individual grid box, we use the following expression (after Foot, 1988):

$$\alpha = \frac{3}{2}\frac{\mathrm{IWC}}{r_{ei}\rho_i} + \frac{3}{2}\frac{\mathrm{LWC}}{r_{el}\rho_l}, \tag{5.2}$$

where IWC is the model ice water content and LWC is the model liquid water content at that particular grid box. The calculation uses the ECMWF model's parameterizations of the effective radius of ice, r_{ei}, which is taken as a function of temperature following Ou and Liou (1995), but setting the constraint that r_{ei} can only vary between 30 and 60 μm. Liquid water effective radius, r_{el}, follows the parameterization of Martin *et al.* (1994), with the concentration of cloud condensation nuclei over the ocean held constant at 50 cm^{-1}. Over the land, this value is again

constant, but this time at 900 cm^{-1}. The values ρ_l and ρ_i are the densities of liquid water and solid ice, respectively. Once the profiles of extinction coefficient have been calculated, the lidar forward model can be run but it is important that it takes account of the cloud overlap scheme used within the ECMWF model. This is discussed further in section 5.2.6.

5.2.2 Calculation of the Multiple-Scattering Factor

An important factor in equation 5.1 is the inclusion of the multiple-scattering factor, η, suggested by Platt (1973). This can vary between 0.5 and 1 depending on the altitude of the satellite, the wavelength of the radiation and the size of the particles the radiation encounters. A multiple-scattering factor of 1 is the single scattering limit, often appropriate for a ground-based lidar, where all the scattered photons are lost, except for those directly backscattered to the instrument. The value of 0.5 is the wide field-of-view limit, often more appropriate for spaceborne lidars, where narrowly forward scattered photons remain within the telescope field-of-view.

The multiple scattering factor can be calculated accurately using a method such as Eloranta (1998). However, this method is too computationally expensive to run on a large amount of ICESat data, so quicker yet accurate solutions had to be found.

Hogan (2006) developed a faster method for calculating η than that of Eloranta, by separating the outgoing photons into distributions that have had zero, one or more than one multiple scattering event. However, this method would still be too computationally expensive to run in operational data, so it was decided to use Hogan (2006) to estimate suitable values of η through various different idealised stratocumulus cases that were similar to those present throughout the period of study.

Equation 3 of Hogan *et al.* (2003b) state that for an optically thick stratocumulus layer, the integrated backscatter (γ_w) is given as

$$\gamma_w = \frac{1}{2\eta s}, \tag{5.3}$$

hence given the value of s of 18 (a typical value for liquid water droplets, see section 5.2.3) and the integrated backscatter from the Hogan (2006) code it is possible to obtain a mean value of the multiple-scattering factor, η. Eight different experiments were run by changing the effective radius values and liquid water contents of the clouds, using the properties of ICESat listed in table 5.1. In each case, the thickness of the stratocumulus cloud was adjusted so that it was at the

minimum vertical thickness to allow it to be optically thick. A demonstration of the backscatter generated is shown in figure 5.1. This shows that the backscatter using the multiple-scattering limit ($\eta = 0.5$) gives similar results to the code of Hogan (2006). The same is true for the results of all eight experiments, which are shown in table 5.2. Using the single-scattering limit ($\eta = 1$, shown as the blue line in figure 5.1) would give incorrect values of backscatter for this profile.

Using table 5.2, the values of η for the eight experiments were found to be 0.500 for 532–nm backscatter data. Hence the value of η for all forward model calculations was chosen to be 0.500. As we are at the wide field-of-view limit, this method should be adequate for this work, but a sensitivity to η will be included in the error analysis in section 5.4. Inclusion of a small estimated experimental error (e.g ± 0.02) on the measurement should not vary the results of model backscatter more than a few percent. It should also be noted that with ice clouds, the forward scattering is even more peaked and so these should be even closer to the wide field-of-view limit. It should be noted that Platt (1973), Eloranta (1998) and Hogan (2006) only consider narrow forward scattering and not wide angle forward scattering. This can result in apparent pulse stretching (Winker and Poole, 1995). There is no fast method to include this within a forward model at present, so this effect has not been included here. However, with currently available codes this is the limit of what can be achieved.

5.2.3 Lidar Ratio

The other unknown variable within equation 5.1 is the value of the lidar ratio, s. This takes the values of 18.8 $\pm$ 0.8 sr for liquid water (O'Connor *et al.*, 2005) but can vary between 10 and 40 sr for ice particles (Platt *et al.*, 1999; Chen *et al.*, 2002). For the purposes of this experiment, we shall be taking the value of the lidar ratio to be 20 (close to the constant for liquid water), but shall examine the sensitivity of changing the lidar ratio between the extreme values on the final result incorporating in the error estimation in section 5.4.

5.2.4 Interpolation of model data on to an ICESat height grid

Due to the relatively low resolution of the model height grid, sharp transitions would occur in water contents, producing an unrealistic profile of the lidar backscatter. In some cases, this could mean the attenuation of the simulated lidar signal would be too great. For example, if we had

Property	Value
Orbit Altitude	600 km
Wavelength	532 nm
Sampling Frequency	5 Hz
Latitude Range	$\pm 86°$
Repeat Orbit Cycle	8 days
Orbit Speed	7 km s^{-1}
Footprint Size	70 m
Minimum Detectable Backscatter at 10 km	1.6 $\times 10^{-6}$ sr^{-1} m^{-1}
Laser Divergence Angle	75 μrad
Telescope field-of-view	375 μrad

Table 5.1: *ICESat characteristics relevant to this study, from Zwally* et al. *(2002). The minimum detectable backscatter is the lowest value observed from molecular scattering over the 15-day study period.*

LWC (g m^{-3})	R_e (μm)	η
0.025	**7.5**	**0.5**
0.025	5.0	0.5
0.025	10.0	0.5
0.025	15.0	0.5
0.010	7.5	0.5
0.050	7.5	0.5
0.100	7.5	0.5
0.500	7.5	0.5
1.000	7.5	0.5

Table 5.2: *Results of experiments to determine the value of the multiple-scattering factor, η. The control run is shown in bold.*

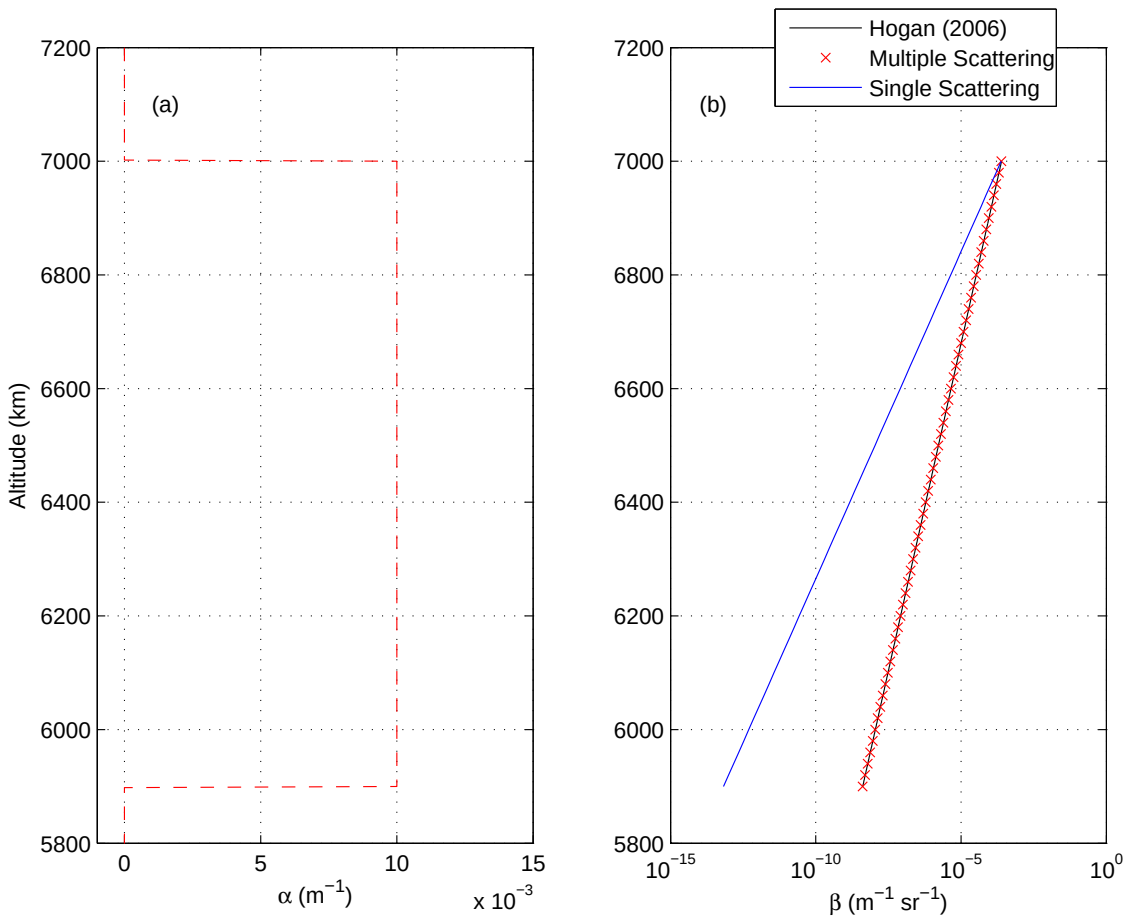

Figure 5.1: *An example of the process to calculate the value of the multiple-scattering factor (η) using code by Hogan (2006). Plot (a) shows a profile of extinction coefficient (α) which shows the location of the cloud from 5.9–7 km altitude, with a liquid water content roughly equivalent to 0.05 g m^{-3}. Plot (b) shows the attenuated backscatter generated by the method of Hogan (2006) as a black line, with the estimation of attenuated backscatter with η set to 0.5 (maximum multiple-scattering) shown as red crosses. The blue line represents the attenuated backscatter profile if the value of η was set to 1 (single scattering limit).*

a large ice water content in one model level, the attenuation could potentially be exaggerated through a depth of the atmosphere of several hundred metres. To allow a smooth transition in the lidar forward model output, a linear interpolation was used for the model variables of ice water content and liquid water content. However, the cloud fraction was interpolated using a nearest-neighbour interpolation method. This was because the amount of cloud is very important to the forward model calculations. Consider a cloud with high ice water content or low liquid water content, represented in the vertical over two model grid boxes. The cloud fraction in the highest grid box is 0.5 while the one immediately beneath has a cloud fraction of 1. Use of a

linear interpolation would increase the cloud fraction on the lidar forward model grid between the two ECMWF model grid points and hence would result in less clear sky and less radiation unaffected by cloud in the depth of atmosphere between the two grid points. A nearest-neighbour interpolation would be more accurate in these circumstances.

However, this higher resolution is only used to run the lidar forward model. In section 5.2.7 we shall see how the cloud fraction is recalculated on the model grid, allowing a direct comparison between the ICESat lidar and the ECMWF model before and after running of the lidar forward model.

5.2.5 Selecting Model Grid Points

Since the aim of using a lidar forward model is to enable a fair comparison between the ECMWF model and ICESat, it is vital that the model and the ICESat data are on the same grid to be compared accurately. To analyse one day of ICESat data, the time and location (latitude and longitude) of the satellite are extracted from the orbit files. The ECMWF analyses are available at 0000 UTC and 1200 UTC, with intervening forecasts available in 3-hour intervals. The ICESat track points are grouped into nine time groups corresponding to the closest ECMWF data available. ICESat points between 0000 UTC and 0130 UTC are associated with the 0000 UTC model analysis and similarly, the ICESat points between 0130 UTC and 0430 UTC are associated with the 0300 UTC model forecast. This process continues in three hour groups, until 2230. The points between 2230 UTC and 00 UTC are associated with the relevant 0000 UTC analysis of the following day.

Once the ICESat points have been grouped, ECMWF model grid profiles closest to the ICESat ground track containing a vertical profile of the model's cloud fraction, relative humidity, temperature, wind speed, ice and liquid water contents are extracted from the ECMWF model output.

5.2.6 Cloud Overlap

An important factor in the lidar forward model calculations is the use of maximum-random overlap as currently implemented in the ECMWF model (Morcrette and Jakob, 2000). To achieve maximum-random overlap, each model grid box is first divided into a set number of sub-columns horizontally. The choice of the number of sub-columns is a trade-off between computer run time

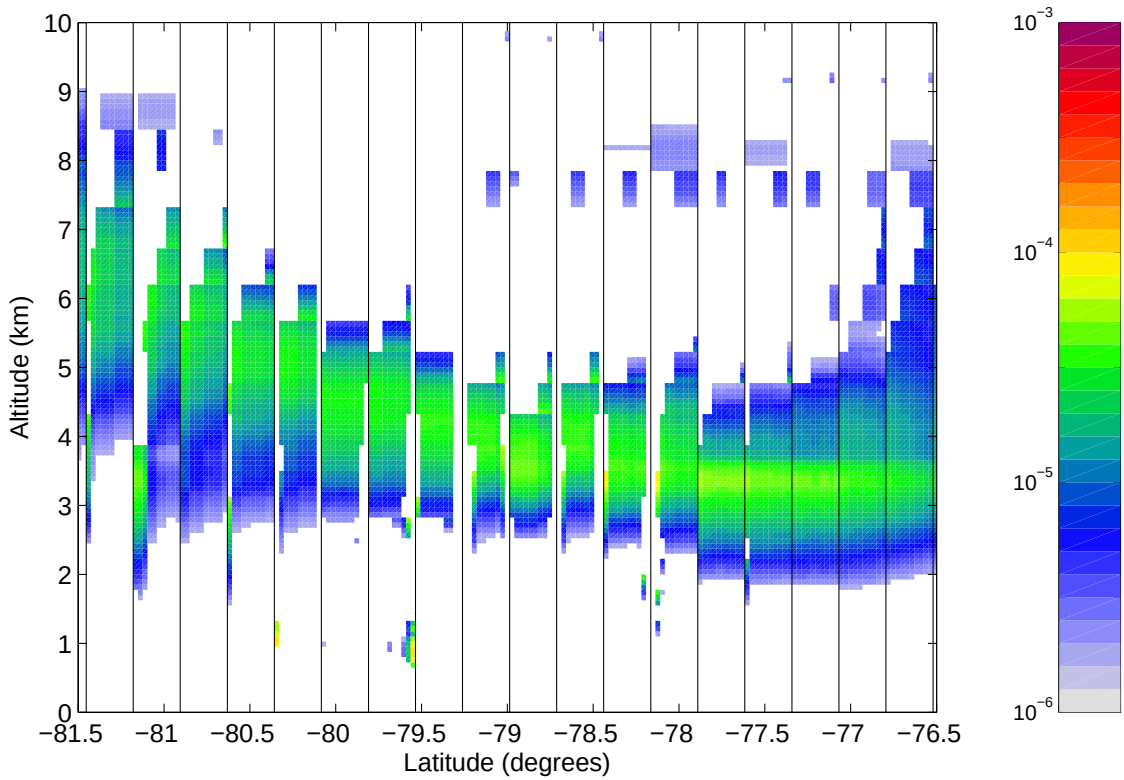

Figure 5.2: *An example of the high-resolution backscatter simulated from model data on 30 September 2003. The thin vertical black lines show the ECMWF model horizontal grid spacing. Where there is cloud cover of one (e.g. latitudes $-77.5°$ to $-77.0°$ and altitudes 2–6 km), the model grid points totally overlap those above. Where there is a cloud-free gap between two cloudy layers, the overlap is random, as seen at latitudes $-80°$ to $-77°$ and altitudes above 8 km. For adjacent cloudy layers, the overlap is maximised with the layer above.*

and accuracy. For these experiments, 10 sub-columns were used. This means that the cloud fraction in each model grid box was rounded to the nearest 10%, giving a good balance between computer run-time and accuracy.

The lidar forward model follows the ECMWF model in using a maximum-random overlap method, as shown in figure 2.7. The backscatter that results from this process is shown in figure 5.2. Although looking at this figure, there appears to be an artefact in the shape of the clouds, this is entirely due to the nature of the overlap scheme and no attempt has been made to try and get the cloud structure realistic, simply to represent what would actually happen in the ECMWF model. The cloud in each grid box is aligned so as to achieve maximum overlap with that immediately above it, as the cloud fraction gets larger, this can mean that the cloud eventually aligns itself to the left or the right hand side of the grid box. The values of interest are actually only the cloud

fraction on the model grid, and not the location of individual clouds in the sub-grid displayed in figure 5.2. If the position of the overlapped cloud were altered within the grid box, say by moving the cloud that is aligned on the right hand side of the grid box to the left hand side of the grid box, without changing the maximum-random overlap assumption, there would be no effect on the final result.

Once the details of the maximum-random overlap are known and the values of all the variables in equation 5.1 are known, the lidar forward model can be applied to each sub-layer to calculate backscatter using the model variables interpolated on to the ICESat height grid.

5.2.7 Cloud Fraction Resampling

In order to compare the cloud fraction from the lidar forward model with cloud fraction from ICESat, cloud fraction data are 'resampled'. At this stage, the ECMWF lidar forward model values are on a high-resolution grid with 10 sub-columns to each model grid box in the horizontal and the data lie on an ICESat height grid in the vertical. To resample the cloud fraction, a model grid is superimposed on to the high resolution data and the percentage of points containing backscatter data above the sensitivity threshold of ICESat (minimum detectable backscatter; see table 5.1) is counted.

Figure 5.3 shows an example of backscatter from the lidar forward model on the ECMWF model grid along with the raw ECMWF mean cloud fraction and the lidar forward model cloud fraction. The length of this swath is approximately 5000 km. From the lidar forward model cloud fraction, it can be seen that the cloud fraction has reduced both above (where the cloud would be too tenuous for the lidar to detect) and below (where attenuation would mean that there would be no cloud observed).

5.3 Processing of Lidar Data

In addition to running the lidar forward model, processing of the ICESat lidar data must take place to remove any return that is not cloud. The properties of the ICESat lidar as used in these experiments are shown in table 5.1.

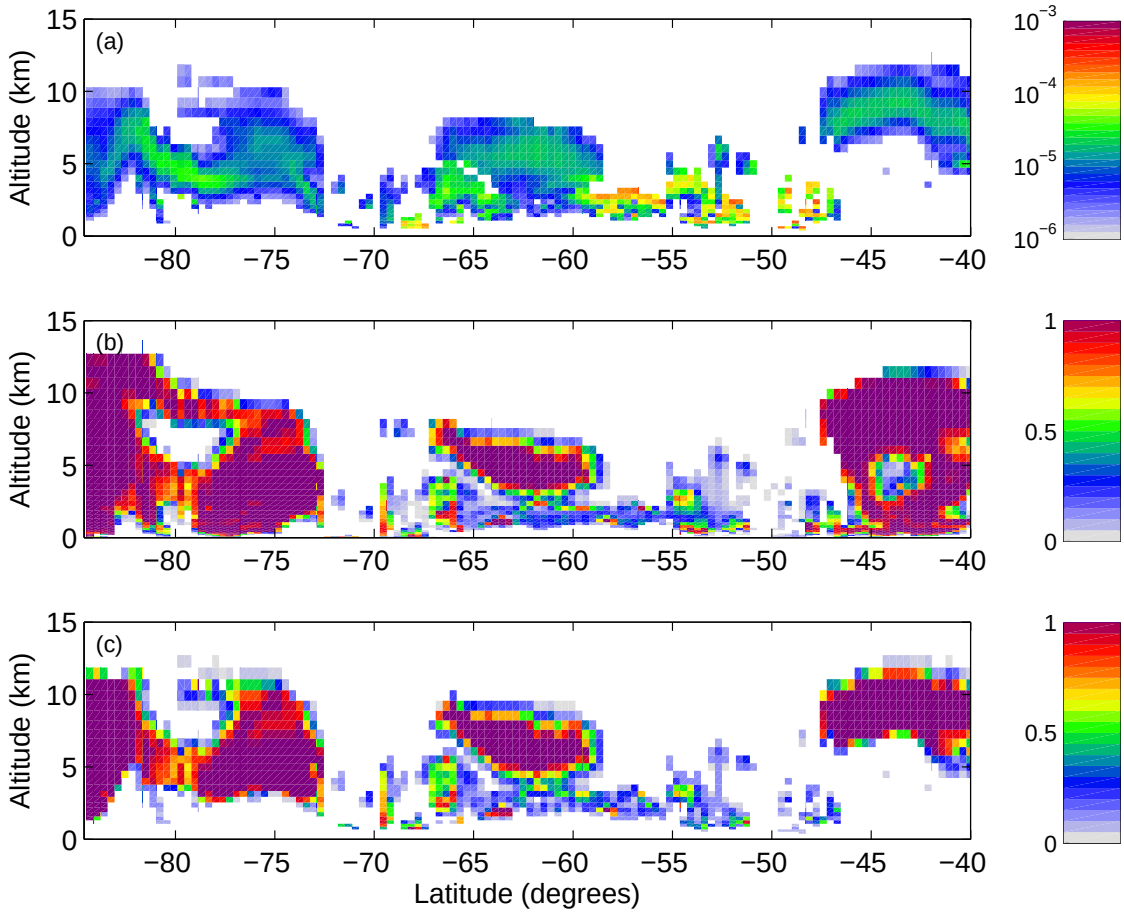

Figure 5.3: *Demonstration of the processing of ECMWF model data from 30th September 2003, from 0117–0137 UTC (a) Lidar forward model backscatter in* sr^{-1} m^{-1} *on a model grid. (b) ECMWF model cloud fraction in its raw state. (c) The model cloud fraction after the lidar forward model has been run. The backscatter data from figure 5.2 forms part of the left hand side of plot (a).*

5.3.1 Rejection of Unwanted (Non-Cloud) Signal

To clean molecular return and instrument noise from the data, the data are divided into 4 minute sections (equivalent to 1680 km) and the mean backscatter above 15 km for this period is used to remove the molecular noise from the lower levels for the whole of the period. It is assumed that at this level, there is no cloud and all the signal received is molecular backscatter or instrument noise. The mean and standard deviation of the linear backscatter at these heights are obtained. These values are only just above the minimum detectable backscatter given in table 5.1 and is due to molecular backscatter. The mean and standard deviation are used to set a noise threshold for the rest of the profile. The threshold at which a signal is accepted to be a cloud signal rather

than molecular or noise is 2 standard deviations above the mean, chosen empirically. If a higher threshold is set, then the clouds start to be removed. With a lower threshold, obvious molecular data still remains within the data. Although the return due to molecular scattering increases with decreasing altitude, the threshold of 2 standard deviations is sufficient to remove the molecular signal down to ground level. A speckle filter is then used to remove any isolate pixels that may remain within the data.

In addition to the removal of noise outlined above, aerosol has also to be removed from the data. Since aerosol data have similar values of backscatter as thin ice cloud, aerosol pixels would be above the noise threshold defined for the 4 minutes period. Aerosol pixels tend to exist as small groups of adjacent data points with backscatter high enough to allow them to exist after the single pixels have been removed from the data.

To remove the aerosol data, the lowest 3 km of the data is divided into a series of grid boxes. As aerosol tends to have quite low backscatter values, all points within the box with low backscatter (values less than 5×10^{-5} m^{-1} sr^{-1}) are located and the standard deviation of these points is calculated. Since aerosol has a low standard deviation and cloud a higher standard deviation, the points with a very low standard deviation (less than 3×10^{-6} m^{-1} sr^{-1}) are assumed to be aerosol and removed.

Naturally, the choice of aerosol removal box size is important to the aerosol removal process. If the grid boxes are too large, a lot of low backscatter will be removed, but if the grid boxes are too small then there will be insufficient data to provide a good sample of the variance of the low backscatter used to remove the aerosol. Best results occurred when grid boxes of 50 by 20 pixels were used. This gives 1000 data points in total in each grid box which is a large enough sample for variance measurements.

Another obvious issue with the aerosol removal method is the removal of any low-backscatter cloud data that occurred in the same box as aerosol we were trying to remove. In some cases, the edges of the clouds were actually removed from grid boxes containing data. However, upon closer examination, this would only lead to the removal of a few points which would equate to less than a 4% error in the cloud fraction calculated.

A digital elevation model was used to remove the high backscatter return from the ground up to and including 75 metres above the surface. Figure 5.4 shows the processing of ICESat lidar data to remove noise and to average on to a model grid to give mean backscatter and cloud

fraction.

5.3.2 Averaging of ICESat Backscatter Data

To compare backscatter from the ECMWF model and backscatter from the ICESat lidar, ICESat profiles which correspond to the same ECMWF model grid box were averaged in the horizontal while maintaining the ICESat vertical resolution.

Figure 5.4 shows the averaging process for a selection of ICESat data over the Arctic, corresponding to the ECMWF values shown in figure 5.3. The ICESat data were averaged on to the model grid, selecting and averaging ICESat track points to the nearest ECMWF model grid point. It can be seen that the data neatly averages on to the ECMWF model grid. Occasionally observed is apparent horizontal stretching and squashing of the original data as it is transformed on to the model horizontal grid. This phenomena is due to the grouping of ICESat track points to individual ECMWF model grid points, which was described in section 5.2.5. Some model grid points will be the average of many ICESat track points while some will only be the average of a few. For this reason, any model grid point that corresponded to less than 5 ICESat track points was rejected from the analysis. Cloud fraction was then calculated on the model grid by using the same method as used for the lidar forward model cloud fraction resample, described in section 5.2.7, with the number of ICESat profiles replacing the sub-columns used in the lidar forward model.

5.4 Results

The lidar forward model has been run on 15 days of ICESat and model data from 30 September 2003 to 14 October 2003 inclusive. This has generated a data set where the length of the ICESat track is over 9 million kilometres. This is equivalent to over 14 years of continuous observations at a mid-latitude ground-based station, assuming a mean wind over the station of 20 m s^{-1}. Although one of the possibilities of the data is to examine the seasonal variations in cloud climatology, this study is restricted to a short data period only due to the computational expense of processing the data and the availability of ICESat data at the time of processing that was of the same release version and of good quality. Data was specifically selected from a period just after a new laser was switched on, to avoid the problems caused by laser signal degradation.

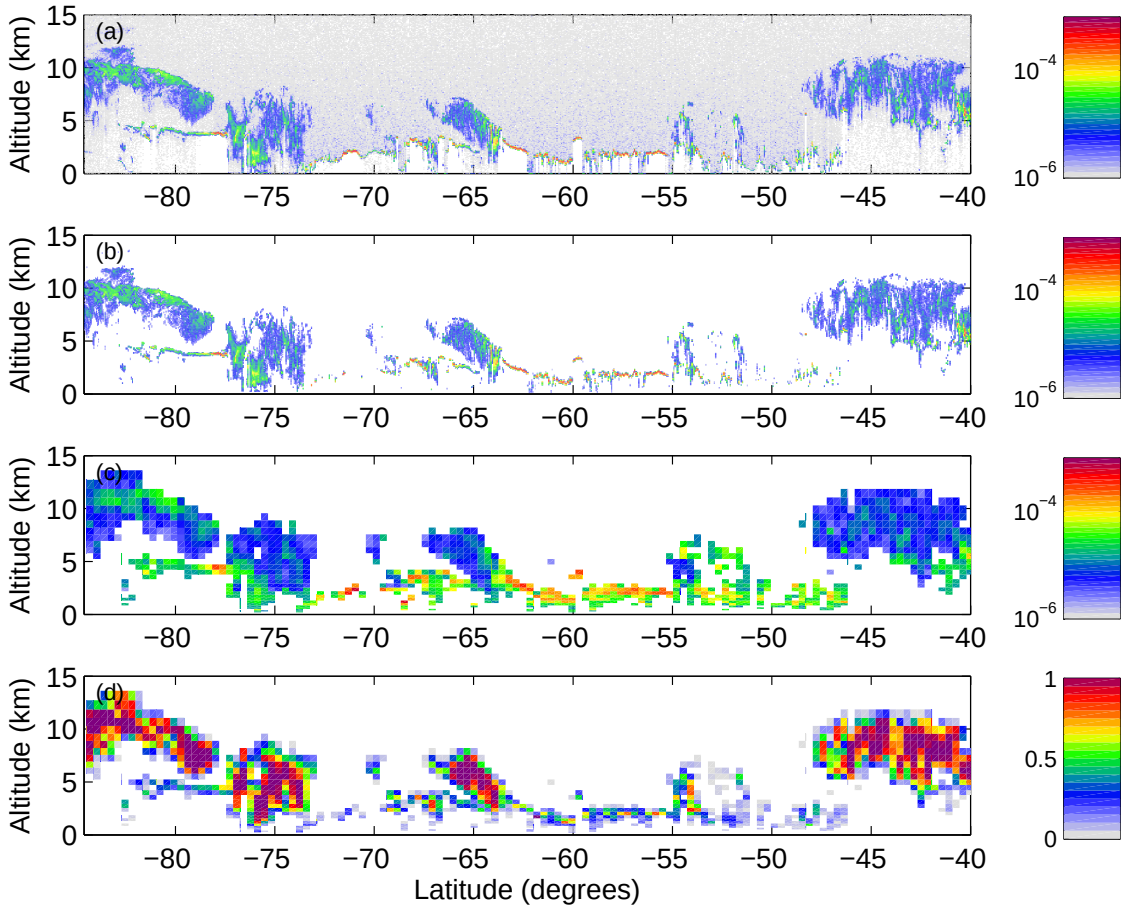

Figure 5.4: *Demonstration of the processing of ICESat lidar data, for the same time period as the model data in figure 5.3. (a) Raw attenuated backscatter data in* m^{-1} sr^{-1}*. (b) After processing to remove noise (molecular backscatter, aerosol and ground layers). (c) After averaging the backscatter to a model grid. (d) cloud fraction calculated on the model grid, (dimensionless).*

5.4.1 The Effect of the Lidar Forward Model

As we saw in figure 5.3, there was a reduction of model cloud fraction due to the processing of the lidar forward model. Cloud fraction is reduced at high altitudes due to the backscatter it would produce being lower than the sensitivity of the ICESat lidar. These clouds are sometimes referred to as "ghost clouds" as they have ice water contents of 10^{-5} g m^{-3} or less and cannot be easily detected. Cloud fraction is also reduced at lower altitudes due to attenuation of the lidar beam as it passes through thick cloud.

Figure 5.5 shows the effect of running the lidar forward model on the ECMWF model mean cloud fraction over the whole globe. There is a reduction of model cloud fraction in the tropics,

at heights above 14 km. In mid and high-latitudes and at high altitudes, the cloud fraction after running the lidar forward model almost matches the original model cloud fraction, but there is an obvious reduction of cloud at lower altitudes and all latitudes. At the lowest altitudes over the poles, mean cloud fraction is reduced from around 0.3 to around 0.05. This is important for any comparison between model and lidar that are made; comparing the ICESat-derived cloud fraction directly with the model would be rather unfair to the model, as can be seen by comparing figures 5.5 and 5.6, the latter of which represents the cloud data obtained from the ICESat analyses in this study.

Although figure 5.6 is an average over 15 days, it shows the general location of global mean cloud during early October. The location of ice cloud outflow from the ITCZ is shown at a height of roughly 15 km. Thicker ice clouds are observed over both poles and extend over the mid-latitude storm track regions, where the cloud extends down to 2 km. Boundary layer cloud is noted over much of the globe. There is a large amount of boundary layer cloud around $-60°$, and as this corresponds to the area of the Southern Hemisphere where there is no land, this is most likely to be marine stratocumulus. There appears to be very little cloud within the tropical mid-troposphere. One possible explanation is that cloud in these regions is very thin, and the attenuation of the lidar signal in the thickest ice clouds of the ITCZ has meant that the signal sensitivity has dropped so these clouds cannot easily be detected.

5.4.2 Location of Cloud with Latitude

In order to examine the performance of the ECMWF model over several different latitude bands and different altitudes, each hemisphere was divided into three latitude regions. In each region, following the work of Hogan *et al.* (2001), the mean frequency of cloud occurrence and mean cloud amount when present was calculated for altitudes up to 20 km. Frequency of occurrence for a particular region, or model grid box, is defined as the fraction of times that cloud fraction exceeds a threshold value of 0.05 within the model or observations. Amount when present is the mean cloud fraction over the grid boxes of interest when cloud fraction exceeds 0.05. To a rough approximation, the two variables can then be multiplied together to give the mean cloud fraction with altitude for each of these six regions. Each region is an average of many thousands of lidar forward model and ICESat profiles, once averaged on to a model grid.

To examine the errors on the lidar forward model, the sensitivity of the multiple-scattering

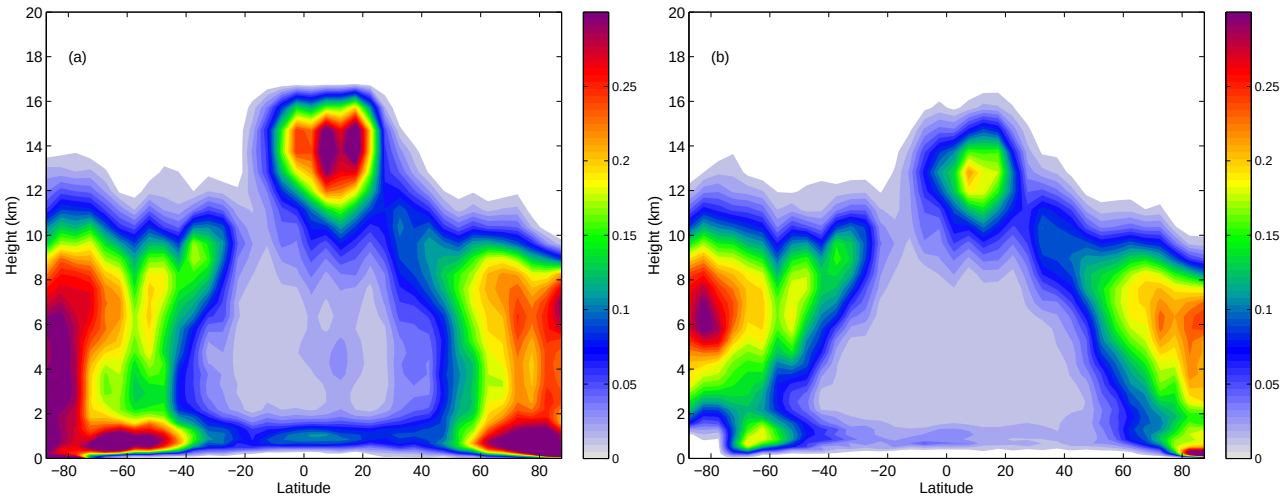

Figure 5.5: *(a) Latitude and height variation of ECMWF model cloud fraction for 15 days from 30/09/2003 0000 UTC to 14/10/2003 2359 UTC under the ICESat track. (b) Cloud fraction from the ECMWF model from the same time period as (a) but after the lidar forward model had been run and the cloud fraction resampled.*

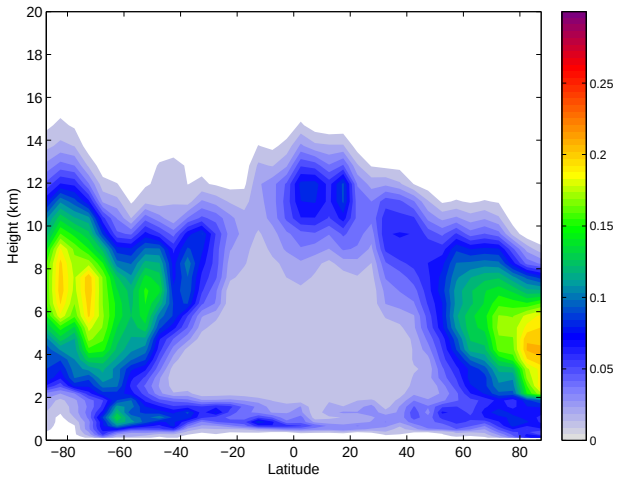

Figure 5.6: *Mean Cloud Fraction from ICESat lidar observations from 30/09/06–14/10/06*

.

factor and the lidar ratio only are allowed to vary. However, as can be seen from table 5.2, the values of the multiple-scattering factor are around the minimum value suggested by Platt (1973) and a solution lower that 0.5 would be unphysical. So the multiple-scattering factor within these experiments was allowed to vary between 0.5 and 0.6. The lidar ratio can vary from 10–40 as noted earlier in section 5.2.3. Examining equation 5.1, it can be seen that a high value of the multiple-scattering factor causes the most attenuation and the smallest value of the attenuated

backscatter and vice-versa. The highest value of the lidar ratio causes the smallest value of attenuated backscatter and vice-versa. Hence to assess the errors on the lidar forward model, three experiments were performed on one day of ECMWF model data (10 October 2003, chosen as the ICESat latitude-altitude analysis showed cloud in many different regions of the globe and more so than any other day). The first experiment was run with lidar ratio of 20, and multiple-scattering factor of 0.5 (as the lidar forward model); the second had a value of lidar ratio to be 40, and multiple-scattering factor 0.6; the third had lidar ratio of 10, and multiple-scattering factor 0.5.

The results of this analysis are displayed in figure 5.7. The errors due to varying the multiple-scattering factor and the lidar ratio are included in this figure. The most striking difference is the reduction in model quantities following the processing of the lidar forward model. In the polar regions the low-altitude cloud fraction and frequency of occurrence are substantially reduced by the model processing. In the equatorial regions there is a reduction of mean cloud fraction and amount when present at high altitudes, caused by very low ice water contents within the model that would not be detected by ICESat. At these low latitudes, there is a large reduction in cloud frequency of occurrence within the lower and mid-troposphere. This is caused by a combination of clouds beneath the ICESat sensitivity threshold and reduction in the sensitivity of the ICESat lidar as it is attenuated through the thick ice clouds that are associated with tropical convection in this region of the atmosphere that occurs in some of the model data.

After processing of the lidar forward model has taken place, the results seen by comparing figure 5.5 to figure 5.6 and examining figure 5.7 show that the ECMWF model is making a reasonable job of representing the mean cloud fraction, with a few exceptions. There is a slight underestimate of mean cloud fraction in tropical low clouds. This is most likely due to the lack of shallow cumulus convection within the model and poor representation of the processes causing convection within the model. In the mid-latitudes and polar regions, the model has too large a mean cloud fraction within the mid-troposphere and in the vicinity of the equator, the cloud fraction for high altitude ice cloud is too great by up to 0.15. Within these same regions, the frequency of occurrence is slightly too high, by around 5%. The modelled amount when present is also too high for these areas. Both the mean cloud fraction and amount when present for the cloud in these locations is too large even when the errors on the lidar forward model are taken into consideration.

The most likely explanation for too large amounts of cloud in these regions is a problem with

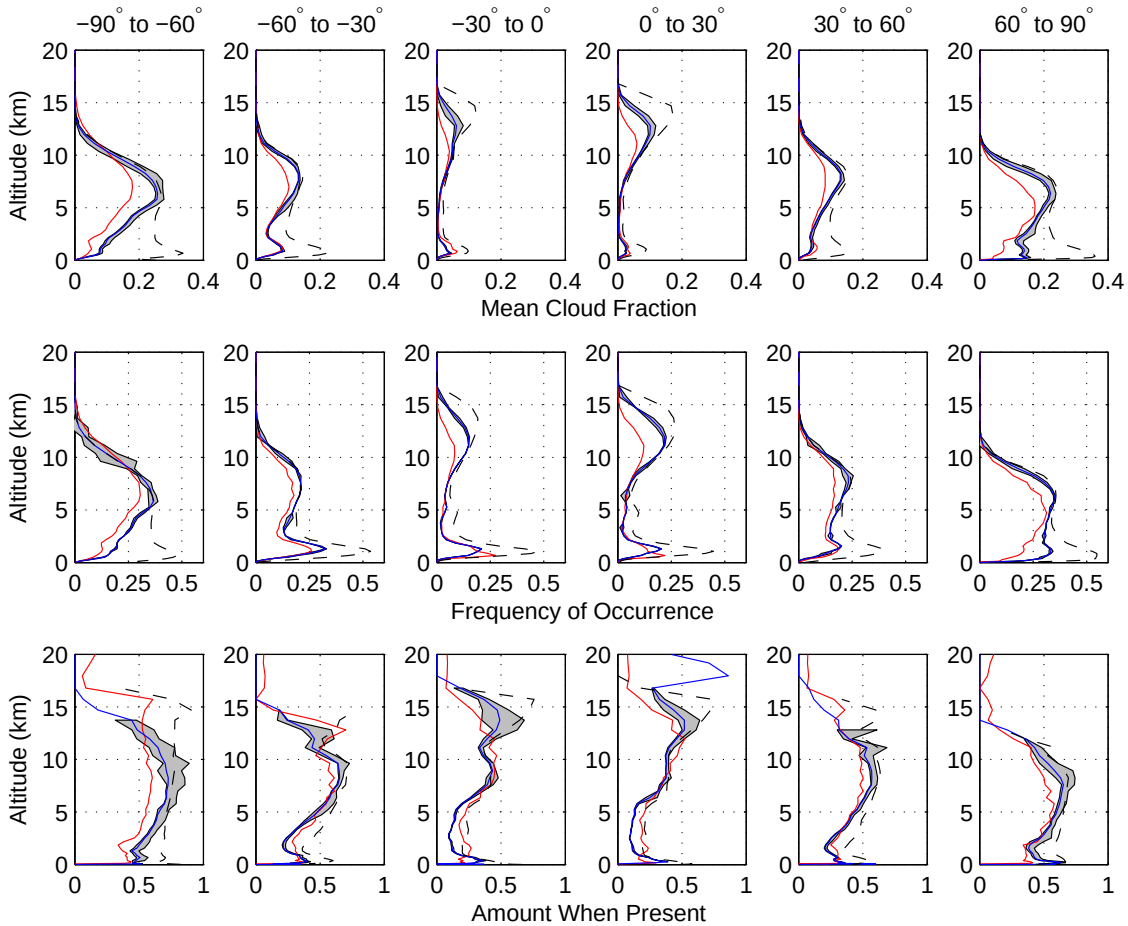

Figure 5.7: *Mean cloud fraction (top row), mean frequency of cloud occurrence (middle row) and mean amount when present (bottom row) for the equatorial latitudes, subtropics and polar regions in each hemisphere. The red solid line indicates the ICESat lidar measurements, the blue solid line shows the results of the lidar forward model and the black dashed line shows the ECMWF model cloud fraction before processing of the lidar forward model took place. The grey regions show the extent of the errors likely on the lidar forward model (see text for error estimation method). The latitude bands to which each column of plots are referring to is given at the top of each column.*

the ice scheme within the model. Most of the regions where the mean cloud fraction is high are regions in which we would expect to find ice clouds. Mace *et al.* (1998) in the Southern great plains, Beesley *et al.* (2000) in the polar regions and Hogan *et al.* (2001) in the mid-latitudes all noticed instances where the ECMWF model had too much ice cloud. The results here show that there is is often too much ice present within the higher altitudes. This is most clearly seen by the higher amount when present in the mid-latitudes above 7 km.

Although the ECMWF frequency of occurrence and amount when present are accurate to

within 0.05 for most of the lower troposphere beneath 5 km, around the equator the amount when present is often slightly underestimated by the model. This could be due to one of two reasons, either the model underestimates the amount of low cloud around the equator or that the large amount of ice cloud is attenuating the lidar forward model backscatter sufficiently that some of the lowest clouds are not detected by the lidar forward model. Although in these regions the retrievals have low error in the frequency of occurrence, the results must be interpreted with caution for these regions of the globe. For any region where the lidar forward model is overestimating the amount of cloud we can be confident that the ECMWF model has a genuine overestimate. However, where the lidar forward model underestimates cloud, we cannot be entirely certain, unless there is little cloud detected above it, and therefore the effects of the attenuation are small. In the majority of cases the model is overestimating cloud, so we can be confident of this result.

5.4.3 Land and Sea Comparisons

In order to test how the performance of the model varies over land and sea, model grid boxes were divided into those over the land surface and those above the sea surface. Theoretically the model may perform better over the land surface close to where there are observations which it has assimilated, but there are other factors such as the orographic effects of the land surface, the heterogeneous variation of the land surface making weather more difficult to simulate. Also, more satellite data can be assimilated over the sea surface, so the model could potentially perform better here.

Results from performing the analysis over land surface are shown in figure 5.8 and the results over the sea are shown in figure 5.9. In both sets of plots the ECMWF lidar forward model accurately represents the location of most of the features seen by ICESat. There are noticeable errors in the ECMWF-lidar forward model representation of the cloud fraction, frequency of occurrence and amount when present over Antarctica; the mean cloud fraction is 0.4 in the model where the lidar measurements show it to be closer to 0.25 and the frequency of occurrence is similarly at 0.35 when in reality it is measured to be closer to 0.3. The amount when present is again too large, in the ECMWF it is shown to be 0.75 but in the ICESat measurements it is closer to 0.5. This again is most likely due to the ECMWF model having difficulty in representing the ice cloud. Similar results can also be seen in the northern hemisphere polewards of 60°, although the amount of cloud detected by both ICESat and the ECMWF model is much lower at these

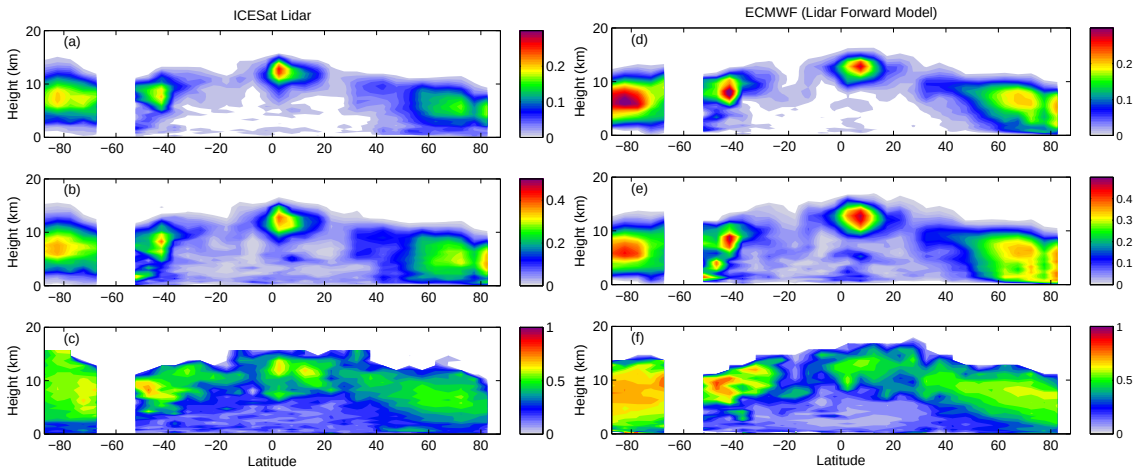

Figure 5.8: *Data from the ECMWF model and ICESat lidar over the 15 day comparison period, where the only points are selected are those above the land surface. (a) ICESat lidar mean cloud fraction; (b) ICESat lidar frequency of occurrence; (c) ICESat lidar amount when present; (d) ECMWF-lidar forward model mean cloud fraction; (e) ECMWF-lidar forward model frequency of occurrence; (f) ECMWF-lidar forward model amount when present. The lowest contour interval in the cloud fraction plots is 0.01.*

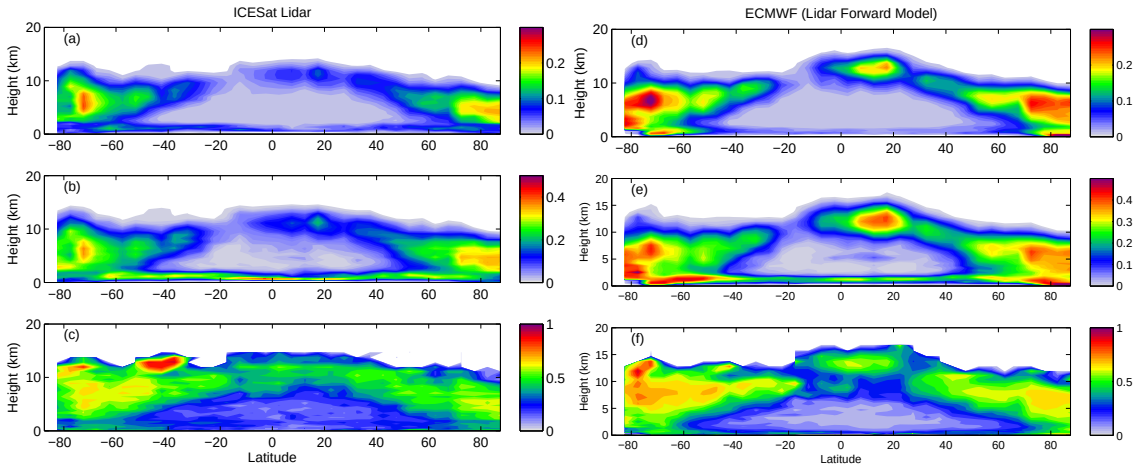

Figure 5.9: *As for figure 5.8, but for grid point selected that were over the sea only.*

latitudes. Observed mean cloud fraction peaks at around 0.15 while the ECMWF model through the lidar forward model is showing a mean cloud fraction peaking at 0.2; frequency of occurrence shows the same bias. However, the amount when present at these latitudes is only overestimated by a very slight amount— the error here is closer to 0.2.

In the tropics and between 10–15 km, the ECMWF lidar forward model over land shows a large mean cloud fraction that although appears fairly correct, the largest cloud fraction and

associated frequency of occurrence covers too large an area. Amount when present in this region is slightly too low by around 0.15, so again cloud can be seen to be modelled more readily at these regions than observed in nature. Finally, mean cloud fraction, frequency of occurrence and amount when present are all overestimated by up to 0.15 by the lidar forward model in the region between $25°$S and $50°$S and at most altitudes cloud is present.

Over the sea surface, a similar picture emerges. Tropical ice cloud within the upper troposphere is too frequent; in the ICESat measurements the frequency of occurrence is around 0.1 between 0° and 20°N and above 10 km, yet in the ECMWF lidar forward model the frequency of occurrence is closer to 0.4, which reflects in the mean cloud fraction the ECMWF lidar forward model is showing at these latitudes and altitudes. The amount when present is overestimated, but only slightly. In both hemispheres, polewards of 40° the frequency of occurrence is overestimated by as much as 0.2 and this causes the mean cloud fraction to be overestimated by a similar amount. Over much of the region between 20° and the pole in each hemisphere, the amount when present is too high by 0.1–0.15, which is again most likely a problem with the amount of ice cloud given within the model.

Some of the lowest clouds are represented quite accurately within the ECMWF model. Looking at the boundary layer and marine stratocumulus which exists between $40°$S to $40°$N, it can be seen that although the mean cloud fraction is too low, the amount when present is only underestimated by 0.05, although the frequency of occurrence is again too low in these regions by 0.15, meaning that the ECMWF model is having some difficulties in representing the boundary layer clouds that exist over the ocean.

Generally, the performance of the model appears from these plots to be approximately the same over both locations. However, in section 5.4.5 we shall examine the skill of the model over each location as well as the overall skill and give different skill scores for both land and sea, which will help determine whether the model is more accurate over land or over sea.

5.4.4 Backscatter Comparison

In addition to assessing the ECMWF model's performance with mean cloud fraction, frequency of occurrence and amount when present, the analysis can be extended to see how well the ECMWF model predicts the backscatter that would be observed by the ICESat satellite. This can be done by comparing the mean backscatter over time for different locations around the globe. In addition, a

new variable, 'backscatter when present' (represented by the symbol βWP) can be derived. This is analogous to the amount when present variable used earlier; the backscatter when present variable consists of the mean backscatter of all the detected cloud pixels, while the mean backscatter includes all pixels, including those which have no cloud. Hence, for this reason, it should be noted that mean backscatter can drop beneath the ICESat sensitivity threshold, but βWP should remain above the sensitivity threshold.

Analysis of the mean backscatter and βWP has been completed for the same 15-day study period as the cloud fraction climatology analysis. The results have been binned into six latitude bands as before and are shown in figure 5.10. Errors in the lidar forward model have been included on the plots and are useful in determining the validity of the results. In general, the backscatter when present derived from the ECMWF lidar forward model is closer to the measurements from ICESat than the mean backscatter; this is most noticeable equatorward of 30° and above 10 km in altitude. A likely explanation is that this effect is due to the ECMWF model overestimating the frequency of occurrence of the clouds in these regions, noted in sections 5.4.2 and 5.4.3.

In different regions the lidar forward model results show better agreement with the measurements from ICESat, yet in other regions there are noticeable differences. The high-altitude ice cloud equatorward of 30° in the lidar forward model results shows a higher backscatter than expected, which is too high even when the errors on the lidar forward model are taken into consideration. The βWP in these regions is again too high, although within the bounds of error, this is in agreement with the ICESat measurements. Polewards of $-60°$, it appears that the lidar forward model is actually underestimating the backscatter from ICESat. However, referring back to figures 5.8 and 5.9, it can be seen that there is little model cloud above 12 km but cloud exists within the ICESat measurements to 15 km over the land. When backscatter when present is examined, there is a better agreement, only a slight underestimate most likely caused by the ice cloud being too thin in the model, while ICESat is detecting a thicker ice cloud.

In addition to the high backscatter in the ice cloud equatorward of 30°, there is also too large a backscatter and backscatter when present at lower altitudes beneath 3 km. This implies that although the model cloud due to convection and the boundary layer has too low a frequency of occurrence in the land and sea comparison (section 5.4.3), where it does occur, the backscatter is actually too high. As we have seen from earlier comparisons, the amount when present in these regions is roughly correct (possibly slightly too large over the ocean surface), so this result could

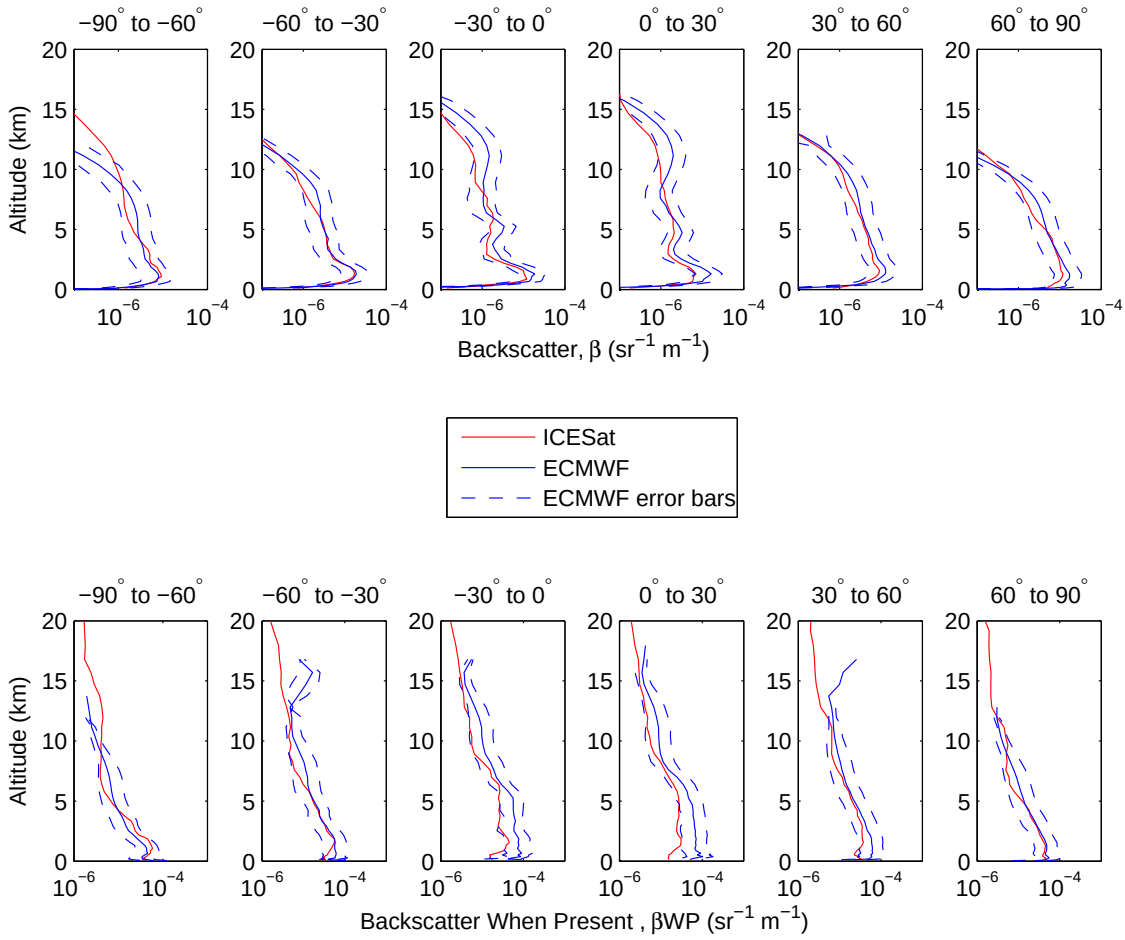

Figure 5.10: *Plots of mean backscatter (top row) and backscatter when present (bottom row) taken from ICESat and the ECMWF model over the 15 day study period. The latitude region of each profile is denoted at the top of the plot. The blue dashed lines on each plot show the error in the backscatter defined from the error analysis, corresponding to the edges of the grey region in figure 5.7.*

be due to a higher value of effective radius for liquid water clouds in the model. The sensitivity to effective radius will be examined later in section 5.4.6. Elsewhere in the lidar forward model, the backscatter and backscatter when present is a fair representation of the observations from the ICESat lidar.

5.4.5 Skill Scores

The comparisons of mean cloud fraction, frequency of occurrence and amount when present evaluates the climatology of the model. In addition, we can evaluate the quality of individual forecasts using skill scores. This is done simply by comparing each model grid box of cloud

fraction data with each point of ICESat data averaged on to the model grid. Using a cloud fraction threshold of 0.05, that grid box can then be determined as a "hit", a "miss", a "false alarm" or a "correct rejection" as shown in Table 5.3.

Many different skill scores have been developed for cloud fraction evaluation within models. Mace *et al.* (1998) and Miller *et al.* (1999) used hit rate, threat score, false alarm rate and probability of detection. Palm *et al.* (2005) defined their own skill score by subtracting the misses from the hits and dividing by the total pixels. However, a good skill score will have a low dependence on the frequency of occurrence and a random (no skill) forecast will always get a low score, close to zero. Hence, this study will concentrate on two more useful skill scores, the equitable threat score, (ETS), used by Illingworth *et al.* (2007) and the odds ratio, (θ; Stephenson, 2000), defined as follows:

$$\mathrm{ETS} = \frac{A - (A+B)(A+C)/N}{A+B+C-(A+B)(A+C)/N} \tag{5.4}$$

$$\theta = \frac{AD}{BC} \tag{5.5}$$

The equitable threat score removes any points that might have occurred due to chance, with random forecasts having a score of zero and one where the ECMWF lidar forward model agrees perfectly with ICESat having a score of 1. The odds ratio is also useful, however it is more common to take the natural log of the odds ratio for each point, as the linear odds ratio can vary over several orders of magnitude. The log of odds ratio gives a zero score for random noise, but tends to break down where N is small, as large variations can occur in θ. The equitable threat score should therefore be more reliable at showing model performance in areas where there are only a few points. However, for a random forecast where equal numbers of A, B, C and D are recorded, the odds ratio will be one and the log of odds ratio will also be zero.

Figure 5.11 shows both skill scores for the different latitude regions. The results from both skill scores show that the ECMWF model is most skillful within the southern hemisphere mid-latitude storm tracks and is least skillful within the equatorial low-altitude regions. This is because the equatorial regions have strong convection which is not accurately forecast within the model. The earth's surface within the southern hemisphere storm tracks is mostly made up of sea and is more uniform in nature and hence doesn't suffer from the same problems in representing the small-scale convection observed over the land.

Both sets of scores show an increase in skill as we progress from the surface of the Earth to

	ICESat grid point full	ICESat grid point empty
Model grid point full	Hit (A)	False Alarm (B)
Model grid point empty	Miss (C)	Correct Rejection (D)

Table 5.3: *Definition of skill score parameters, the letters denote the symbols used to represent these variables in the skill score equations. An extra variable, N, is the sum of A, B, C & D. This follows table 2.2, but is repeated here for clarity.*

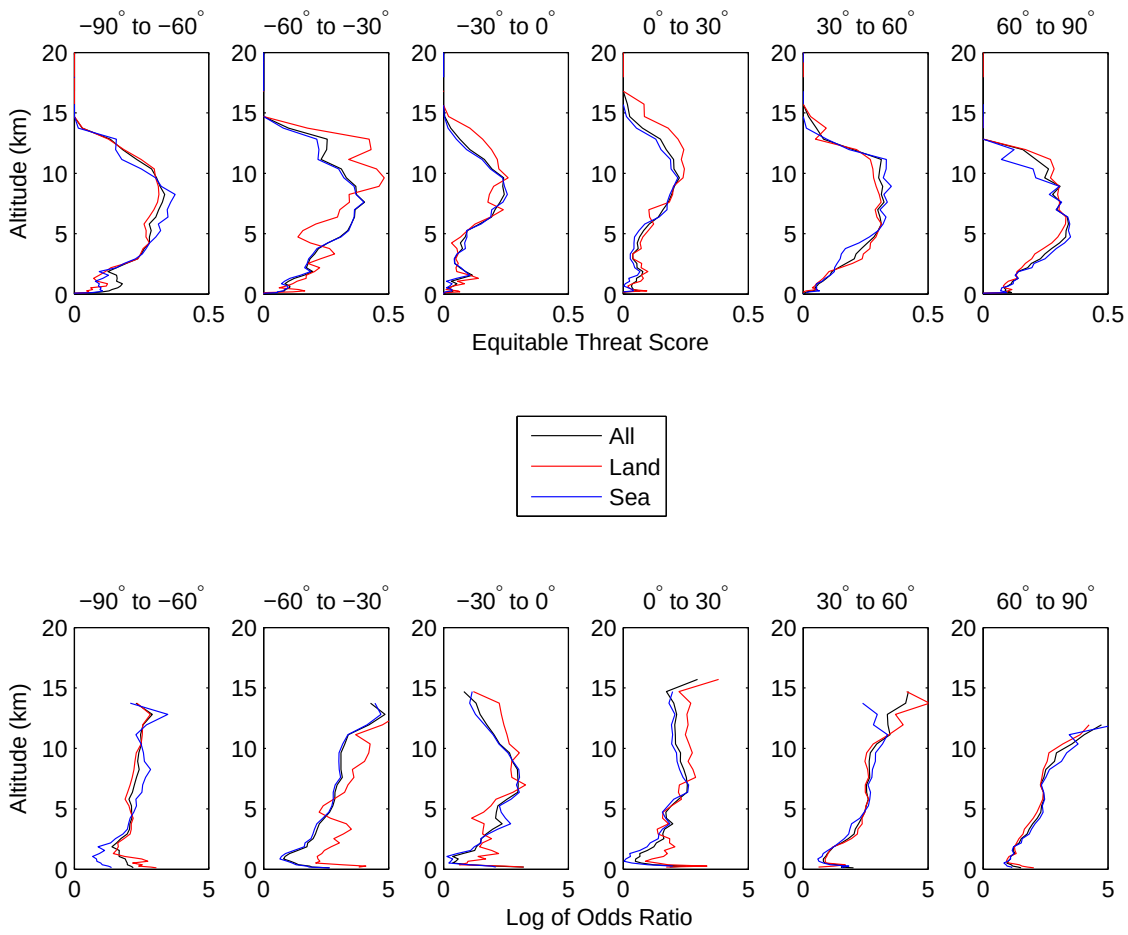

Figure 5.11: *Figures showing the latitude (grouped into bands of 30° width) and height variation of the equitable threat (top row) and log of odds ratio (bottom row) scores for the ECMWF model, after the lidar forward model has been run. The black line represents all data; the blue line shows the scores for data above the sea surface only and the red line shows scores for the data above the land surface only.*

mid-altitude regions around 5–10 km. This is most likely due to the model being able to successfully produce higher cloud, which is generally associated with large-scale features, but having difficulty in resolving the small-scale boundary layer and convective cloud at lower altitudes. This could also be a sampling feature where high, thick ice clouds obscure the lower clouds and in order to get good skill in a profile, both the low and high ice clouds need to be right.

At mid-altitudes (5–10 km) there are more larger-scale features present, due to a lot of the cloud being associated with transient weather systems or large-scale features. Hence the skill score is better. From this altitude upwards, the log of odds ratio score shows an increase in the skill of the model.

The equitable threat score gradually tends to fall as we pass through the highest cloud bands—the gradually thinner ice clouds. Skill scores are generally low within the tropical bands (equatorward of 30°) above 12.5 km and for polar clouds tend to drop off sharply above 10 km. This is most likely due to the model incorrectly representing cloud, which is not in the observations as discussed earlier. However, due to the smaller number of points included within the study from these regions, these results are less robust. At higher altitudes, as the number of cloud points within both ICESat and the ECMWF lidar forward model decrease, the two scores produce different values of skill which may be hard to interpret, but at altitudes from 5–10 km, the results of the skill scores should be fairly robust.

5.4.6 Sensitivity to Effective Radius

The results of equation 5.1 are sensitive to the values of the water contents (ice and liquid), the effective radii of liquid and ice particles assumed, the lidar ratio and the multiple scattering value assumed. As mentioned earlier, the water contents and effective radii are determined directly from the ECMWF model assumptions; as this study intends to compare this model to ICESat, should the values of effective radius and water content be wrong, it is a problem with the ECMWF model parameterizations and not the lidar forward model. However, it is of importance to test the sensitivity of the results to changes in effective radius as a reduction in effective radius may lead to less ice cloud in the model, which was noted in sections 5.4.2 and 5.4.3 or a reduction in the backscatter of tropical clouds below 3 km, which was seen to be too high in section 5.4.4.

In order to test the lidar forward model response to changes in effective radius, two simple experiments were performed: one with both liquid and ice effective radius doubled and the other

with liquid and ice effective radius halved. Results from both experiments are shown in two figures; figure 5.12 shows the changes to mean cloud fraction, frequency of occurrence and amount when present, while figure 5.13 shows the sensitivity in the backscatter and backscatter when present.

Changing the effective radius makes changes to ice phase in a different way to the liquid phase. Referring back to equation 5.1 we can see that the equation is made up of two forms, the α within the exponential reducing the backscatter and the α outside the exponential increasing the backscatter. For ice clouds, the attenuation term is small when compared to the attenuation by liquid clouds and the terms outside the exponential. Hence a decrease in effective radius will lead to an increase in α (following equation 5.2) and as the term within the exponential is small, the backscatter will increase and more cloud will be detected within the ICESat sensitivity threshold. In the liquid water case, the value of extinction coefficient α is large with respect to other phases and the exponential term will dominate. A decrease in effective radius will lead to more attenuation and a smaller backscatter, meaning less cloud is detected. Hence the sensitivity lines in each plot cross at some altitude within the profile.

From the backscatter plot shown in figure 5.13, the sensitivity to effective radius is greatest within the ice cloud phase towards the top of the atmosphere. However, there is generally more sensitivity to the ice phase; this is probably due to the larger uncertainty in effective radius of ice when compared to liquid water. If we were to assume that most of the cloud observed between $-60°$ and $-90°$ latitude was ice it can be seen that the sensitivity to backscatter is large at 5 km. In the polar regions in the βWP measurements, where there is little sensitivity variation with altitude. Small backscatter and βWP sensitivity is noted equatorward of 30° latitude within the boundary layer and small convective cloud, which suggests that the cloud in these regions could have too high a backscatter noted in section 5.4.4 due to an incorrect value of effective radius, but an incorrect value of liquid water content cannot be ruled out in these areas.

In figure 5.12, the changes in the extinction fed back into the amount of cloud; again the sensitivity lines cross in the middle of each profile as a decrease in ice effective radius leads to more ice cloud coming within the ICESat sensitivity threshold and in the liquid phase, effective radius decrease leads to more attenuation and less cloud being detected. Sensitivity to mean cloud fraction and amount when present is generally greater in the ice phase clouds, apart from within the storm tracks, where the greatest sensitivity is within the mixed phase clouds— this is likely

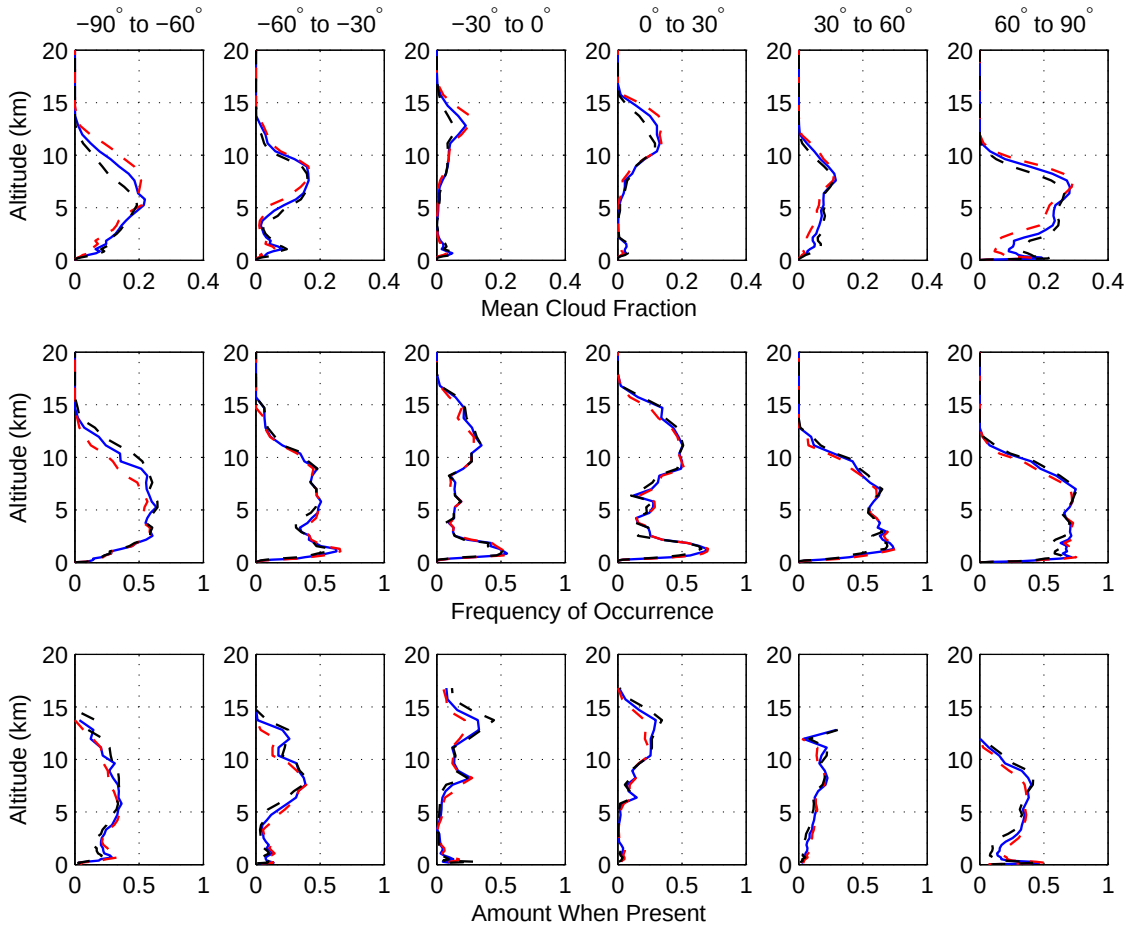

Figure 5.12: *Plots of mean cloud fraction (top row), Frequency of occurrence (middle row) and amount when present (bottom row) from the ECMWF model after running the lidar forward model (blue line) and showing the sensitivity to changes in effective radius. The points where the effective radius is halved are shown as red dashed lines and those where the effective radius is doubled are shown as black dashed lines.*

to be due to the thickness of the ice cloud in these regions, and increases in effective radius lead to decreases in the amount of attenuation by the thick ice clouds and hence more lower cloud is visible. Apart from above the antarctic, frequency of occurrence is very insensitive to changes in effective radius. Over the antarctic, the frequency of occurrence is affected as the changes in effective radius allow more or less cloud to fall within the ICESat sensitivity threshold and be detected. Elsewhere, changes in frequency of occurrence will occur when the cloud is so optically thick that it totally extinguishes the lidar signal. Reducing the optical thickness by means of a change in effective radius will increase the frequency of occurrence of some low clouds. In all cases, the changes in effective radius do not alter mean cloud fraction or amount when present by

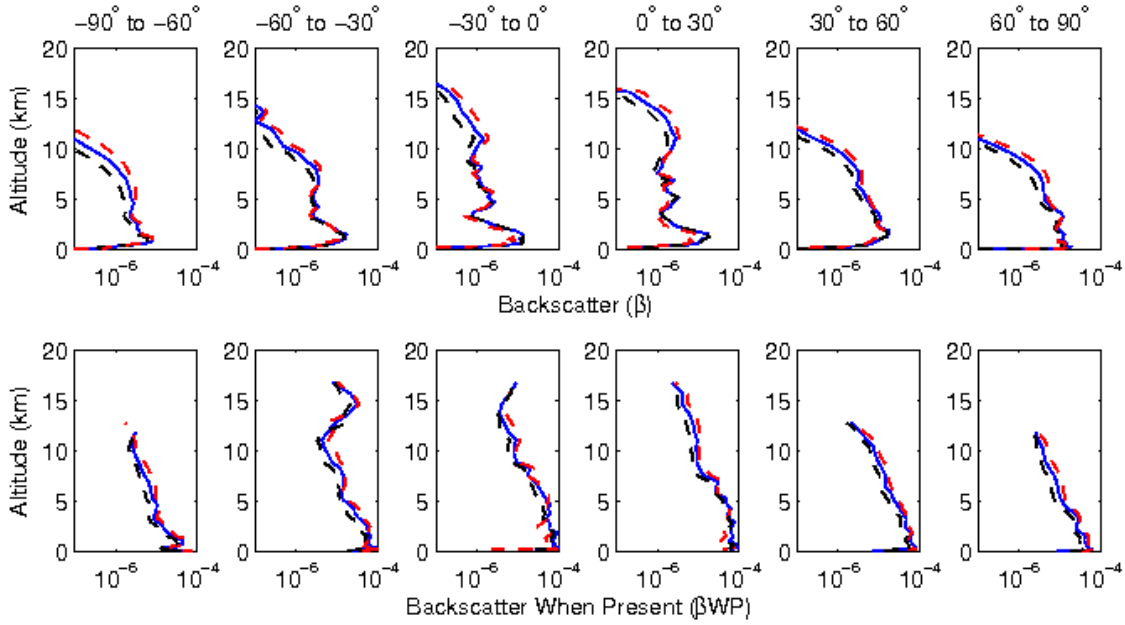

Figure 5.13: *Plots of backscatter (top row) and backscatter when present (bottom row) taken from the ECMWF model (blue line) and showing the sensitivity to effective radii. The points where the effective radius is halved are shown in red dashed lines and those where the effective radius is doubled are shown as black dashed lines .*

more than 0.05, which is less than many of the errors noted in cloud fraction and amount when present in section 5.4.2; so it can be concluded that the water contents or cloud fractions of the ice and liquid clouds are the largest contributors to the apparent overestimate in cloud fraction.

5.5 Conclusions

This study has developed techniques to compare a forecast model with attenuated backscatter from global lidar observations from space and demonstrated their use on 15 days of ECMWF model data. The method of using model output to derive the quantities observed by the instruments are in this case far more satisfactory than trying to use the instrument to derive the model variables. It is important for any study which compares radar or lidar from space to remove any clouds from the model which would not be seen by the instruments making the observations. Previous studies using lidar to model comparisons did not take account of the lidar attenuation may have produced misleading results.

Comparison has been made between the ECMWF global model and observations from the

ICESat lidar. They have shown that the model has a tendency to get most features of the mid-latitude storm tracks correct, although there is too much ice cloud within the model, which will reduce the skill score of the model as well as affecting the way the model behaves towards incoming and outgoing radiation. If the model does not have the correct amount of ice, this could lead to incorrect representation of the radiation budget of the model and although the ECMWF model is not a climate model, these problems within a climate model could potentially lead to incorrect estimates of temperature in future climate.

The model also has problems in representing the low-altitude clouds in the equatorial regions. This is probably a combination of two reasons, the model incorrectly representing the shallow convection which is taking place, particularly due to its stochastic nature. Also, the processing of the lidar forward model data will remove some of the low equatorial cloud due to extinction of the lidar signal by the large amount of ice present within the model. Later versions of the ECMWF model have reduced the amount of ice (A. Tompkins, Personal Communication) and hence once the data for this period is available, it should be possible to rerun the lidar forward model to give a more accurate prediction of the representation of the lower clouds that may have previously been obscured by the attenuation from the high altitude ice clouds. Results show that the model performs in a similar manner over the oceans to over the land, but the problem with the increased amount of ice cloud is more prevalent over the ocean. Tests have also shown that the model has only a 10% error due to the largest unknowns within the lidar forward model: the lidar ratio and the multiple-scattering factor.

The performance of the model has been examined over land and sea regions. Comparison of cloud fraction indicate that there is too much ice cloud over both surfaces in the tropics, that the model has too high a frequency of occurrence within the ice cloud regions, most notably around the poles and the upper-level tropical ice clouds. Over the sea, boundary layer and marine stratocumulus clouds have too low a frequency of occurrence, particularly in the tropics. Over the land surface, model amount when present is too large, particularly in the polar regions, possibly due to thick ice cloud. Skill scores indicate that the model performs the best over the land surface, but the skill of the model reduces as altitude decreases. The equitable threat skill score is a robust method suitable for cloud fraction comparisons and is not particularly sensitive to the number of points included in the calculation of the score; log of odds ratio is generally robust, but has no upper bound and is not as accurate when only a few data points are considered.

Backscatter and backscatter-when-present comparisons have been performed. In most cases the backscatter produced by the lidar forward model is accurate within the error bounds of the model; however, the backscatter is too high within the tropical high-altitude ice clouds and within the tropical and sub-tropical marine and boundary layer stratocumulus clouds observed around the equator.

Sensitivity studies show that doubling or halving the ice cloud effective radius makes a change of up to 5% in the cloud fraction and amount when present. Since this is not enough to change the amount of ice cloud within the model to values equivalent to those observed by ICESat, it is likely that the model is producing too much ice cloud, rather than an error in effective radius. These sensitivity studies also reveal that the backscatter in the tropical boundary layer and lower free atmosphere liquid clouds is too high and this could be due to a high effective radius within the liquid cloud phase.

Comparison of the ECMWF model to lidar observations is an essential precursor to systems involving the data assimilation of lidar data into a forecast model. In this case, the model can be used to predict backscatter from the laser and then inaccuracies in backscatter can be satisfied by changing the liquid or ice water contents or cloud fraction to allow the two backscatter signals to agree. This method can also be used for testing new cloud physics schemes which appear within the model.

5.6 Future Work

Although this study has shown the value of active remote sensing from space, it has concentrated on only a few days of data. Longer periods of lidar data is now available from the CALIPSO lidar, which is part of the A-Train of satellites (Vaughan *et al.*, 2004). This data will be over longer time periods and hopefully should not suffer from the laser deterioration problems that have affected long-term measurements with the ICESat satellite. However, due to the strong attenuation of liquid water clouds from the lidar, measurements by radar from space, such as CloudSat will be more suited to model evaluation for the thicker ice clouds. However, shorter wavelength radars or lidars could be used to sense the thin ice clouds. Working together with longer wavelength radars (Hogan and Illingworth, 1999), the vast majority of clouds within the atmosphere could be detected, allowing for fairer evaluation of models of the earth's climate system and in principle

leading to fewer inaccuracies of forecasts of future climate. This work can lead on to assimilation of cloud properties into numerical weather prediction models, which should improve the quality of cloud forecasts. Further radar measurements will improve our understanding of future climate and the cloud feedbacks on future climate. Simulators are currently being developed by the Met Office and elsewhere for CloudSat (for example Bony-Lena (2006) and Stephens (2006), discussed at the ECMWF workshop on cloud parameterizations) and this work has proved that the simulation method works and will be useful in these future studies.

CHAPTER SIX

Summary, Conclusions and Future Work

Clouds are an important part of the radiation budget of the Earth, yet they remain one of the largest uncertainties within the climate system, with many numerical models disagreeing on the sign and magnitude of the change in cloud radiative forcing in the future climate system. This thesis has examined use of the simulation (or model-to-observations) method for evaluating different aspects of how clouds are represented within numerical models.

6.1 Summary of Findings and Conclusions

As part of this thesis, simulation has been used for two separate experiments. Firstly, it has been used to convert the cloud scheme output from the Met Office model into Doppler radar observations of the clouds above Chilbolton, to examine where the model may have errors in the evaporation of ice. In the case of the Doppler velocity, it would have been very difficult to derive the model parameterized ice particle fall speeds and hence simulation has proved of use in this area.

Secondly and arguably the most useful application of the simulation method has been made in developing a lidar forward model to predict observations from the ICESat lidar using the ECMWF model. This allows a fair comparison between the ECMWF model and the ICESat lidar and the findings will be looked at in detail in section 6.1.2. Although a comparatively new field for cloud studies, simulation has applications in the data assimilation of radar variables, which are different in nature from the variables of cloud fraction and water contents used by models to represent clouds. It also has practical applications in evaluating models; for example the change of a parameterized ice particle spectrum within the model can be evaluated by comparing simulated radar or lidar data to the corresponding observations.

6.1.1 Evaporating Ice within Operational Models

In chapters, 3 and 4, 94-GHz Doppler cloud radar measurements have been used to see how well the evaporation zone beneath ice cloud is represented in operational models. The work was inspired by Forbes (2002) who found in his thesis (subsequently published; Forbes and Hogan, 2006) that the depth of the evaporation of ice (defined as the change in ice water content from the maximum within the profile to 10% of this maximum value in the area beneath the maximum) was 2–3 times the depth of that in radar observations. Observations made with Doppler radar (not available at the time of Forbes' thesis) has shown that the depth of the evaporation zone in the Met Office model is on average, 2.55 times that observed by IWC measurements calculated using radar reflectivity and model temperature. This feature is not unique to the Met Office model, with several operational models from the Cloudnet programme all showing increased evaporation depth of 2–3 times the radar observations. Various candidates for the increased depth of the evaporation zone within the Met Office model have been considered. In addition, a simple numerical model of ice evaporation has been constructed, allowing a realistic representation of ice evaporation within the Met Office model, but with a high resolution grid. Following the results of these two chapters, the following possible causes of the error are discarded:

- The model parametrized fall velocity being too high. Simulations of model parameterized fall velocity show that in the middle of the cloud (where the effects of the vertical air velocity are small), the modelled particle fall speed is around 30% too low.
- The lack of turbulence in the model at ice cloud altitudes. Measurements of turbulence and evaporation zone depth show no evidence of any correlation.
- The parametrized density of the ice particles. When simulating radar measurements using a wide variety of ice particle density functions suggested by recent studies, the depth of the evaporation zone within the Met Office model is found to change by less than 10%.

The humidity gradient within the evaporation zone or immediately beneath the ice cloud is much smaller in model profiles than in radiosonde ascents from Larkhill. The drop off from moist air with 100% relative humidity to dry air with 20–30% relative humidity within the radiosonde observations takes place in a shallow layer with depths of around 500 m. Studies of the layer mean evaporation rate show that the model's parametrized evaporation rate is about one third of

that derived using radar observations and model temperature. The parametrized evaporation rate equation used in the parameterization scheme is based on well-established cloud physics and is dependent on the temperature, humidity, particle diameter and pressure. The error in evaporation rate is thought to be due to incorrect humidity as unrealistic changes in the other parameters would be required. The sharp drop in humidity would take place over the space of one model grid box and would be represented as a step function, but the numerics of the model are presumably too diffusive and so the sharp humidity gradient cannot be maintained.

As it is difficult to test the problems within the Met Office model, this thesis has introduced the ELePhANT model, an explicit microphysics model which has tested the hypothesis that the deeper evaporation zone depth in the operational models were due to the models incorrectly representing the sharp drop in humidity within the evaporation zone. This contains the parameterizations of the Met Office model but with high resolution (5 m grid spacing), to allow any sharp changes in humidity gradient that take place over a few hundred metres to be accurately represented. It has been used both to examine the sensitivity of the Met Office model to cloud and thermodynamic variables relevant to cloud formation, and to represent evaporation from radar and radiosonde case studies.

The evaporation zone depth is most sensitive to changes in the humidity gradient. If the humidity gradient increases from 0.02% m^{-1} then the evaporation zone depth decreases from 1 km to 500 m. Evaporation depth is also sensitive to changes in the temperature profile, due to the effect on the specific humidity within the evaporation zone. Changes in the initial ice water content, made by changing the equivolumetric mean diameter (D_0) of the ice particles are also important. Doubling the value of D_0 leads to an increase in the evaporation depth by 200 m.

The evaporation zone depth is not sensitive to changes in pressure or changes in ice water content made by changing particle number concentration. Changing the starting pressure from 500 to 1000 mb changed the depth of the evaporation zone by less than 100 m.

The ELePhANT model can predict evaporation depths for both radar and model profiles of ice water content to within 200 m of those observed by the radar. Systematic inaccuracies occur from the differences in grid spacing between the models, the parameterization scheme differences and that the sonde may have a lag of a few seconds when it passes from dry to moist air. Random inaccuracies may occur when the profiles of humidity may not be from the same cloud the radar is seeing over Chilbolton, depending on the direction of the wind and the sonde drift.

The results from the ELePhANT model show that if the Met Office model had the correct humidity gradient it could accurately represent evaporation zone depths. The evaporation zone depth is more sensitive to humidity gradient changes than changes in any other variable and hence the results from the ELePhANT model give strong evidence that the shallow humidity gradient within the evaporation zone in the Met Office model causes the deeper evaporation zone in this model.

There has been some consideration (Westbrook *et al.*, 2007a) that the Met Office model may (by assuming all particles are spheres) be underestimating the capacitance of the evaporating ice and hence affecting the evaporation rate. This needs to be tested in further studies with the ELePhANT model, but experiments show that using a lower capacitance, yet keeping all other factors the same, would actually increase the depth of the evaporation zone in the model to greater depths than with the present scheme, and that humidity gradient is still the most obvious cause of the deep layer within the Met Office model.

6.1.2 Assessment of the Performance of the ECMWF model using ICESat

Chapter 5 has developed techniques to compare models with attenuated backscatter from global lidar observations from space and demonstrated their use on 15 days of ECMWF model data. Although previous authors (Miller *et al.*, 1999; Palm *et al.*, 2005) have examined the performance of the cloud scheme within the ECMWF model using spacebourne lidar, they have not accounted for the attenuation of the lidar signal when making their comparisons. While this may be good for thin ice clouds, where extinction of the lidar signal takes place, an unfair comparison of the model may result. Comparison has been made between the ECMWF global model and observations from the ICESat lidar. Fifteen days of ICESat and model data have been examined, which is equivalent to over 9 million kilometres of ground-based radar data and assuming a mean wind speed of 20 m s^{-1}, is around 14 years of observations made at a mid-latitude ground-based station such as Chilbolton. Using the lidar forward model, the following conclusions can be drawn:

The method of simulation (in the form of a lidar forward model) is in this case far more satisfactory than trying to use the lidar data to derive the model variables. Importantly, the comparison removes any clouds from the model which would not be seen by the instruments making the observations.

- Results of mean cloud fraction, frequency of occurrence and amount when present have shown that in general the model has a tendency to get most features of the mid-latitude storm track resulting in an error in the frequency of occurrence in the high altitude ice cloud in the tropics of 10–15% and over the polar regions of up to 15%. This large amount of ice will change the model behaviour towards incoming and outgoing radiation and could potentially affect surface temperature forecasts.

- The model also has problems in representing the low-altitude clouds in the tropics. This is probably a combination of two reasons, the model being able to accurately represent the shallow convection which is taking place, and the processing of the lidar forward model data removing some of the low equatorial cloud due to extinction of the lidar signal by the large amount of ice present within the model. It is likely that only one of these errors is present, but the at this stage it is not possible to say which one.

- Tests have also shown only a 10% error in the comparison due to the largest unknowns within the lidar forward model: the lidar ratio and the multiple-scattering factor. When the effects of a reasonable range of values of the forward model are included, there is very little change in the results.

- Comparisons into the performance of the model have been carried out over land and sea regions, and results for each region have been derived separately. Cloud fraction evaluations indicate that there is too much ice cloud over both surfaces above the tropics and the model has too high a frequency of occurrence within the ice cloud regions, most notably around the poles and the upper-level tropical ice clouds.

- Over the sea, boundary layer and marine stratocumulus clouds have too low a frequency of occurrence, particularly in the tropics. There is evidence that misrepresentation of mountain ranges affect boundary layer clouds (Xu *et al.*, 2004) and it could be that this is the case with the ECMWF model. Over the land surface, model amount when present is too large, particularly over the polar regions, possibly due to thick ice cloud that may be present in the model. Evidence from Beesley *et al.* (2000) produces similar results and it can be concluded that generally, the ice cloud scheme within the model needs revision as the radiation budget of the polar regions, an area of importance to climate due to the melting of the ice caps will not be accurately represented within the ECMWF model.

- Skill scores of equitable threat score and log of odds ratio have been calculated for the model performance and indicate that the model performs the best over the land surface, but in general the skill of the model reduces as altitude decreases. The equitable threat skill score is suitable for cloud fraction comparisons and is not particularly sensitive to the number of points included in the calculation of the score; log of odds ratio is generally robust, but has no upper bound and is not as accurate when only a few data points are considered.

- Backscatter and backscatter-when-present comparisons have been made using model data. In most cases the backscatter produced by the lidar forward model is accurate within the error bounds of the model; however, the backscatter is too high within the tropical high-altitude ice clouds and within the marine and boundary layer stratocumulus clouds observed around the equator to 30° north and south. These comparisons prove useful in validating the way the model will behave to short wave radiation.

- Sensitivity studies show that doubling or halving the ice cloud effective radius makes a change of up to 5% in the cloud fraction and amount when present. Since this is not enough to change the amount of ice cloud within the model to ICESat levels, it is likely that the model is producing too much ice cloud. These sensitivity studies also reveal that the backscatter in the equatorial boundary layer and lower free atmosphere liquid clouds is too high and this could be due to a high effective radius within the liquid cloud phase.

Comparison of the ECMWF model to lidar observations is an essential precursor to systems involving the data assimilation of lidar data into a forecast model. In this case, the model can be used to predict backscatter from the laser and then inaccuracies in backscatter can be satisfied by changing the ice water contents. This method can also be used for testing new cloud physics schemes which are being considered for inclusion within the model.

6.1.3 Spacebourne Radar and Lidar Cloud Climatology

In chapter 5, 15 days of ICESat data were used to obtain global averages of cloud location and amounts. With the launch of the CALIPSO lidar in 2006, this study could potentially be extended to provide long-term climatologies of clouds for use in validating climate models, as well as advancing our knowledge of global clouds where current observations are not always available.

However, one of the key issues raised in chapter 5 was that the lidar signal is attenuated (and in some cases extinguished) as it passes through thick cloud. Although this study has made efforts to account for attenuation to be fair to the model, one obvious shortfall of global spacebourne lidar measurements will be that low altitude clouds are not always detected.

However, CALIPSO is part of the A-train of satellites along with the CloudSat radar, which orbit the Earth along the same track, a few minutes apart. Hence, combined radar and lidar observations of the same cloud profiles are now available. The synergy of the two instruments allows both the detection of liquid cloud by the radar, (which the lidar will not detect) as well as very thin ice cloud (which the radar will not always detect). So although on its own, lidar measurements will not be able to validate every type of model cloud, the two sets of observations coupled together will allow very powerful evaluations of cloud climatology and model performance in the future.

6.2 Future Work

Work in this thesis and climate science has shown the need to improve the way clouds are represented within GCMs, to constrain the error on estimates of future temperature due to poor cloud representation.

The first step is to see which GCMs are performing well and which have large errors. Although the Cloudnet programme (Illingworth *et al.*, 2007) has gone some way towards evaluating European models and is undergoing expansion to include ARM (Atmospheric Radiation Measurement) data from the USA; the inclusion of further models to this programme should be encouraged. Using data from multiple ground-based studies, the operational models can be evaluated to examine which ones perform well over a long period of time at individual locations.

In addition, global profiles of clouds have been made from space by ICESat and are currently being made by the CALIPSO lidar and the CloudSat radar (Stephens *et al.*, 2002), which form part of the A-train of satellites. In future more such satellites are planned to be launched, such as the EarthCare satellite (Bezy *et al.*, 2002), which will have radar and lidar on board the same platform and is scheduled for launch in 2012. This will be of particular use in examining the performance of GCMs in the areas where radar and lidar observations are difficult, such as the polar regions, tropical upper troposphere and over the oceans, where few cloud observations exist.

With the extra measurements, the extraction of observation and model profiles of cloud properties, similar to that with the ECMWF model in chapter 5 can be used and a Cloudnet-style programme on model evaluation from space can be set-up. This should include all global GCMs available for evaluation, in order to reduce the error in how clouds are represented.

In addition, conclusions may be drawn for the short-term development of the studies in this thesis. Section 6.2.1 at the ice evaporation problem, section 6.2.2 examines the further developments in the ECMWF model evaluation and section 6.2.3 looks at how simulation may develop in the future.

6.2.1 Ice Evaporation

As noted in chapter 4, Westbrook *et al.* (2007a) have found that the Met Office may underestimate the capacitance of ice particles. The spherical assumption could be relaxed within the ELePhANT model and using the work of Westbrook *et al.* (2007a), a re-run of the ELePhANT model can be attempted with the new particle shapes to see how the results are affected.

In addition, tests using the ELePhANT model can be made to determine a critical grid resolution threshold, where any grid spacing greater than this threshold would result in the model being unable to represent the humidity gradient properly. The results could, in principle be used to change the grid resolution of the Met Office model in future versions.

Although evaporation has been studied using four models from across Europe in chapter 3, only the Met Office parameterization has been studied in detail. The ELePhANT model could be run with the ECMWF or Météo-France parameterization scheme to assess where these models may have problems in representing evaporation.

6.2.2 ICESat and the ECMWF model

More recently, the ECMWF model has reduced the amount of ice in its cloud scheme (A. Tompkins, personal communication) and therefore a rerun of the analysis of the ECMWF model on a later time period (from early 2005 onwards) would be of use. However, there have been problems with the availability of good quality ICESat data from a later period; the signal strength of the lasers has reduced somewhat while the satellite has been in orbit. If good quality ICESat data is available, this comparison should be possible. However, as an alternative, attenuated backscatter

data of good quality is now available from CALIPSO and could be used for the evaluation. It would be particularly of use to see how the ECMWF model represents lower-level clouds once the amount of ice and hence the amount of attenuation is reduced at upper levels.

In addition, the work can easily be extended to include other operational models, such as the Met Office global model. As the ECMWF model is not specifically a climate model, it is difficult to specifically use the results from chapter 5 to show how climate models are performing. Instead, the ECMWF model cloud scheme can be improved and then used as the basis as a cloud scheme for a climate model, such as the RACMO model examined in chapter 3. Knowledge of the major pitfalls in cloud schemes can then be used to write better cloud schemes and hence this methodology can directly affect the predictions of future climate and reduce the uncertainty caused by clouds.

6.2.3 Simulation

This thesis has undoubtedly proved the use of simulation in future work and it is useful to develop the method for future spacebourne missions. This is currently being done for CloudSat (Bony-Lena, 2006; Stephens, 2006; Haynes and Stephens, 2006, document in preparation) and CALIPSO (Bony-Lena, 2006) and should be attempted for EarthCARE before its 2012 launch. They are valuable in model evaluation studies, particularly for lidar studies where signal attenuation takes place and for high-frequency radar studies (e.g. 94-GHz) where some signal attenuation takes place in thicker water clouds.

In addition, simulation of ground-based radar signals should continue from the methods developed by Chiriaco *et al.* (2006) and applied to the Cloudnet programme. This will enable accurate comparisons of models in a similar way to the methods of Hogan *et al.* (2001), who removed ice cloud that could not be seen by the radar. Simulation would offer an alternative method to this, as well as testing the model parameterization schemes in their effectiveness at reproducing the observations. This would give additional insight to the cloud model comparisons already undertaken (Illingworth *et al.*, 2007).

In addition, simulation can be used for data assimilation purposes. Work in variational retrievals are already being done in the radar group at Reading using CloudSat data (Delanoë and Hogan, 2007, document in preparation) and could potentially be extended to a combination of CALIPSO and CloudSat data, EarthCARE after its 2012 launch and future Cloudnet work. The

simulated radar and lidar signals can be used to make a comparison with the observations and the results applied into model cloud schemes. This should allow more accurate representations of clouds for NWP models.

Due to the increasing number and complexity of data assimilation methods, more variables are set to be assimilated into operational models and hence simulation has a positive outlook for the future. As we continuously wish to examine model performance, simulation provides scientists the only way to represent radar and lidar signal attenuation, and hence the most accurate tests of model performance. This study has barely scratched the surface of the simulation technique, which can be adapted for many different instruments, but is especially useful for radar and lidar. Simulation methods should be used in many future studies and would be especially relevant within the Cloudnet programme, as it expands to evaluate more models with more radar data. The results of further published simulation experiments are eagerly anticipated.

Glossary

ACTIVE REMOTE SENSING *The detection of an object's properties at a distance by sending out electromagnetic or sound waves from a transmitter and receiving them some time later.*

AEROSOL *An airbourne solid or liquid particle which may be of natural or anthropogenic origin and of size of the order of micrometres. These can be detected by some* ***lidar*** *wavelengths.*

AMOUNT WHEN PRESENT *The mean* ***cloud fraction*** *detected by* ***radar*** *or* ***lidar*** *or observed in a model grid box, with the condition that the mean grid box cloud fraction is above a certain threshold (usually 5%, but sometimes 50%).*

ATTENUATED BACKSCATTER *The* ***backscatter*** *observed by a lidar, including a transmission term for the* ***attenuation*** *of the lidar signal:* $\beta' = \frac{\alpha}{s} \exp\left[-2\eta \int_0^r \alpha dr\right]$*, where* β' *is the attenuated backscatter,* α *is the* ***extinction coefficient****,* r *is the range from the lidar and* η *is the* ***multiple-scattering factor****.*

ATTENUATION *The loss of a* ***radar*** *or* ***lidar*** *signal as they pass through a dense medium, such as cloud, atmospheric constituents or rain.*

BACKSCATTER *Similar to* ***Reflectivity*** *factor, the backscatter is a measure of the signal returned to a* ***lidar*** *and can be expressed in linear or logarithmic form. It contains information about the target and is related to properties of the target.*

BACKSCATTER WHEN PRESENT (βWP) *Analogous to* ***Amount When Present****, backscatter when present is the mean attenuated backscatter, ignoring zero values from the calculation.*

BINARY SKILL SCORE *See* ***Skill Score***

CALIPSO *Acronym for Cloud-Aerosol Lidar and Infrared Pathfinder Satellite Observation, launched in April 2006. This is a 2 year spacebourne* ***lidar*** *mission, with one of its aims to monitor clouds.*

CAPACITANCE *Making an electrostatics analogy, capacitance is a variable which refers to the ability of a particle shape to allow diffusion and evaporation of water vapour on to its surface. The highest values are for spheres, with capacitance decreasing for different particle habits.*

CLOUD FRACTION *The fraction of cloud filling a model grid box, defined in terms of its volume or area in 3 dimensions. This is different from cloud cover, which is the fraction of a model grid box filled with cloud when observed from beneath.*

CLOUDNET *A European experiment using ground-based cloud* ***radar*** *and* ***lidar*** *to evaluate properties of clouds in operational models.*

CLOUD PHASE *Referring to whether clouds are composed of liquid water, ice or a combination of the two. Cloud phase of 1 is totally liquid; 0 is totally solid ice.*

CLOUDSAT *Launched on 28 April 2006, this is a satellite with a cloud profiling* ***radar*** *on board, which is making orbits of the Earth and able to observe snapshots of clouds.*

DEPTH FACTOR *A variable introduced for comparing model and* ***radar evaporation zone*** *depth. It is simply the ratio of model* ***evaporation zone*** *depth to* ***radar evaporation zone*** *depth, so that a model having a depth factor of 2 has an* ***evaporation zone*** *depth of double the* ***radar****.*

DIAGNOSTIC VARIABLE *A variable in the model which is not carried between timesteps, yet instead is Diagnosed from relations with* ***Prognostic***

Variables.

DOPPLER RADAR *A **radar** which in addition to measuring **reflectivity** factor, is Dopplerised, enabling it to obtain information on the Doppler shift of scatterers in its beam. When the **radar** is vertically pointing, Doppler shift is useful to obtain estimates of particle terminal velocity and turbulence at cloud base in **nephological** research.*

DUAL WAVELENGTH RADAR *Use of two (or more) **radars** simultaneously to remotely sense objects. In **nephological** studies it has applications in determining cloud particle size.*

EARTHCARE *A planned spacebourne **radar** and **lidar** mission, due for launch in 2012.*

EFFECTIVE RADIUS *A measure of the radius of a particle from the point of view of it's interaction with radiation. This is defined as* $r_e = \frac{\int_0^\infty n(r)r^3dr}{\int_0^\infty n(r)r^2dr}$, *where* r *is the radius of the particles and* $n(r)$ *is the number of particles of size* r.

ELEPHANT *Evaporation LEvel PHysics and Numerical ice Transport. A model created for this thesis to simulate **evaporation zones**.*

EVAPORATION ZONE *Coined by Forbes (2002), an evaporation zone is the area close to the base of ice clouds in which the particles evaporate (strictly sublimate, see **Ice Evaporation**). It is defined as the depth of atmosphere between the maximum **Ice Water Content** in the profile to 10% of this maximum value at some altitude between the maximum value and the Earth's surface.*

EXTINCTION COEFFICIENT *For a particular substance, the extinction coefficient is a measure of how well it absorbs electromagnetic radiation. Sub-*

stances with higher extinction coefficients absorb more radiation. In this thesis, extinction coefficient represents the reduction in a lidar signal as it interacts with atmospheric constituents. A high extinction coefficient leads to a weaker lidar signal further away from the instrument, yet a higher attenuated backscatter from the particles interacting with the radiation.

EXTINCTION-TO-BACKSCATTER RATIO *See **Lidar Ratio**.*

FREQUENCY OF OCCURRENCE *A measure of cloud climatology, being the fraction of times cloud is above a detection threshold in a particular location. See also **Amount When Present** and **Mean Cloud Fraction**.*

GENERAL CIRCULATION MODEL (GCM) *A model with large grid resolution which is concerned with representing the general circulation of the earth's atmosphere rather than small-scale variations in weather.*

GEOSCIENCE LASER ALTIMETER SYSTEM (GLAS) *See **ICESat**.*

ICE EVAPORATION *Strictly, the sublimation of ice to vapour bypassing the liquid phase. Termed evaporation in this thesis to avoid confusion with sublimation from vapour to ice.*

ICESAT *Acronym for Ice, Cloud and Land Elevation Satellite. It was launched in 2003, which carries a **lidar** platform on board (**GLAS**), which is capable of making profiles of clouds as one of the secondary aims of the mission.*

ICE WATER CONTENT (IWC) *A measure of the amount of ice contained within a cloud or model grid box. Ice water content is the mass of ice per unit volume.*

INTEGRATED BACKSCATTER *The lidar* ***backscatter*** *summed over a profile. This may be done to calibrate the lidar (O'Connor* et al.*, 2004), to determine the* ***multiple scattering factor*** *through a cloud of which the properties are known, to predict the* ***Lidar Ratio****, or to estimate the cloud optical depth.*

LIDAR *Acronym for Light Detection and Ranging.* ***Active remote sensing*** *instrument which operates at wavelengths centred around the visible, ultraviolet and infrared wavelengths.*

LIDAR IN-SPACE TECHNOLOGY EXPERIMENT (LITE) *Experiment where a* ***lidar*** *flew on board the space shuttle "Discovery" in 1996 to determine whether future spacebourne* ***lidar*** *missions would be possible.*

LIDAR RATIO *The ratio of* ***extinction*** *to* ***backscatter*** *observed by a lidar instrument. For liquid water, it is nearly constant at* 18 ± 0.8 *sr, however it varies within ice clouds, largely due to variable habits.*

LIQUID WATER CONTENT (LWC) *See also* ***Ice Water Content****. A measure of the amount of liquid water contained within a cloud or model grid box, defined as the mass of liquid water per unit volume.*

MAXIMUM OVERLAP *See* ***Overlap****.*

MAXIMUM-RANDOM OVERLAP *See* ***Overlap***

MEAN CLOUD FRACTION *The average cloud fraction for one particular model grid box or location; hence a measure of cloud climatology.*

MULTIPLE SCATTERING FACTOR *Defined by Platt (1973), the multiple scattering factor is a scaling factor for optical depth due to the amount of radiation from a lidar that is scattered out of the beam. It has an up-*

per limit of one, where there is only single scattering and a lot of radiation is scattered outside of the lidar field-of-view. This is probably most suitable for ground-based instruments. The lower limit is 0.5, which represents the maximum amount of multiple scattering and all scattered radiation remaining within the lidar field-of-view. This value is particularly suitable for spacebourne instruments.

NEPHOLOGY *Term for the scientific study of clouds.*

NUMERICAL WEATHER PREDICTION (NWP) *A model or models usually with smaller grid spacing and timesteps than a **GCM**, used for forecasting of the weather up to a few days in the future.*

OVERLAP *Specifically Cloud overlap; a term that is applied to an assumption of how clouds from different model grid boxes in the vertical overlap each other, which is important for cloud radiation calculations. Usually there are three main types that are used in models: Random, where the clouds are overlapped randomly; maximum, where at all times maximum extent of overlap is maintained and maximum-random overlap, where clouds with vertical extent over one or more grid boxes are maximumly overlapped or otherwise randomly overlapped.*

PARAMETERIZATION *In a numerical weather model, parameterization is the representation of small-scale processes (with scales of less than the model grid), yet important for the model large-scale physics which are represented in terms of a series of expressions allowing their effects to be felt on the large-scale grid. For example, cloud condensation is parameterized to form cloud and to modify the model's large-scale humidity.*

PARTICLE SPECTRUM *Another name for size distribution of particles. This refers*

to the number of particles available for a specific size of cloud droplet or ice particle and the variation of number of particles with particle size.

PASSIVE REMOTE SENSING *Remote sensing technique where distant information about an object is determined by observing radiation that is received from the object.*

PROGNOSTIC VARIABLE *A model variable that is carried from timestep to timestep with a equation for its time derivative.*

RADAR *Acronym for RAdio Detection And Ranging;* ***Active Remote Sensing*** *instrument that works at radio and microwave wavelengths. For cloud studies, wavelengths are on the order of centimetres or millimetres.*

RANDOM OVERLAP *See* ***Overlap****.*

REFLECTIVITY *Also known as Reflectivity Factor, it is the variable measured by a* ***radar****:* $Z = \int_0^\infty N(D)D^6 dD$*, where* $N(D)$ *is the number of particles of size* D*. It can be expressed in logarithmic (dB) or linear (mm*^{6} *m*$^{-3}$*) form.*

SIMULATION *Using model variables to predict (or simulate) measurements made by an instrument, where the model variables are not directly measured by the instrument.*

SKILL SCORE *A binary score of determining model performance when compared to the observations. Used in this thesis for examining how well clouds are forecast in models. Each model grid box is compared to the* ***radar*** *or* ***lidar*** *measurements and each model grid box is categorized as either a hit, a miss, a correct rejection or a false alarm (see table 2.2). A skill score uses this categorization to judge*

the skill of the model's forecast cloud.

TROPICAL RAINFALL MEASURING MISSION (TRMM) *An early space-bourne* ***radar*** *that was launched in 1997 for the purpose of measuring rainfall in the tropics.*

VENTILATION COEFFICIENT *A variable used in evaporation growth and diffusion calculations to model the airflow around the particle, which can lead to increased vapour diffusion or evaporation.*

Symbols

Chapter Two

Using Radar and Lidar for Model Evaluation

P_R	*Power returned to the radar receiver*
r	*Range of the targets from the radar*
C_{rad}	*Radar constant; dependent on radar hardware*
P_T	*Power transmitted from the radar*
ΔV	*Radar pulse volume*
σ	*Backscatter cross section of particles detected*
λ	*Radar or lidar wavelength*
K	*Dielectric factor*
N	*Number of particles of a specified diameter or within a specified diameter bin*
D	*Particle Diameter*
m	*Complex refractive index*
γ	*Mie-to-Rayleigh ratio*
K_{water}	*Dielectric factor of liquid water*
K_{ice}	*Dielectric factor of ice*
ϵ	*Complex dielectric constant of ice*
γ_g	*Attenuation of radar signal due to atmospheric gases*
γ_w	*Attenuation of radar signal due to cloud liquid water.*
γ_i	*Attenuation of radar signal due to cloud ice.*
C_{lid}	*Lidar constant; dependent on lidar hardware*
β'	*Attenuated lidar backscatter*
β	*Lidar backscatter*
r'	*Dummy variable of range,* r
η	*Multiple scattering factor*
α	*Lidar extinction coefficient*
s	*Lidar (or extinction-to-backscatter) ratio*

q	*Specific humidity of a model grid box*
q_t	*Total cloud water content of a model grid box*
q_l	*Cloud liquid water fraction of a model grid box*
q_i	*Ice water fraction of a model grid box*
q_{sat}	*Saturation specific humidity of a model grid box*
$_{ADV}$	*Subscript to denote change in cloud prognostic variables due to advection*
$_{DIFF}$	*Subscript to denote change in cloud prognostic variables due to diffusion*
$_{TM}$	*Subscript to denote change in cloud prognostic variables due to turbulent mixing from the boundary layer*
$_{ST}$	*Subscript to denote change in cloud prognostic variables due to stratiform cloud formation or dissipation processes.*
$_{P}$	*Subscript to denote change in cloud prognostic variables due to precipitation*
$_{CV}$	*Subscript to denote change in cloud prognostic variables due to convective activity*
$_{EV}$	*Subscript to denote change in cloud prognostic variables due to cloud evaporation*
α_{CP}	*Cloud phase function, where a phase of 1 is entirely liquid and 0 is entirely ice.*
RH_{crit}	*Critical value of relative humidity, at which cloud formation can begin*
$\mathcal{C}_{\mathcal{F}}$	*Cloud fraction*
LWC	*Liquid water content*
IWC	*Ice water content*
$\hat{a}$, $\hat{b}$, $\hat{c}$, $\hat{d}$	*Coefficients in the Hogan* et al. *(2006) relation of ice water content to radar reflectivity*
A	*Skill score hit*
B	*Skill score false alarm*
C	*Skill score miss*
D	*Skill score correct rejection*
HR	*Skill score of hit rate (Wilks, 1995)*

POD	*Skill score of probability of detection (Wilks, 1995)*
TS	*Skill score of threat score Wilks (1995)*
FAR	*Skill score of false alarm rate Wilks (1995)*
PSS	*Skill score developed by Palm* et al. *(2005)*
ETS	*Equitable threat skill score*
E	*Component of equitable threat score which removes randomness from the score*

Chapter Three

Doppler Radar Evaluation of the Representation of Evaporating Ice in Operational Models

N	*Ice crystal concentration*
D	*Maximum crystal diameter*
N_0	*Number concentration at zero particle diameter*
T	*Temperature*
Λ	*Parameter used to express the exponential decay of the ice particle size spectrum.*
D_0	*Equivolumetric median diameter of the ice particle spectrum*
a	*Coefficient of mass-diameter as used in the Met Office model*
b	*Exponent of mass-diameter as used in the Met Office model*
ρ_i	*Ice particle density*
IWC	*Ice water content*
m	*Mass of an individual ice particle*
Z	*Radar Reflectivity*
dB	*Indicates that a quantity is measured in decibels*
V_{Dop}	*Radar measured vertical Doppler velocity*
$\lvert K_{ice}\rvert$	*Dielectric factor of ice*
γ	*Mie to Rayleigh ratio*
v_c	*Ice crystal terminal velocity*

α	*Coefficient of velocity-diameter as used in the Met Office model*
β	*Exponent of velocity-diameter as used in the Met Office model*
ρ_0	*Density of 1 kg m*$^{-3}$
ρ_a	*Density of air*
R	*Gas constant for dry air*
p	*Atmospheric pressure*
q_i	*Ice water mixing ratio*
ϵ	*Turbulent kinetic energy dissipation rate*
$\sigma_{\bar{\mathrm{v}}}$	*Standard deviation of mean Doppler velocity*
v_a	*Vertical air velocity*
v_t	*Reflectivity-weighted particle terminal velocity*
D_a	*Area averaged particle diameter*
RH	*Relative humidity*
t	*Time*
C	*Capacitance of an ice crystal*
F	*The ventilation coefficient*
S_i	*Saturation ratio*
X	*Diffusivity*
e_{satice}	*Saturation vapour pressure*
L_s	*Latent heat of sublimation of ice*
k_a	*Thermal conductivity of air*
μ	*Dynamic viscosity of air*
ρ	*Air density*
z	*Altitude*
z_{adj}	*Adjusted altitude*
Sc	*The Schmidt number, equal to 0.6*
Re	*The Reynolds number*

Chapter Four

Simple Numerical Model Studies of Ice Evaporation

m	*Mass of an individual ice particle*
t	*Time*
C	*Capacitance of an ice crystal*
S_i	*Saturation ratio*
F	*The ventilation coefficient*
L_s	*Latent heat of sublimation of ice*
k_a	*Thermal conductivity of air*
μ	*Dynamic viscosity of air*
X	*Diffusivity*
e_{satice}	*Saturation vapour pressure*
Sc	*The Schmidt number, equal to 0.6*
Re	*The Reynolds number*
T	*Temperature*
ρ	*Air density*
D	*Maximum crystal diameter*
$v(D)$	*Ice particle terminal fall velocity, expressed as a function of D.*
RH	*Relative humidity*
R	*Gas constant for dry air*
p	*Atmospheric pressure*
ρ_i	*Ice particle density*
IWC	*Ice water content*
N	*Ice crystal concentration*
N_0	*Number concentration at zero particle diameter*

Chapter Five

Use of a Lidar Forward model for comparisons between ICESat and the ECMWF model

β'	*Lidar attenuated backscatter*

α	*Lidar extinction coefficient*
z	*Altitude*
s	*Lidar (or extinction-to-backscatter) ratio*
η	*Multiple scatting factor*
z_{lid}	*ICESat orbit altitude (altitude of the lidar)*
z'	*Dummy variable for* z
IWC	*Ice water content*
LWC	*Liquid water content*
r_{ei}	*Ice particle effective radius*
r_{el}	*Cloud droplet effective radius*
ρ_i	*Density of solid ice*
ρ_l	*Density of liquid water*
γ_w	*Integrated backscatter*
βWP	*Backscatter when present*
ETS	*Equitable threat skill score*
θ	*Odds ratio skill score*
A	*Skill score hit*
B	*Skill score false alarm*
C	*Skill score miss*
D	*Skill score correct rejection*
N	*Total number of points used to calculate a skill score (*$= A+B+C+D$*).*

References

Arking, A. (1991). The radiative effects of clouds and their impact on climate. *Bull. Amer. Meteorol. Soc.*, **72**, 795–813.

Atlas, D. (1954). The estimation of cloud parameters by radar. *J. Meteorol.*, **11**, 309–317.

Atlas, D., Matrosov, S. Y., Heymsfield, A. J., Chou, M.-D., and Wolff, D. B. (1995). Radar and radiation properties of ice clouds. *J. Appl. Meteorol.*, **34**, 2329–2345.

Baedi, R. J. P., de Wit, J. J. M., Russchenberg, H. W. J., and Poiares Baptista, J. P. V. (1999). *Alternative algorithm for correcting FSSP measurements*. CLARE'98, ESA-ESTEC.

Battaglia, A., Ajewole, M. O., and Simmer, C. (2007). Evaluation of radar multiple scattering effects in CloudSat configuration. *Atmos. Chem. Phys.*, **7**, 1719–1730.

Battan, L. J. (1973). *Radar Observation of the Atmosphere*. University of Chicago Press.

Beesley, J. A., Bretherton, C. S., Jakob, C., Andreas, E. L., Intrieri, J. M., and Uttal, T. A. (2000). A comparison of cloud and boundary layer variables in the ECMWF forecast model with observations at Surface Heat Budget of the Arctic Ocean (SHEBA) ice camp. *J. Geophys. Res.*, **105**, 12337–12349.

Bengtsson, L., Hodges, K. I., and Roeckner, E. (2005). Storm tracks and climate change. *J. Climate*, **19**, 3518–3543.

Bezy, J. L., Kondo, K., Kumagai, H., Leibrandt, W., Lin, C. C., Poiares Baptista, J. P. V., Silvestrin, P. L., and Suzuki, M. (2002). The EarthCARE mission. In *Proc. Second*

Int. Workshop on SpaceBorne Cloud Profiling Radar, pages 23–32. Communications Research Laboratory (CRL).

Boers, R., Russchenberg, H., Erkelens, J., Venema, V., van Lammeren, A., Apituley, A., and Jongen, S. (2000). Ground-based remote sensing of stratocumulus properties during CLARA, 1996. *J. Appl. Meteorol.*, **39**, 169–181.

Bony-Lena, S. (2006). Cloud feedbacks in GCMs: what did we learn from IPCC? In *Workshop on Parametrization of clouds in large-scale models*. ECMWF.

Born, M. and Wolf, E. (1999). *Principles of Optics: Electromagnetic Theory of Propagation, Interference, and Diffraction of Light, 7th ed*, chapter 13.5, pages 633–644. Cambridge University Press.

Bouniol, D., Illingworth, A. J., and Hogan, R. J. (2003). Deriving turbulent kinetic energy dissipation rate within clouds using ground based 94 GHz radar. In *Proc. 31st AMS Conference on Radar Meteorology*, volume 1, pages 193–196, Seattle, USA.

Bower, K. N., Moss, S. J., Johnson, D. W., Choularton, T. W., Latham, J., Brown, P. R. A., Blyth, A. M., and Cardwell, J. (1996). A parameterizations of the ice water content observed in frontal and convective clouds. *Q. J. R. Meteorol. Soc.*, **122**, 1815–1844.

Brown, P. R. A. and Francis, P. N. (1995). Improved measurements of the ice water content in cirrus using a total-water probe. *J. Atmos. Ocean. Technol.*, **12**, 410–414.

Brown, P. R. A., Illingworth, A. J., Heymsfield, A. J., McFarquhar, G. M., Browning, K. A., and Gosset, M. (1995). The role of spaceborne millimeter-wave radar in the global monitoring of ice cloud. *J. Appl. Meteorol.*, **34**, 2346–2366.

Browning, K. A. (1983). Air motion and precipitation growth in a major snowstorm. *Q. J. R. Meteorol. Soc.*, **109**, 225–242.

Browning, K. A. (1985). Conceptual models of precipitation systems. *Meteorol. Mag.*, **114**, 293–318.

Browning, K. A. and Monk, G. A. (1982). A simple model for the synoptic analysis of cold fronts. *Q. J. R. Meteorol. Soc.*, **108**, 435–452.

Browning, K. A., Clough, S. A., Davitt, C. S. A., Roberts, N. M., Hewson, T. D., and Healey, P. G. W. (1995). Observations of mesoscale sub-structure in the cold air of a developing frontal cyclone. *Q. J. R. Meteorol. Soc.*, **121**, 1229–1254.

Brussaard, G. and Watson, P. A. (1995). *Atmospheric modelling and millimetre wave propagation*. Chapman and Hall.

Burgess, D. and Ray, P. S. (1986). *Mesoscale Meteorology and Forecasting*, chapter 6. American Meteorological Society.

Bushell, A. C., Wilson, D. R., and Gregory, D. (2003). A description of cloud production by non-uniformly distributed processes. *Q. J. R. Meteorol. Soc.*, **129**, 1435–1455.

Carswell, A. I. and Pal, S. R. (1980). Polarization anisotropy in lidar multiple scattering from clouds. *Appl. Opt.*, **19**, 4123–4126.

Chapman, D. and Browning, K. A. (2001). Measurements of dissipation rate in frontal zones. *Q. J. R. Meteorol. Soc.*, **127**, 1939–1959.

Chen, W.-N., Chiang, C.-W., and Nee, J.-B. (2002). Lidar ratio and depolarization ratio for cirrus clouds. *Appl. Opt.*, **41**, 6470–6476.

Chiriaco, M., Vautard, R., Chepfer, H., Haeffelin, M., Dudhia, J., Wanherdrick, Y., Morille, Y., and Protat, A. (2006). The ability of MM5 to simulate ice clouds: Systematic comparison between simulated and measured fluxes and lidar/radar profiles at the SIRTA atmospheric observatory. *Mon. Weather Rev.*, **134**, 897–918.

Clough, S. A. and Franks, R. A. A. (1991). The evaporation of frontal and other stratiform precipitation. *Q. J. R. Meteorol. Soc.*, **117**, 1057–1080.

Clough, S. A., Lean, H. W., Roberts, N. M., and Forbes, R. M. (2000). Dynamical effects of ice sublimation in a frontal wave. *Q. J. R. Meteorol. Soc.*, **126**, 2405–2434.

Cox, G. P. (1988). Modelling precipitation in frontal rainbands. *Q. J. R. Meteorol. Soc.*, **114**, 115–127.

Delanoë, J. and Hogan, R. J. (2007). A variational scheme for retrieving ice cloud properties from combined radar, lidar and infrared radiometer. *Manuscript in Preparation*.

Delanoë, J., Protat, A., Bouniol, D., Heymsfield, A., Bansemer, A., and Brown, P. (2007). The characterization of ice cloud properties from Doppler radar measurements. *J. Appl. Meteorol. Climatol., in press.*

Donovan, D. P. and van Lammeren, A. C. A. P. (2000). Combined lidar and radar cloud particle effective size retrievals made during CLARA. *Phys. Chem. Earth (B)*, **25**(2), 115–120.

Donovan, D. P. and van Lammeren, A. C. A. P. (2001). Cloud effective particle size and water content profile retrievals using combined lidar and radar observations - 1. Theory and examples. *J. Geophys. Res. - Atmos.*, **106**(D21), 27425–27448.

Eloranta, E. W. (1998). A practical model for the calculation of multiply scattered lidar returns. *Appl. Opt.*, **37**, 2464–2472.

Ferrare, R., Melfi, S., Whiteman, D., Evans, K. D., Schmidlin, F. J., and Starr, D. O. (1995). A comparison of water vapour measurements made by Raman lidar and radiosondes. *J. Atmos. Ocean. Technol.*, **12**, 1177–1195.

Field, P. R. and Heymsfield, A. J. (2003). Aggregation and scaling of ice crystal ize distributions. *J. Atmos. Sci.*, **60**, 544–560.

Field, P. R., Hogan, R. J., Brown, P. R. A., Illingworth, A. J., Choularton, T. W., Kaye, P. H., Hirst, E., and Greenway, R. (2004). Simultaneous radar and aircraft observations of mixed-phase cloud at the 100m scale. *Q. J. R. Meteorol. Soc.*, **130**, 1877–1904.

Foot, J. S. (1988). Some observations of the optical properties of clouds. II: Cirrus. *Q. J. R. Meteorol. Soc.*, **114**, 145–164.

Forbes, R. M. (2002). *Numerical Model parametrization of ice microphysics and the impact of evaporative cooling on frontal dynamics*. Ph.D. thesis, Dept. Meteorology, University of Reading.

Forbes, R. M. and Hogan, R. J. (2006). Observations of the depth of ice particle evaporation beneath frontal cloud to improve NWP modelling. *Q. J. R. Meteorol. Soc.*, **132**, 865–883.

Fowler, L. D., Randal, D. A., and Rutledge, S. A. (1996). Liquid and ice cloud microphysics in the CSU general circulation model. Part I: Model description and simulated microphysical processes. *J. Climate*, **9**, 489–529.

Fox, N. I. and Illingworth, A. J. (1997a). The potential of a spaceborne cloud radar for the detection of stratocumulus clouds. *J. Appl. Meteorol.*, **36**, 676–687.

Fox, N. I. and Illingworth, A. J. (1997b). The retrieval of stratocumulus cloud properties by ground-based radar. *J. Appl. Meteorol.*, **36**, 485–492.

Francis, P. N., Hignett, P., and Macke, A. (1998). The retrieval of cirrus cloud properties from aircraft multi-spectral reflectance measurements during EUCREX'93. *Q. J. R. Meteorol. Soc.*, **124**, 1273–1291.

Geleyn, J. F. and Hollingsworth, A. (1979). An economical method for the computation of the interaction between scattering and line absorption of radiation. *Contrib. Atmos. Phys.*, **52**, 1–16.

Ghan, S. J., Leung, L. R., and Hu, Q. (1997). Application of cloud microphysics to NCAR community climate model. *J. Geophys. Res.*, **102**, 16507–16527.

Gregory, D., Wilson, D., and Bushell, A. (2002). Insights into cloud parametrization provided by a prognostic approach. *Q. J. R. Meteorol. Soc.*, **128**, 1485–1504.

Hall, W. D. and Pruppacher, H. R. (1976). The survival of ice particles falling from cirrus clouds in subsaturated air. *J. Atmos. Sci.*, **33**, 1995–2006.

Harris, F. I. (1977). The effects of evaporation at the base of ice precipitation layers: Theory and radar observations. *J. Atmos. Sci.*, **34**, 651–672.

Haynes, J. M. and Stephens, G. L. (2006). A multi-purpose radar simulation package: Quickbeam. *Document in Preparation*.

Heymsfield, A. J. (1977). Precipitation development in stratiform ice clouds: A microphysical and dynamical study. *J. Atmos. Sci.*, **34**, 367–381.

Heymsfield, A. J. and Miloshevich, L. M. (1995). Relative humidity and temperature influences on cirrus formation and evolution. *J. Atmos. Sci.*, **52**, 4302–4326.

Hobbs, P. V., Funk, N. T., Weiss, R. R., Locatelli, J. D., and Biswas, K. R. (1985). Evaluation of a 35 GHz radar for cloud physics research. *J. Atmos. Ocean. Technol.*, **2**, 35–48.

Hogan, R. J. (1998). *Dual-Wavelength Radar Studies of Clouds*. Ph.D. thesis, Dept. Meteorology, University of Reading.

Hogan, R. J. (2006). Fast, approximate calculation of multiply scattered lidar returns. *Appl. Opt.*, **45**, 5984–5992.

Hogan, R. J. and Illingworth, A. J. (1999). The potential of spaceborne dual-wavelength radar to make global measurements of cirrus clouds. *J. Atmos. Ocean. Technol.*, **16**, 518–531.

Hogan, R. J. and Illingworth, A. J. (2000). Developing cloud overlap statistics from radar. *Q. J. R. Meteorol. Soc.*, **126**, 2903–2909.

Hogan, R. J., Illingworth, A. J., and Sauvageot, H. (2000). Measuring crystal size in cirrus using 35- and 94-GHz radars. *J. Atmos. Ocean. Technol.*, **17**, 27–37.

Hogan, R. J., Jakob, C., and Illingworth, A. J. (2001). Comparison of ECMWF winter-season cloud fraction with radar-derived values. *J. Appl. Meteorol.*, **40**, 513–525.

Hogan, R. J., Bouniol, D., Ladd, D. N., O'Connor, E. J., and Illingworth, A. J. (2003a). Absolute calibration of 94/95-GHz radars using rain. *J. Atmos. Ocean. Technol.*, **20**, 572–580.

Hogan, R. J., Illingworth, A. J., O'Connor, E. J., and Poiares Baptista, J. P. V. (2003b). Characteristics of mixed-phase clouds. II: A climatology from ground-based lidar. *Q. J. R. Meteorol. Soc.*, **129**, 2117–2134.

Hogan, R. J., Mittermaier, M. P., and Illingworth, A. J. (2006). The retrieval of ice water content from radar reflectivity factor and temperature and its use in evaluating a mesoscale model. *J. Appl. Meteorol. Climatol.*, **45**, 301–317.

Holloway, J. L. and Manabe, S. (1971). Simulation of climate by a general circulation model. 1: Hydrological cycle and heat balance. *Mon. Weather Rev.*, **99**, 335–369.

Hulbert, E. O. (1937). Observations of a searchlight beam to an altitude of 28 kilometers. *J. Optical Soc. Amer.*, **27**, 377–382.

Illingworth, A. J., Hogan, R. J., O'Connor, E. J., Bouniol, D., Brooks, M. E., Delanoë, J., Donovan, D. P., Eastment, J. D., Gaussiat, N., Goddard, J. W. F., Haeffelin, M., Klein, H., Baltink, O., Krasnov, O. A., Pelon, J., Piriou, J.-M., Protat, A., Russchenberg, H. W. J., Seifert, A., Tompkins, A. M., van Zadelhoff, G. J., Vinit, F., Willén, U., Wilson, D. R., and Wrench, C. L. (2007). Cloudnet—Continuous evaluation of cloud profiles in seven operational models using ground-based observations. *Bull. Am. Met. Soc, in press*.

Intrieri, J. M., Stephens, G. L., Eberhard, W. L., and Uttal, T. (1993). A method for determining cirrus cloud particle sizes using lidar and radar backscatter technique. *J. Appl. Meteorol.*, **32**, 1074–1082.

IPCC (Intergovernmental Panel on Climate Change, 2007). *IPCC Fourth Assessment Report— Climate Change 2007*. UNEP/WMO.

Jakob, C. (1994). The impact of the new cloud scheme on ECMWF's intergrated forecasting system (IFS). In *ECMWF/GEWEX Workshop on Modelling, Validation and Assimilation of Clouds*, Reading, United Kingdom. ECMWF.

Jakob, C. (1999). Cloud cover in the ECMWF reanalysis. *J. Climate*, **12**, 947–959.

Jakob, C. (2003). An improved strategy for the evaluation of cloud parameterizations in GCMs. *Bull. Amer. Meteorol. Soc.*, **84**, 1387–1401.

Jakob, C. and Klein, S. A. (1999). The role of vertically varying cloud fraction in the parameterization of microphysical processes in the ECMWF model. *Q. J. R. Meteorol. Soc.*, **125**, 941–965.

Johnson, E., Meyer, R. C., Hopkins, R. E., and Mock, W. H. (1939). Measurement of light scattered by the upper atmosphere from a search-light beam. *J. Optical Soc. Amer.*, **29**, 512–517.

Karlsson, K. G. (1996). Validation of modelled cloudiness using satellite-estimated cloud climatologies. *Tellus*, **48A**, 767–785.

Kattawar, G. W. and Plass, G. N. (1971). Reflection of light pulses from clouds. *Appl. Opt.*, **10**, 2304–2310.

Kollias, P., Albrecht, B. A., Lhermitte, R., and Savtchenko, A. (2001). Radar observations of updrafts, downdrafts, and turbulence in fair-weather cumuli. *J. Atmos. Sci.*, **58**, 1750–1766.

Krasnov, O. A. and Russchenberg, H. W. J. (2005). A synergetic radar-lidar technique for the LWC retrieval in water clouds:description and application to the CLOUDNET data. In *11th conference on Mesoscale processes and the 32nd conference on radar meteorology*, Albuquerque, New Mexico. American Meteorological Society.

Lhermitte, R. (1987). A 94-GHz doppler radar for cloud observations. *J. Atmos. Ocean. Technol.*, **4**, 36–48.

Lhermitte, R. (1989). Satellite-bourne millimeter wave Doppler radar. In *Union Radio Scientifique Internationale, Open Symposium*, La-Londe-Les-Maures, France.

Lhermitte, R. M. (1990). Attenuation and scattering of millimeter wavelength radiation by clouds and precipitation. *J. Atmos. Ocean. Technol.*, **7**, 464–479.

Liao, L. and Sassen, K. (1994). Investigation of relationships between K-band radar reflectivity and ice and liquid water content. *Atmos. Res.*, **34**, 231–248.

Liebe, H. J. (1985). An updated model for millimeter-wave propogation in moist air. *Radio Sci.*, **20**, 1069–1089.

Liu, C.-L. and Illingworth, A. J. (2000). Toward more accurate retrievals of ice water content from radar measurements of clouds. *J. Appl. Meteorol.*, **39**, 1130–1146.

Locatelli, J. D. and Hobbs, P. V. (1974). Fall speeds and masses of solid precipitation particles. *J. Geophys. Res.*, **79**, 2185–2197.

Lohmann, U. and Roeckner, E. (1995). Influence of cirrus cloud radiative forcing on climate and climate sensitivity in a general circulation model. *J. Geophys. Res.*, **100**, 16305–16324.

Luo, Y., Krueger, S. K., and Mace, G. C. (2003). Cirrus clouds properties from a clou-resolving model simulation compared to cloud radar observations. *J. Atmos. Sci.*, **60**, 510–525.

Luo, Y., Krueger, S. K., and Moorthi, S. (2005). Cloud properties simulated by a single-column model. Part I: Comparison to cloud radar observations of cirrus clouds. *J. Atmos. Sci.*, **62**, 1428–1445.

Mace, G. G. and Benson-Troth, S. (2002). Cloud-layer overlap characteristics derived from long-term cloud radar data. *J. Climate*, **15**, 2505–2515.

Mace, G. G., Jakob, C., and Moran, K. P. (1998). Validation of hydrometeor occurrence predicted by the ECMWF model using millimeter wave radar data. *Geophys. Res. Lett.*, **25**, 1645–1648.

Maiman, T. H. (1960). Simulated optical radiation in ruby. *Nature*, **187**, 493–494.

Manabe, S. and Stouffer, R. J. (1999). The role of the thermohaline circulation in climate. *Tellus*, **51**, 91–109.

Manabe, S., Smagorinsky, J., and Stricker, R. F. (1965). Simulated climatology of a general circulation model with a hydrological cycle. *Mon. Weather Rev.*, **93**, 769–798.

Marshall, J. S. (1953). Precipitation trajectories and patterns. *J. Meteorol.*, **10**, 25–29.

Martin, G. M., Johnson, D. W., and Spice, A. (1994). The measurement and parameterization of effective radius of droplets in warm stratocumulus clouds. *J. Atmos. Sci.*, **51**, 1823–1842.

Mason, B. (1953). The growth of ice crystals in a supercooled water cloud. *Q. J. R. Meteorol. Soc.*, **79**, 104–111.

Mason, B. J. (1971). *The Physics of Clouds*. Oxford University Press, 2nd edition.

Matrosov, S. Y. (1997). Variability of microphysical parameters in high-altitude ice clouds: Results of the remote sensing method. *J. Appl. Meteorol.*, **36**, 633–648.

Matrosov, S. Y., Orr, B. W., Kropfli, R. A., and Snider, J. B. (1994). Retrieval of vertical profiles of cirrus cloud microphysical parameters from doppler radar and infrared radiometer measurements. *J. Appl. Meteorol.*, **33**, 617–626.

Matrosov, S. Y., Heymsfield, A. J., Intrieri, J. M., Orr, B. W., and Snider, J. B. (1995). Ground-based remote sening of cloud particle sizes during the 26 November 1991 FIRE II cirrus case: Comparisons with in situ data. *J. Atmos. Sci.*, **52**, 4128–4142.

Matveev, L. T. (1984). *Cloud Dynamics*. D. Reidel.

McClung, F. J. and Hellwarth, R. W. (1962). Giant optical pulsations from ruby. *J. Appl. Phys*, **33**, 828–829.

McCormick, M. P., Winker, D. M., Browell, E. V., Coakley, J. A., Gardner, C. S., Hoff, R. M., Kent, G. S., Melfi, S. H., Menzies, R. T., Platt, C. M. R., A., R. D., and Reagan, J. A. (1993). Scientific investigations planned for the Lidar In-Space Technology Experiment (LITE). *Bull. Amer. Meteorol. Soc.*, **74**, 205–214.

Mead, J. B., McIntosh, R. E., Vandemark, D., and Swift, C. T. (1989). Remote sensing of clouds and fog with a 1.4-mm radar. *J. Atmos. Ocean. Technol.*, **6**, 1090–1097.

Meneghini, R. and Kozu, T. (1990). *Spacebourne Weather Radar*. Artech House.

Middleton, W. E. K. and Spilhaus, A. F. (1953). *Meteorological Instruments*. University of Toronto Press, Toronto.

Miller, S. D., Stephens, G. L., and Beljaars, A. C. M. (1999). A validation survey of the ECMWF prognostic cloud scheme using LITE. *Geophys. Res. Lett.*, **26**, 1417–1420.

Miloshevich, L. M., Paukkunen, A., Vömel, H., and Oltmans, S. J. (2004). Development and validation of a time-lag correction for vaisala radiosonde humidity measurements. *J. Atmos. Ocean. Technol.*, **21**, 1305–1327.

Morcrette, J.-J. (2002). Assessment of the ECMWF model cloudiness and surface radiation fields at the ARM SGP site. *Mon. Weather Rev.*, **130**, 257–277.

Morcrette, J.-J. and Fourquart, Y. (1986). The overlapping of cloud layers in shortwave radiation parameterizations. *J. Atmos. Sci.*, **43**, 321–328.

Morcrette, J.-J. and Jakob, C. (2000). The response of the ECMWF model to changes in the cloud overlap assumption. *Mon. Weather Rev.*, **128**, 1707–1732.

Naud, C., Muller, J.-P., and de Valk, P. (2005). On the use of ICESAT-GLAS measurements for MODIS and SEVIRI cloud-top height accuracy assessment. *Geophys. Res. Lett.*, **32**, L19815, doi:10.1029/2005GL023275.

O'Connor, E. J., Illingworth, A. J., and Hogan, R. J. (2004). A technique for autocalibration of cloud lidar. *J. Atmos. Ocean. Technol.*, **21**, 777–786.

O'Connor, E. J., Hogan, R. J., and Illingworth, A. J. (2005). Retrieving stratocumulus drizzle parameters using Doppler radar and lidar. *J. Appl. Meteorol.*, **44**, 14–27.

Ou, S.-c. and Liou, K.-N. (1995). Ice microphysics and climatic temperature feedback. *Atmos. Res.*, **35**, 127–138.

Pal, S. R., Steinbrecht, W., and Carswell, A. I. (1992). Automated method for lidar determination of cloud base height and vertical extent. *Appl. Opt.*, **31**, 1488–1494.

Palm, S. P., Benedetti, A., and Spinhirne, J. D. (2005). Validation of ECMWF global forecast model parameters using GLAS atmospheric channel measurements. *Geophys. Res. Lett.*, **32**, L22S09, doi:10.1029/2005GL023535.

Pinnick, R. G., Jennings, S. G., Chýlek, P., Ham, C., and Grandy, W. T. J. (1983). Backscatter and extinction in water clouds. *J. Geophys. Res.*, **88**, 6787–6796.

Platt, C. M. R. (1973). Lidar and radiometric observations of cirrus clouds. *J. Atmos. Sci.*, **30**, 1191–1204.

Platt, C. M. R., Scott, J. C., and Dilley, A. C. (1987). Remote sounding of high clouds. Part IV: Optical properties of mid-latitude and tropical clouds. *J. Atmos. Sci.*, **44**, 729–747.

Platt, C. M. R., Young, S. A., Manson, P. J., Patterson, G. R., Marsden, S. C., and Austin, R. T. (1998). The optical properties of equatorial cirrus from observations in the ARM pilot radiation observation experiment. *J. Atmos. Sci.*, **55**, 1977–1996.

Platt, C. M. R., Winker, D. M., Vaughan, M. A., and Miller, S. D. (1999). Backscatter-to-extinction ratios in the top layers of tropical mesoscale convective systems and in isolated cirrus from LITE observations. *J. Appl. Meteorol.*, **38**, 1330–1345.

Probert-Jones, J. R. (1962). The radar equation in meteorology. *Q. J. R. Meteorol. Soc.*, **88**, 485–495.

Pruppacher, H. R. and Klett, J. D. (1978). *Microphysics of Clouds and Precipitation*. D. Reidel Publishing Company, Boston, USA.

Quante, M. (2004). The role of clouds in the climate system. *J. Phys. IV France*, **121**, 61–86.

Randall, D. A., editor (2000). *General Circulation Model Development. Past, Present and future*. International Geophysics Series. Academic Press.

Sassen, K. (1987). Ice cloud content from radar reflectivity. *J. Climate Appl. Meteorol.*, **26**, 1050–1053.

Sassen, K. and Liao, L. (1996). Estimation of cloud water by a W-band radar. *J. Appl. Meteorol.*, **35**, 932–938.

Sauvegeot, H. and Omar, J. (1987). Radar reflectivity of cumulus clouds. *J. Atmos. Ocean. Technol.*, **4**, 264–272.

Schiffer, R. A. and Rossow, W. B. (1983). The International Satellite Cloud Climatology project (ISCCP): The first project of the world climate research program. *Bull. Amer. Meteorol. Soc.*, **64**, 779–784.

Senior, C. A. and Mitchell, J. F. B. (1993). Carbon dioxide and climate: The impact of cloud paramterization. *J. Climate*, **6**, 393–418.

Simpson, J., Adler, R. F., and North, G. R. (1988). A proposed Tropical Rainfall Measuring Mission (TRMM) satellite. *Bull. Amer. Meteorol. Soc.*, **69**, 278–295.

Slingo, J. M. (1980). A cloud parameterization scheme derived from GATE data for use with a numerical model. *Q. J. R. Meteorol. Soc.*, **106**, 747–770.

Slingo, J. M. (1987). The development and verification of a cloud prediction scheme for the ECMWF model. *Q. J. R. Meteorol. Soc.*, **113**, 899–927.

Smagorinsky, J., Manabe, S., and L., H. J. (1965). Numerical results of a nine-level general circulation model. *Mon. Weather Rev.*, **93**, 727–768.

Smith, R. N. B. (1990). A scheme for predicting layer clouds and their water content in a general circulation model. *Q. J. R. Meteorol. Soc.*, **116**, 435–460.

Spinhirne, J. D., Palm, S. P., and Hart, W. D. (2005). Antarctica cloud cover for October 2003 from GLAS satellite lidar profiling. *Geophys. Res. Lett.*, **32**, L22S05, doi:10.1029/2005GL023782.

Stephens, G. L. (2006). Using satellites to validate clouds: ISCCP, MODIS, and now the Cloudsat era. In *Workshop on Parametrization of clouds in large-scale models*. ECMWF.

Stephens, G. L., Tsay, S. C., Stackhouse Jr, P. W., and Flatau, P. (1990). The relevance of the microphysical and radiative properaties of cirrus clouds to climate and climate feedback. *J. Atmos. Sci.*, **47**, 1742–1753.

Stephens, G. L., Vane, D. G., Boain, R. J., Mace, G. C., Sassen, K., Wang, Z., Illingworth, A. J., O'Connor, E. J., Rossow, W. B., Durden, S. L., Miller, S. D., Austin, R. T., Benedetti, A., Mitrescu, and The Cloudsat Science Team (2002). The CloudSat mission and the A-Train. *Bull. Amer. Meteorol. Soc.*, **83**, 1771–1790.

Stephenson, D. B. (2000). Use of the "Odds Ratio" for diagnosing forecast skill. *Weather and Forecasting*, **15**, 221–232.

Sundqvist, H. (1978). A parameterization scheme for non-convective condensation including prediction of cloud water content. *Q. J. R. Meteorol. Soc.*, **104**, 677–690.

Taylor, P. K., Guyner, T. H., Nicholls, S., Briscoe, M. G., and Pollard, R. T. (1983). The structure of an atmospheric warm front and its interaction with the boundary layer [and discussion]. *Phil. Trans. R. Soc. Lond*, **A 308**, 341–358.

Thorpe, A. J. and Clough, S. A. (1991). Mesoscale dynamics of cold fronts. I: Structures described by dropsoundings in FRONTS 87. *Q. J. R. Meteorol. Soc.*, **117**, 903–941.

Tian, L. and Curry, J. A. (1989). Cloud overlap statistics. *J. Geophys. Res.*, **94**, 9925–9935.

Tiedtke, M. (1993). Representation of clouds in large-scale models. *Mon. Weather Rev.*, **121**, 3040–3061.

Tompkins, A. M. (2002). A prognostic parameterization for the subgrid-scale variability of water vapour and clouds in large-scale models and its use to diagnose cloud cover. *J. Atmos. Sci.*, **59**, 1917–1942.

Tompkins, A. M. (2006). Issues concerning the representation of clouds in GCMs. In *Workshop on Parametrization of clouds in large-scale models*. ECMWF.

Uttal, T., Clothiaux, E. E., Ackerman, T. P., Intrieri, J. M., and Eberhard, W. L. (1995). Cloud boundary statistics during FIRE II. *J. Atmos. Sci.*, **52**, 4276–4284.

Vaughan, M., Young, S., Winker, D., Powwell, K., Omar, A., Liu, Z., Hu, Y., and Hostetler, C. (2004). Fully automated analysis of space-based lidar data: an overview of the CALIPSO retrieval algorithms and data products. In *Laser Radar Techniques for Atmospheric Sensing*, pages U.N. Singh, editor **5575**, 16–30. Proc. SPIE.

Wallace, B. (1988). Millimeter-wave propogation measurements at the ballistic research laboratory. *IEEE transactions on geoscience and remote sensing*, **26**, 253–258.

Washington, W. M. (1974). *NCAR Global Circulation Model*. GARP Publications Series, No. 14.

Weitkamp, editor (2005). *Lidar: range-resolved optical remote sensing of the atmosphere*. Springer.

Westbrook, C. D., Hogan, R. J., and Illingworth, A. J. (2007a). The capacitance of pristine ice crystals and aggregate snowflakes. *Submitted to J. Atmos. Sci.*

Westbrook, C. D., Hogan, R. J., Illingworth, A. J., and J., O. E. (2007b). Theory and observations of ice particle evolution in cirrus using Doppler radar: Evidence for aggregation. *Geophys. Res. Lett.*, **34**, L02824, doi:10.1029/2006GL027863.

Wexler, R. (1955). Radar analysis of precipitation streamers observed 25 February 1954. *J. Meteorol.*, **12**, 391–393.

Wexler, R. and Atlas, D. (1958). Moisture supply and growth of stratiform precipitation. *J. Meteorol.*, **15**, 531–538.

Wexler, R. and Atlas, D. (1959). Precipitation generating cells. *J. Meteorol.*, **16**, 327–332.

Wilks, D. S. (1995). *Statistical Methods in the Atmospheric Sciences*. Academic Press.

Wilson, D. R. and Ballard, S. P. (1999). A microphysically based precipitation scheme for the UK Meteorological Office Unified Model. *Q. J. R. Meteorol. Soc.*, **125**, 1607–1636.

Winker, D. M. and Poole, L. R. (1995). Monte-Carlo calculations of cloud returns for ground-based and space-based lidars. *Applied Physics B: Lasers and Optics*, **60**, 341–344.

Wood, R. and Field, P. R. (2000). Relationships between total water, condensed water, and cloud fraction in stratiform clouds examined using aircraft data. *J. Atmos. Sci.*, **57**, 1888–1905.

Xu, H., Wang, Y., and Xie, S.-P. (2004). Effects of the Andes on Eastern Pacific Climate: A regional atmospheric model study. *J. Climate*, **17**, 589–602.

Xu, K.-M. and Krueger, S. K. (1991). Evaluation of cloudiness parameterizations using a cumulus ensemble model. *Mon. Weather Rev.*, **119**, 342–267.

Yeh, H.-Y. M., Prasad, N., Meneghini, R., Tao, W.-K., Jones, J. A., and Adler, R. F. (1995). Cloud model-based simulation of spacebourne radar observations. *J. Appl. Meteorol.*, **34**, 175–197.

Zwally, H. J., Schutz, B., Abdalati, W., Abshire, J., Bentley, C., Brenner, A., Bufton, J., Dezio, J., Hancock, D., Harding, D., Herring, T., Minster, B., Quinn, K., Palm, S., Spinhirne, J., and Thomas, R. (2002). ICESat's laser measurements of polar ice, atmosphere, ocean and land. *Journal of Geodynamics*, **34**, 405–445.